Decay of a High Arctic Lake Ice Cover

By

Richard Heron, B.Sc., M.Sc.

A Thesis

Submitted to the School of Graduate Studies

in Partial Fulfilment of the Requirements

for the Degree

Doctor of Philosophy

McMaster University

December 1985

ISBN 0-315-30594-0

DECAY OF A HIGH ARCTIC LAKE ICE COVER

DOCTOR OF PHILOSOPHY (1985)

McMASTER UNIVERSITY
Hamilton, Ontario

TITLE: Decay of a High Arctic Lake Ice Cover

AUTHOR: Richard Heron, B.Sc. (Trent University)
M.Sc. (McMaster University)

SUPERVISOR: Dr. M.K. Woo

NUMBER OF PAGES: xvii, 189

ABSTRACT

This is a study of the decay processes of an ice cover on a small Arctic lake. The study was carried out near Resolute, N.W.T., Canada, for two melt seasons commencing in late May prior to melt and continuing until the lake was ice-free in late July. During this period, ice thickness, other ice properties and melt from the upper and lower ice surfaces were measured regularly. In addition, environmental conditions which affect the melt rate, such as air and water temperature and net radiation were obtained to permit a computation of the energy balance for the ice.

A one-dimensional energy balance model used to calculate the ice melt at a site performs well in predicting the ablation from the upper ice surface, melt from the lower ice surface and the internal melt and ice density. For the two study years, 49 percent of the melt (in water equivalent units) occurred in the ice interior due to absorbed radiation while ice melt at the upper ice surface (in water equivalent) amounted to 40 percent. Melt at the lower ice surface was only 11 percent of the total ice melt. Seventy five percent of the change in ice

thickness occurred at the upper ice surface where much of the internal ice melt was concentrated, producing low surface ice densities.

The formation of a moat along the edge of the ice cover and its subsequent growth was investigated. The results were incorporated in a two-dimensional model of ice decay along a transect normal to the shore. A series of transects allowed a simulation of the behaviour of the entire ice cover. The modelled results agree closely with the observed ice decay events from the beginning of melt until the fragmentation of the ice cover. Although the ice decay period was emphasized, the two-dimensional model can be expanded to include the season of ice growth.

ACKNOWLEDGEMENTS

I wish to thank Dr. M. K. Woo for his supervision and encouragement throughout this study and the other menbers of my supervisory commitee, Dr. S. B. McCann and Dr. W. P. Adams, for their useful discussions and review of the manuscript. Funding for this study was provided by the Natural Sciences and Engineering Research Council of Canada, The Arctic Institute of North America and the Presidential Committee on Northern Studies of McMaster University. Generous logistical support was provided by the Polar Continental Shelf Project, Department of Energy, Mines and Resources and the National Hydrology Research Institute, Department of the Environment who provided accomodation in Resolute.

Thanks also go to Dr. Philip Marsh, Peter Steer and Marie-Andre Dubreuil for their companionship during the study and help in the field. I am grateful for the assistance provided by Peter Low and Dan Orr under difficult conditions in the field. Special thanks to George Hobson and Frank Hunt of Polar Continental Shelf Project and their staff at Resolute, Fred, Bill, Emile, George, Lief and Frank, their assistance and support.

TABLE OF CONTENTS

LIST OF FIGURES

LIST OF TABLES

NOTATION

Symbol	Variable Description	Dimensions
a	absorption coefficient	m^{-1}
b	coefficient	dimensionless
B	Stefan-Boltzman constant	$m^{-2}\ K^{-4}$
C_a	heat capacity of air	J/kg K
C_i	heat capacity of ice	J/kg K
C_w	heat capacity of water	J/kg K
d	distance from reference point	m
d_e	distance to ice edge from shore	m
d_{fz}	distance to edge of frozen zone	m
D	drag coefficient	dimensionless
D_s	drag coefficient adjused for atmospheric stability	dimensionless
D_H	sensible heat drag coefficient	dimensionless
D_E	latent heat drag coefficient	dimensionless
e	extinction coefficient	m^{-1}
E	surface emissivity	dimensionless
F	ice layer bouyancy	kg/m^2
h	ice thickness (water equivalent)	m
h_b	basal ice thickness	m
h_f	critical ice thickness for fracture	m
h_m	depth of snowmelt during ripening	m
h_s	snow depth	m
h'_s	adjusted snow depth	m

h_w	water level	m
h_{wl}	hydrostaic water level	m
H	ice thickness	m
h_{ie}	ice edge thickness	m
I_{zi}	irradiance at depth d	W/m²
I_o	irradiance at surface	W/m²
J	heat required to melt ice layer	J/m²
k_i	thermal conductivity of ice	W/m² K
K	Von Karman constant	dimensionless
K↓	incident shortwave radiation	W/m²
L_f	latent heat of fusion	J/kg
L_v	latent heat of vapourization	J/kg
$L\uparrow_{sg}$	emitted longwave radiation from ground surface	W/m²
$L\uparrow_i$	emitted longwave radiation from ice surface	W/m²
L^*_g	ground surface net longwave radiation	W/m²
L^*_i	ice surface net longwave radiation	W/m²
L^*_s	snow surface net longwave radiation	W/m²
n	ice layer number	dimensionless
n_w	distance from top of ice layer to hydrostatic water level	m
N	total number of ice layers	dimensionless
p	air pressure	Pa
q_s	surface vapour pressure	Pa
q_z	vapour pressure at height z	Pa

Q_L	latent heat flux	W/m²
Q_H	sensible heat flux	W/m²
Q_I	heat flux into ice cover	W/m²
Q^*_i	ice surface radiation balance	W/m²
Q^*_{ic}	ice coven radiation balance	W/m²
Q^*_s	snow surface radiation balance	W/m²
Q_{mu}	upper surface melt energy flux	W/m²
Q_{ml}	lower surface melt energy flux	W/m²
Q_{in}	internal melt energy flux	W/m²
Q_P	precipitation heat flux	W/m²
Q_R	radiation flux absorbed in an ice layer	W/m²
Q_W	heat flux from water	W/m²
R	precipitation rate	m/s
Ri	Richardson Number	dimensionless
S	heat content of ice cover	J
t	time	s
T	time	days
T_a	air temperature	K
T_i	ice temperature	K
T_o	surface temperature	K
T_r	temperature of rainfall	K
T_s	ice surface temperature	K
T_{sg}	ground surface temperature	K
T_w	water temperature	K
T_z	temperature at height z	K

u_s	surface wind speed	m/s
u_z	wind speed at height above ice surface	m/s
v	temporary variable	
W_n	weight of ice layer	kg/m2
x	horizontal distance	m
y	ice cover deflection	m
z	distance above ice surface	m
zi	depth below ice surface	m
zw	distance from lower ice surface	m
z_0	surface roughness	m
z_{os}	snow surface roughness	m

GREEK

α_i	ice albedo	dimensionless
α_s	snow albedo	dimensionless
α_{s1}	initial snow albedo	dimensionless
α_{s2}	final snow density	dimensionless
ϵ	ratio of the molecular weights of air and water	dimensionless
ρ_a	air density	kg/m^3
ρ_i	ice density	kg/m^3
ρ_{pi}	density of pure ice	kg/m^3
ρ_{sd}	density of dry snow	kg/m^3
ρ_{sw}	density of wet snow	kg/m^3
ρ_w	water density	kg/m^3

SUBSCRIPTS

us	upper ice surface
ls	lower ice surface
in	internal
λ	wavelength

CHAPTER 1

INTRODUCTION

The decay of lake ice in spring is an important annual event. It marks the commencement of navigation and the end of the use of the floating ice as a bearing surface for winter roads, air strips and other uses. During the decay period, the ice cover conditions have a profound influence upon the physical, chemical, biological, hydrological and geomorphological processes operating in the lake (Carson and Hussey 1960, Adams 1981, Schindler et al 1974, Alestalo 1980).

In the scientific literature, this period of ice decay is sometimes referred to as the break-up period. Starosolszky (1980) defines it as the period of disintegration of an ice cover, beginning with the first visual evidence of deterioration along the shoreline and the appearance of shore leads and ending on the date when the water body is clear of ice. In many cases, these features may occur after ice melt has started. Other authors, such as Kivisild (1970), Allen (1977), Greene (1981) used a more general definition to include the period commencing from the end of ice growth when the ice melt processes become active. However, when applied to

river ice, the break-up period begins with the first movement of the ice (Starosolszky 1980). To avoid ambiguity in the definition, the term break-up will be avoided in this study. Instead, the ice decay period will be used to describe the duration from the first deterioration of the ice cover due to melting until the ice is completely gone.

1.1 Process Studies

The decay of lake ice and its controlling factors have been described qualitatively by many authors (e.g. Barnes 1960; Williams 1967). However, quantitive studies of melting lake ice are few and limited and many of the necessary parameters, such as the aerodynamic roughness and the shortwave radiation extinction coefficient of ice, required to model lake ice decay are unavailable. More research has been performed on melting sea ice (Langleben 1966, Grenfell and Maykut 1977). While the melt processes are similar, certain information is not readily transferable to lake ice due to the differences in ice properties and behaviour as well as thermal conditions of the sea water. A large amount of data has been obtained from growing lake ice, but much of this information is not applicable because the ice structure changes once melt starts.

1.2 Models

In their review of limnologic models, Fox et al (1979) found that the existing models cannot describe lake processes during the period of ice growth and decay. This is in part due to the absence of process-oriented ice melt models suitable for use on small lakes. The degree-day method (Bilello 1980, Ashton 1983) and a more comprehensive energy balance approach (Maykut and Untersteiner 1971, Rumer and Yu 1978, Greene and Outcalt 1985) have been used to estimate the ice thickness at a point. The spatial models available have been developed for large lakes (Wake and Rumer 1979) and sea ice (Parkinson and Washington 1979, Hibler 1979). The spatial resolution of these models is on the order of kilometers, too coarse to represent the melt pattern on most lakes. In addition, their scale allows the ice-shore interaction to be treated in a simple manner without much loss of accuracy, but this is not sufficiently detailed for modelling the spatial ice characteristics during ice decay period in small lakes.

1.3 Objectives

Within the context of the above discussion, the objectives of this study are:

1) to examine the ice decay processes of a small lake in order to provide a better understanding

of the behaviour of the decaying ice cover

2) to model the spatial variability of the ice cover during its decay period.

For the first objective, detailed observation of the ice cover conditions were made during the decay period. At a site, a one dimensional energy balance model is used to determine the contributions of the energy sources to melting on the upper and lower ice surfaces as well as internal melt. These results are compared to the measured ice thickness. To accomplish the second objective, a series of computational transects are established normal to the shore. The one dimensional site model is used to calculate the ice thickness at a number of locations along the transect with additional relationships used to describe the behaviour of the ice at the edge of the ice cover. The combined results from these transects are verified by field observations

1.4 Study Site Selection

A small High Arctic lake, near Resolute on Cornwallis Island (74° 40' N, 95° 00' W) was chosen for the study. The relatively uniform ice covers and continuous daylight during the decay period result in ice conditions which are simpler than those found on more southerly lakes. This permits the melt processes to be isolated and the requisite parameters estimated. The greater ice

thickness extends the melt period which allows a longer period of study. However, the types of ice found in High Arctic lake covers do not differ greatly from lakes in other areas and thus the results of this study are transferable to the ice covers on lakes elsewhere.

1.5 Presentation of Thesis

The literature on ice decay is reviewed in Chapter 2 followed by a description of the study site and field methods in Chapter 3. In Chapter 4, the ice conditions and ice melt processes that were observed on the lake during the ice decay period are described. A one-dimensional model is used in Chapter 5 to simulate the change in ice thickness at a site. In Chapter 6, a two-dimensional model is developed to describe the spatial properties of the decaying ice cover. The final chapter summarizes the major findings of this study and indicates the general applicability of the results.

CHAPTER 2

LITERATURE REVIEW

The physical properties and behaviour of lake ice during the growth phase are well known (Michel 1978, Adams 1981). For the period of decay, however, lake ice covers have not been studied sufficiently. In the late 19th century, the rapid clearance of ice from lakes late in the melt season led to the speculation that it sank overnight (Barnes 1910). Since then, field observations have provided qualitative descriptions of the processes and factors influencing the decay of the lake ice covers (Williams 1965, Barnes 1960, Hobbie 1973). There is little quantitative information on the rate of ice melt and most of the data are limited to the change in ice thickness (Bilello 1980, Shaw 1965, Hobbie 1961, Williams 1968), though much detailed research has been performed on individual melt processes. For one-dimensional ice melt, these processes can be categorized as internal, surface and bottom ice melt.

2.1 Internal Ice Melt

Internal melt in ice is primarily the result of absorbed radiation. Laboratory and field studies have

shown that the interior of multi-grained ice begins to melt just before the ice warms to 0° C. The first locations to melt are the triple grain boundaries where an increase in surface energy depresses the freezing point (Ketcham and Hobbs 1969). Browman (1974) observed this melting phenomenon in clear lake ice at ice temperatures down to -0.5° C. These features appear as thread-like channels which become more numerous as the ice warms and eventually become interconnected. The presence of impurities trapped at the crystal boundaries during ice formation may also contribute to the early melt at the triple grain boundaries and at the remaining crystal boundaries (Muguruma and Kikuchi 1963).

Radiation is also absorbed within ice crystals, producing features that are known as ice flowers or Tyndall figures after their discoverer. These are thin inclusions of water and vapour with hexagonal symmetry located along the basal plane of the crystal (Shumskii 1964, Hobbs 1974). Additional structures that are not Tyndall figures can grow along the plane parallel to the optical or c-axis. These dendritic structures may be inclined up to 45° from the plane and like the Tyndall figures, require superheating to form (Hobbs 1974).

The crystallography of the ice strongly influences the behaviour of the melt water inclusions. Where the

c-axis is horizontal, the trapped air bubbles and Tyndall figures can migrate upwards along the basal plane to the ice surface. The air bubbles are replaced by water and the albedo decreases (Barnes 1960). If the c-axis is vertical, no migration occurs, and with continued melt, the ice albedo increases.

Besides controlling the strength of the ice cover (Barnes 1960, Polyakova 1977, Ashton 1983), the ice skeleton density determines the thickness of ice melted for a given energy input. A knowledge of the radiation attenuation characteristics of the melting ice is required when modelling the internal melt and ice density, but there is little information on radiative transfer in melting lake ice. Only Goldman et al (1967), Hobbie (1973), Bolsenga (1978) and Gorelkin et al (1980) provide radiation extinction coefficients for melting lake ice. However, many studies have determined extinction coefficients for non-melting ice (Maguire 1975, Bolsenga 1978, Roulet 1981) and snow (Warren 1982). The results of laboratory studies of the absorption coefficients for pure ice over a broad spectral range can be found in Goodrich (1970), Irvine and Pollack (1968), Hobbs (1974), and Grenfell and Perovich (1981). It is the values for non-melting ice that many of the physically based ice decay models have used (Rumer and Yu 1978, Wake and Rumer 1979b, Greene 1981, Dilley 1978). More work has been done on the

radiation regimes in sea ice (Grenfell and Maykut 1977, Grenfell and Perovich 1981, Grenfell and Perovich 1982, Grenfell 1983). In these studies, the vertical variation of the extinction coefficients in sea ice have been determined for a wide spectral range. Using this information, Grenfell (1979) applied a two stream model to predict the energy absorbed by the sea ice, but such information has not yet been incorporated into any sea ice decay model. An exception is Ashton (1984), who applied the vertically variable absorption coefficients of Maykut and Grenfell (1977) to lake ice since no other adequate data were available.

2.2 Surface Ice Melt

Scott and Ragotzkie (1961) observed that 70 percent of the change in ice thickness during the melt season occurred at the upper ice surface, indicating the importance of melt from the top. However, few field studies have distinguished the surface and the bottom ablation components, preventing a thorough validation of many models which make use of the energy balance and estimated ice densities to compute the changing ice thickness (Langleben 1972, Maykut and Untersteiner 1971, Wake and Rumer 1979b).

Most existing studies only consider the melting of well drained ice. Where water is ponded on the ice

surface, the melt processes are modified. The ponds have a lower surface albedo (Langleben 1968, Bolsenga 1980, Maykut and Grenfell 1977) and the temperature of the ponded water may reach 2° C or more (Adams 1975). Wake and Rumer (1979) investigated ice melt under ponded water but their model shows little difference between the ablation rate of bare ice and water covered ice because the influence of the water in retarding the melt offsets the increased radiation melt due to a lowered albedo.

2.3 Bottom Ice Melt

Numerous water temperature measurements have been made beneath melting ice (Hobbie 1962, Hill 1967, Bilello 1967, Williams 1969, Rigler 1975, LaPerriere et al 1978). Williams (1969) observed temperatures below the ice up to 7.5° C and he concluded that the water was warmed by absorbed radiation.

Williams (1969) computed melt at the bottom of the ice cover using a heat conduction model with measured water temperatures and assuming still water conditions. Recognizing that absorbed radiation was the only heat source for their lake water, Barnes and Hobbie (1960) first calculated the heat absorbed by the water before computing the heat conducted to the ice cover. A detailed ice bottom melt model, developed by Pivovarov (1972), routed radiation through the ice and water using the

Bouguer-Lambert Law and calculated the water heat flux. This model was able to demonstrate that a diurnal water temperature cycle could be expected. By 1500 h, an unstable temperature inversion of 2.5° C developed under the ice but this inversion decayed almost completely overnight. The peak melt rate computed was 5.5 mm/h. Pivovarov's (1972) model does not consider the effects on the thermal profile caused by chemical stratification developed as the ice melts (Hill 1967, Schindler et al 1974) or water currents effecs.

Scott and Ragotzkie (1961) noted that 30 percent of the lake ice loss occurred at the ice bottom. This shows that in modelling ice melt, the water heat flux should not be ignored, though it has been left out in certain models (Wake and Yu 1978, Chien et al 1983).

2.4 Loss Of Ice From The Ice Cover

The loss of ice around the perimeter of a lake ice cover has received little attention. Barnes (1960) destribes the formation of the moats around an Arctic lake ice cover, and outlined the manner in which the ice breaks free of the shore. Doronin and Kheisin (1977) used a two dimensional model to examine the accelerated melt along the edges of sea ice floes due to a diffusion of heat from the water. Absorbed solar radiation provided the energy source for the water. This approach is inadequate for lake

ice which is also affected by the input of warm stream water and by the thermal stratification and variable circulation pattern in the lake (Carson and Hussey 1960).

Recent interest in towing icebergs from Antarctica for supplying water has stimulated laboratory and computational studies of melting processes on a vertical ice face in both saline and fresh water (Huppert and Josberger 1980, Russell-Head 1980, Josberger 1980). These studies demonstrate a complex pattern of vertical convection for which only steady state solutions can be obtained. In addition, only a narrow range of conditions is examined since waves and currents are ignored. The applicability of the resulting models (Josberger 1980) is thus limited.

All of these studies deal with well bonded ice that undergoes minimal internal melting. For lake ice, internal melt loosens the crystals, permitting individual crystals to detach along the ice edge. This non-thermodynamic component of ice edge retreat has not been considered in the literature.

2.5 Modelling Ice Cover Decay

Many models focus upon the change in ice thickness during the melt period to predict the time when the lake becomes ice-free. Williams (1965) employed a statistical approach to determine the date on which a lake is clear of

ice. Similar procedures, using means or probability distributions, are useful for describing the ice climate for the lakes of a given region but require longterm observations to derive the pertinent statistics. Such techniques cannot predict the ice conditions for specific years and do not take into account the ice decay processes.

Statistical correlation is the most common technique used to determine the rate of decay and the ice-free date. Ice conditions are correlated between locations (Baker et al 1976) and the prediction is reasonably accurate if the sites are not far apart and are subject to similar ice decay processes and rates. Historical records are again required to determine the relationship between stations. Another method employs the degree-day equation to determine the ice thickness during melt (Baker et al 1976, Bilello 1980, Ashton 1983). This is the melt equivalent of Stefan's Equation which is commonly used to predict the growth of ice and has a better theoretical basis since ice growth occurs primarily on the lower ice surface. For ice decay, the various melt processes are indexed only by the thawing degree-day and therefore this approach has little physical basis. Despite such limitation, the results are surprisingly good. This is primarily due to the strong relationship between air temperature and solar radiation which is a significant

contributor to melt. Bilello (1980) recognized the importance of solar radiation and included it in his analysis, but obtained no significant improvement in accuracy. Williams (1965) condensed his energy balance, using only the two major components, air temperature and solar radiation to compute his heat index. In the USSR, a regional heat index is used in a regression relationship to determine ice melt (Shulyakovski 1966).

The most detailed models are those based on the energy balance of the ice cover. While they require a substantial amount of meteorological data, the processes are modelled more realistically. As a result, simulations can be performed to test the response of the ice cover under varying climatic conditions (Maykut and Untersteiner 1971, Semtner 1976). The first energy balance study of a melting lake ice cover was part of a winter lake energy budget for Lake Mendota in Wisconsin (Scott and Ragotskie 1961). Although various energy components were observed, the resulting change in ice thickness was measured and not computed. Williams (1965) also used the energy balance approach for a lake in southern Ontario. He ignored the heat flux from the water but in spite of this his end-of-melt energy totals were comparable to those required to melt the ice. Wake and Yu (1978) performed a similar operation for Lake Erie, using land based meteorological data and ignoring the water heat flux.

Since Lake Erie is covered by pack ice in continuous motion, verification of ice thickness is difficult. However, the model performed well for the short period when data was available. This one dimensional model was expanded to three dimensions by Wake and Rumer (1979) and Chieh et al 1983 with the addition of a two dimensional water circulation subroutine to drive the ice drift. These computations were performed on a square 5 km grid. When the model was calibrated, the computed results were comparable to observed ice cover distribution on the lake. In this model, ice drifting and ice thickness increase due to ice rafting are both ignored, and no allowance is made for the overlying snowcover. The most complex of the physically-based ice decay models is the two dimensional numerical model of Dilley (1978). This was designed to simulate the growth and decay of the border ice along a transect normal to the shore of lakes which do not freeze over. Unlike many of the earlier studies, abundant field data were collected from Lake Ontario, for which the model performed well. The complete thermal regime of the soil, water, ice, snow and air was modelled but no provision was made for mechanical action along the ice edge.

Physically-based models have also been developed for the decay of river and sea ice. The river ice model of Greene, 1981 and Greene and Outcalt 1985 is similar to that of Rumer and Yu (1978) but includes a term to account

for the flux of heat from the flowing water. In most of the models mentioned above, an arbitrary ice density, or the density of pure ice was used in the computation of change in ice thickness. In the one dimensional sea ice model of Maykut and Untersteiner (1971), the ice density could not be ignored due to the presence of brine in the ice. Ice density was determined from a relationship involving salinity and ice temperature which was influenced by the absorbed radiation. This permitted more realistic modelling of the change in ice thickness. Hibler (1979), Parkinson and Washington (1979) and others have constructed three dimensional ice models that includes the ice drift and deformation of the sea pack ice. These models are more complex and advanced than any of the lake ice models.

None of the models available can be applied easily to ice melt on small lakes. The three dimensional models are developed for large bodies of water and lack the spatial resolution required for small lakes for studying the interaction between the ice and the shoreline. The only two dimensional model is that developed for the border ice situation, but no provisions are included for ice movement. The one dimensional models do provide the basis upon which a spatial model can be developed for small lakes. Such models were originally meant for sea ice and the relevant parameters for lake ice do not exist or

are poorly defined.

2.6 Summary

Lake ice decay has received less attention than the decay of river and sea ice or lake ice during the growth period. Most observations of lake ice decay consist of qualitative descriptions and ice thickness measurements. Energy balance calculations and some process oriented studies have been carried out for specific sites, but many of the spatially important ice decay processes active on lakes have not been adequately examined. Available spatial decay models are applicable only for large lakes. Field observations are required to gain an understanding of the decay processes active smaller on lakes, to enable an appropriate model to be constructed, and to provide data to verify the model.

CHAPTER 3

STUDY AREA AND METHODS

3.1 Research Area

This study was carried out at Small Lake, about 5 km north of Resolute, Cornwallis Island, N.W.T. (Figs. 3.1 and 3.2). The area is underlain with palaeozoic rock and is in the Cornwallis Fold Belt on the southern edge of the Innuitian Region (Energy, Mines and Resources 1974, Bostock 1972).

The region has been glaciated at least once (Thorsteinsson 1958) but little is known about the detailed glacial history. Deglaciation occurred about 10,000 years B.P. followed by submergence. Emergence commenced approximately 9000 years ago (Washburn and Stuiver 1985). Marine shells are found at elevations of 150 m while the highest strand lines reach 105 m and possibly higher (Washburn and Stuiver 1985). Glacial action deprived many areas of a soil cover and the surface material is composed mainly of rock fragments and fine sands and silts. The parent material is till and locally-derived rock fragments but solifluction and cryoturbation have modified their original properties. Cruikshank (1971) classified the soils around Resolute

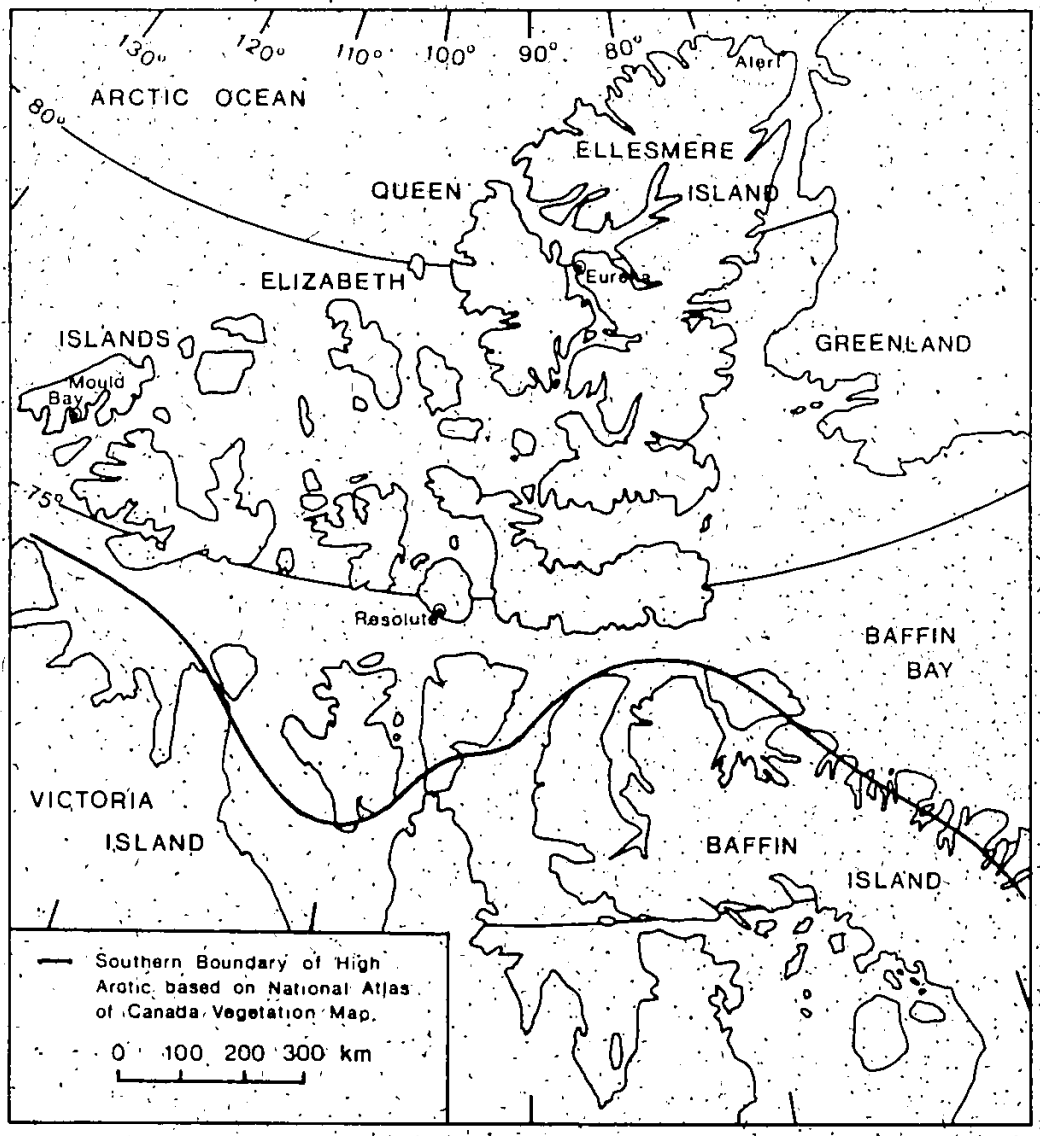

Figure 3.1. Location of the study site at Resolute on Cornwallis Island in the Canadian High Arctic. The southern limit of the High Arctic is determined by the tundra vegetation boundary.

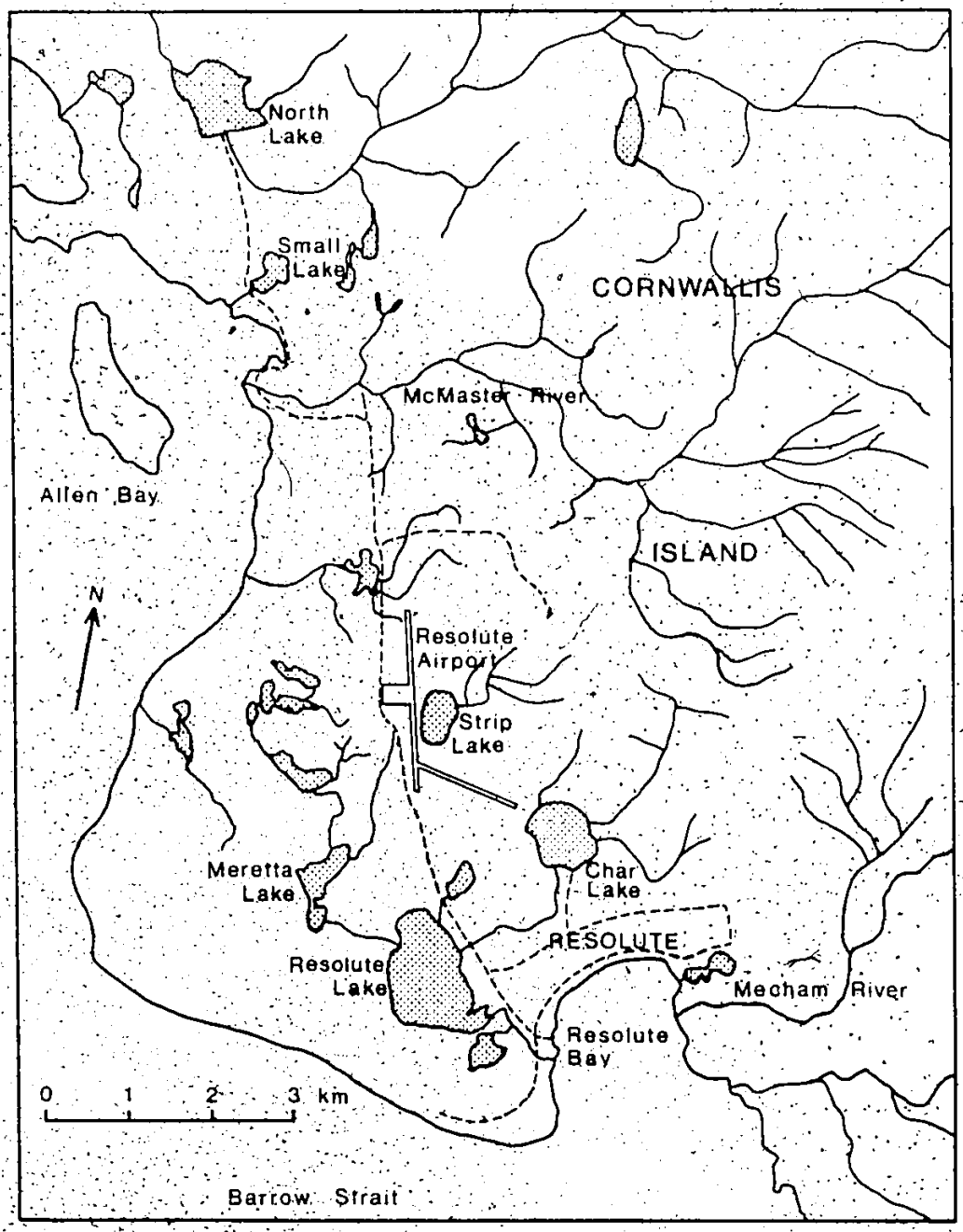

Figure 3.2. The study site at Small Lake, near Resolute, is one of a large number of lakes found along the coast of Cornwallis Island.

into three groups. Lithosols are composed of fragmented limestone and dolomite gravels located near the bedrock outcrops. The polar desert soils are very sparsely vegetated and consist of limestone and dolomite gravels in a sand and silt matrix. The fine grained tundra gleys with bog soils are restricted to slopes and depressions that remain wet all summer and are completely vegetated with black lichens, mosses, sedges and grasses. Due to the spatial domination of the polar desert soils and lack of vegetaion, Cornwallis Island lies in the High Arctic vegetation zone (Fig. 3.1) (Energy, Mines and Resources 1974).

This study area lies in the northwestern climatic zone of the Canadian Arctic (Maxwell 1980). Polar night with 24 hours of darkness lasts from November 4th to February 5th. By April 30th daylight lasts 24 hours and this continues until August 15th. This extreme radiation regime produces extremely low temperatures in winter. At Resolute Airport, the mean annual temperature is -13.5° C. (Fig. 3.3). Peak summer temperatures are generally below 10° C while winter temperatures reach -35° C. Mean daily temperature rises above 0° C on June 10th and falls below zero on August 24th. However, the air temperature can drop below zero on any day in the summer. The thermal regime produces approximately 300 thawing degree days and more than 6000

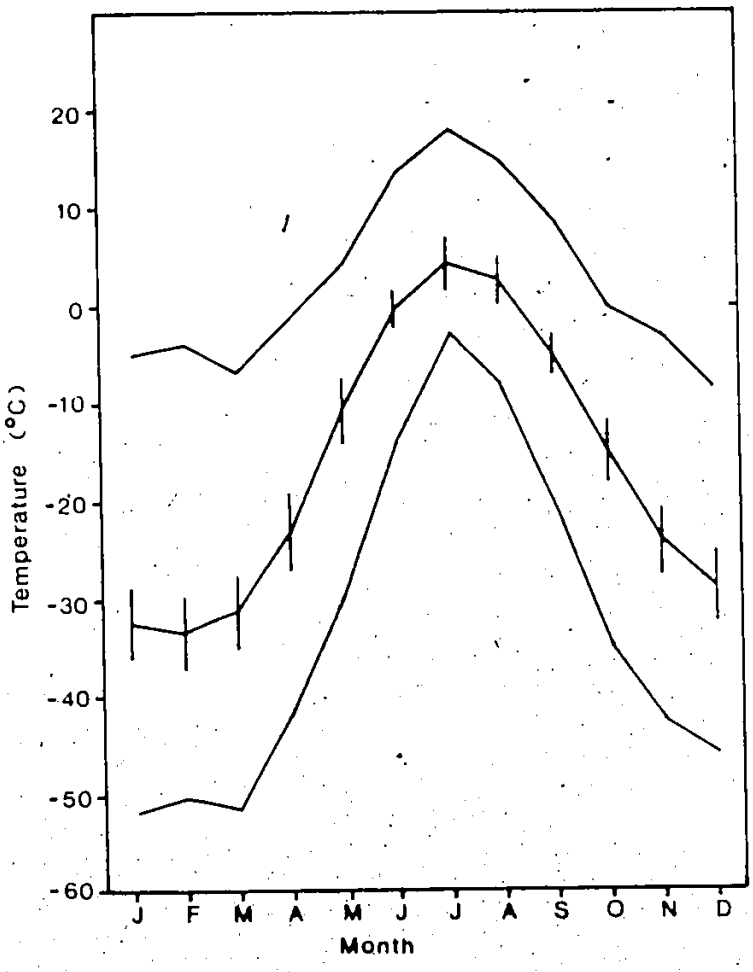

Figure 3.3. Mean monthly and extreme air temperatures for Resolute. The mean daily maximum and air temperatures for each month are indicated by the bars on the mean curve (after Maxwell 1980).

freezing degree days annually (Energy, Mines and Resources 1974).

Resolute has low precipitation with the weather station recording only 130 mm annually (Maxwell 1980). However, Woo et al (1983) have shown that the High Arctic weather stations greatly underestimate the snow received in the surrounding catchments due to the many blowing snow and trace precipitation events. A mean annual precipitation total of 180 to 210 mm is a more reasonable value. The monthly variation of precipitation is indicated in Fig. 3.4. The highest snowfall occurs in the spring and fall when atmospheric moisture is available, though snow can fall at any time of the year. The peak precipitation period is in the summer with rainfall being dominant, although it accounts for less than 20 percent of the total annual precipitation (Woo et al 1983). Drifting snow is common in the winter, producing an extremely uneven snowcover. Hilltops and exposed locations may be bare while the snowpacks of lee slopes and sheltered depressions are many metres thick (Woo et al 1983).

The predominant wind directions at Resolute are northwesterly and southeasterly, the latter being prevalent in the summer months. The least frequent wind direction is the southwest. The mean summer wind speed is 21 km/h (Maxwell 1980).

The cold climate favours the development and

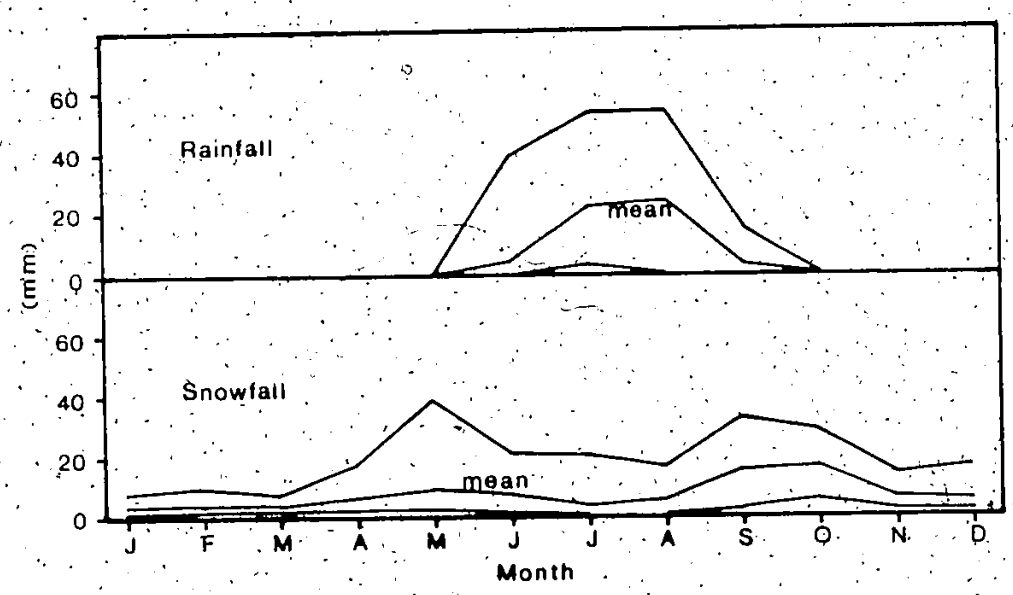

Figure 3.4. Annual variation in precipitation received at Resolute. The maximum and minimum monthly values are also plotted though the snowfall record is of uncertain accuracy (after Maxwell 1980).

maintenance of permafrost to great thickness. Based on ground temperature measurements down to 195 m, Meisner (1955) estimated the permafrost thickness to be 390 m (Fig. 3.5). The zero amplitude point is located at 19.2 m where the temperature is -12.6° C. The thickness of the active layer, in which thawing occurs, rarely exceeds 0.75 m in polar desert soils and 0.5 m in the tundra gleys.

While the High Arctic has less than 1 percent of its surface covered by standing water (Energy, Mines and Resources 1974), Cornwallis Island has many lakes along the coast. The location of most of these lakes are related to glacial action (Thorsteinsson 1958). The largest lake has an area of 6 km². The limnology of High Arctic lakes was established by an International Biological Project carried out at Char and Meretta Lakes, 1 km from Resolute Airport (Fig. 3.2) (Schindler et al 1974, Rigler 1974). Char Lake lies in the marine submergence zone and through isostatic uplift, it was separated from the sea about 5,300 years ago (Rigler 1975). Char Lake remained meromictic for several thousand years until the trapped sea water was flushed. At present, both Char and Meretta Lakes can be considered as cold monomictic lakes (Wetzel 1975).

The productivity and other aspects of the limnology of these lakes are strongly influenced by the lake ice

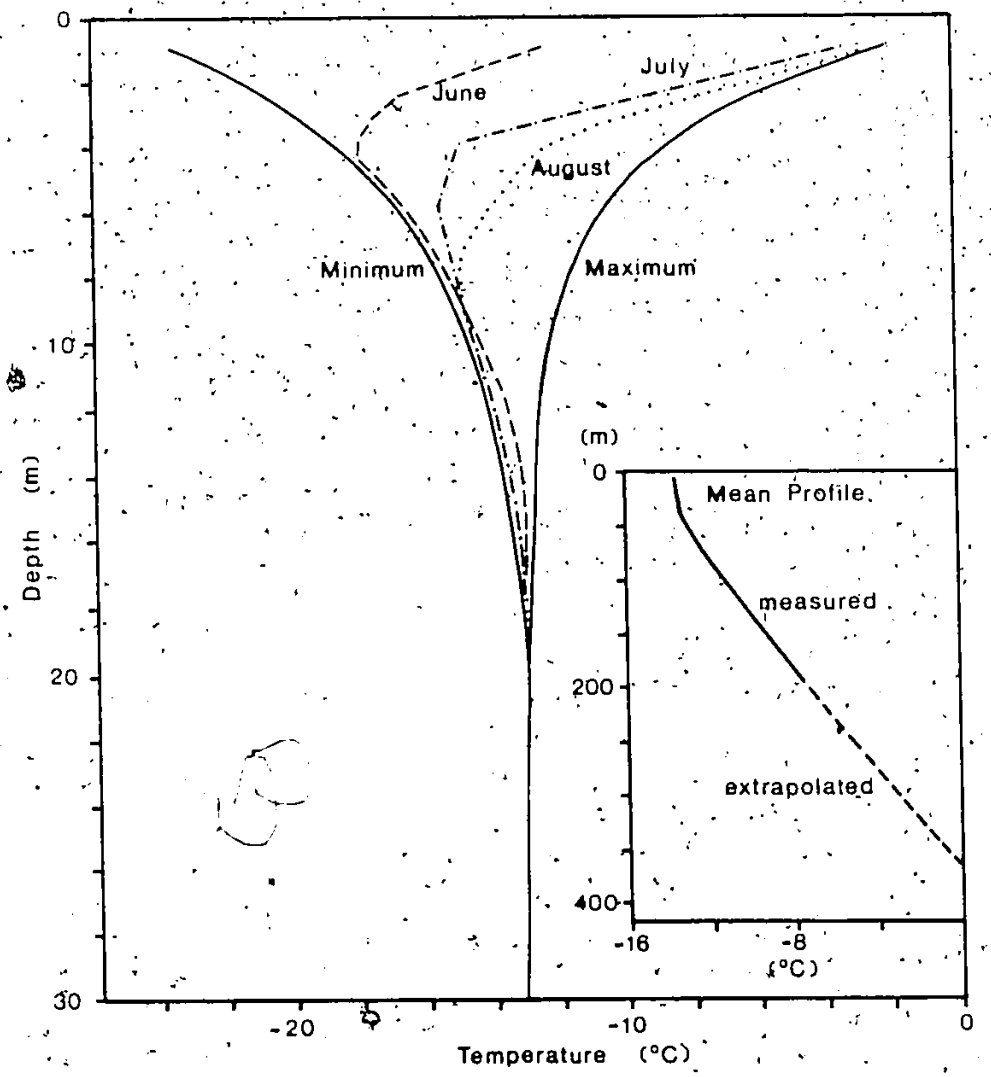

Figure 3.5. Ground temperature regime for Resolute. The monthly temperature profiles for June, July, and August are shown along with the annual maximum and minimum ground temperatures (after Meisener 1955, Cook 1958).

cover. Freeze-over of High Arctic lakes occurs in September (Fig.3.6) with the small, high altitude lakes freezing first and the large, coastal lakes freezing last. Changing weather patterns cause substantial year to year variations, but all the ice growth processes outlined by Adams (1976) are found on High Arctic lakes. However, the formation of black ice is the primary ice growth mechanism. The annual growth of ice on High Arctic lakes has been monitored only at Alert (Dumbell Lake) (Fig. 3.7) and Mould Bay (an un-named lake) for more than a decade. Ice thickness increases almost linearly for 7 months but the growth rate decreases rapidly near the end of the winter. The annual maximum ice thickness depends mainly upon the severity of the of the winter and the depth of snow upon the ice cover. In the Resolute area, snow-free lakes can have ice 2.4 m thick while others may have only 1.5 m of ice due to the insulating effect of snow. Ice melt begins in June or July after snowmelt has commenced and the duration of the decay period is typically 50 days. For some lakes, however, the ice cover melt may be incomplete in certain years. Dumbell Lake experiences complete decay only 25 percent of the time while on Resolute Lake, incomplete decay occurs less than 45 percent of the time (Allen 1977).

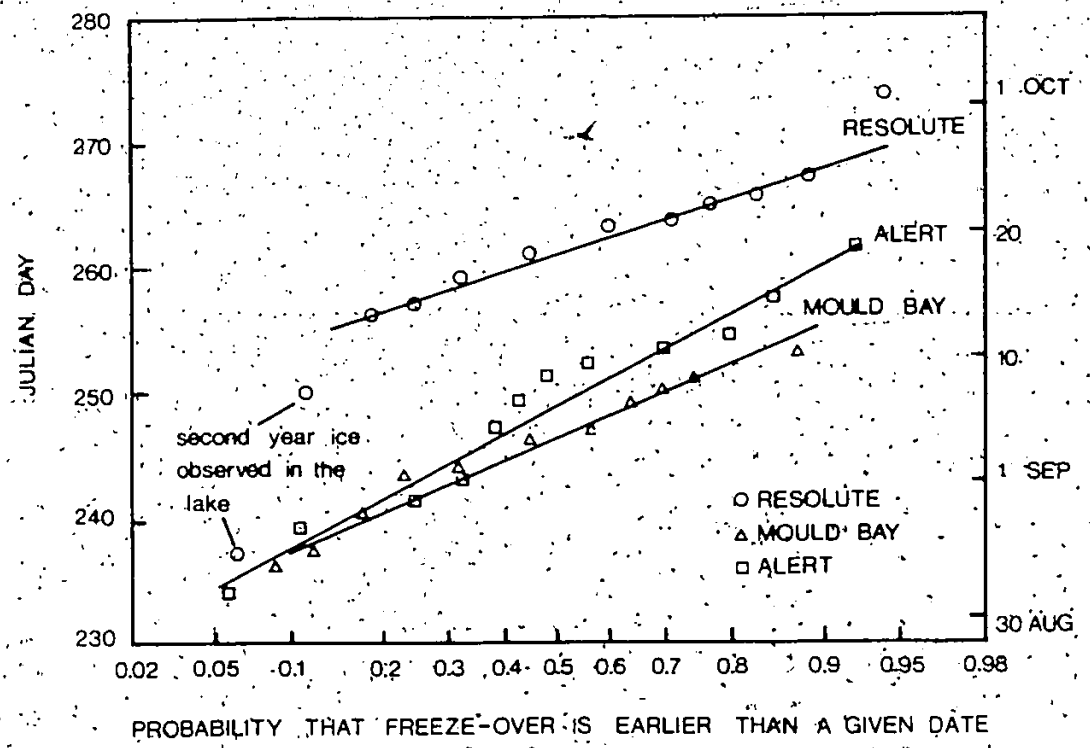

Figure 3.6. Exceedance probabilities for dates of freeze-over for three lakes in the High Arctic. The differences are due to variations in weather and the physical charactistics of each lake.

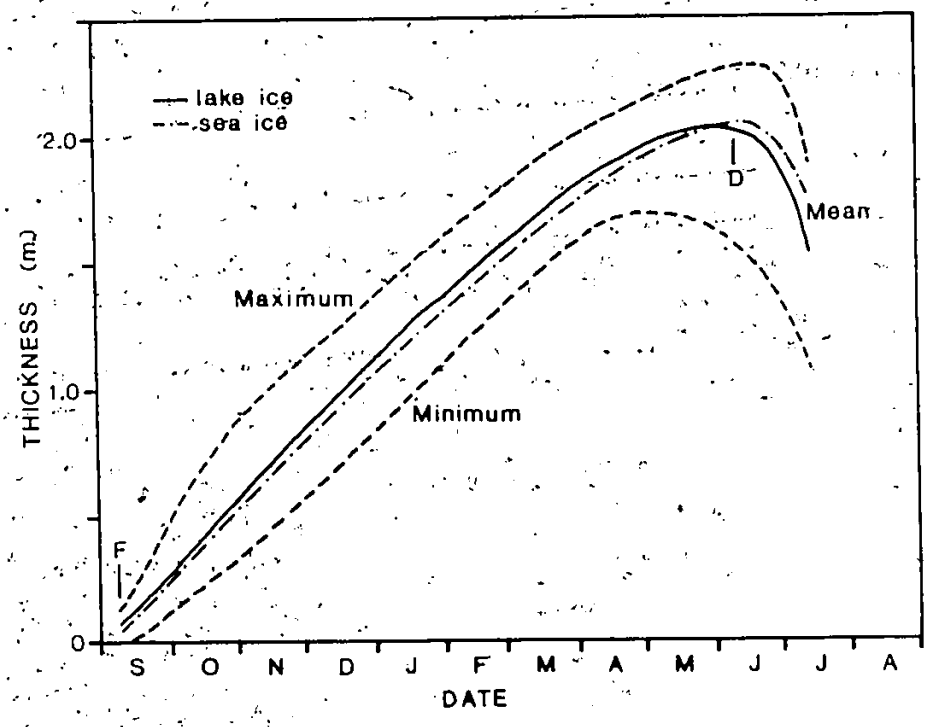

Figure 3.7. Annual growth of ice for Dumbell Lake, Alert. The maximum and minimum ice thicknesses are also given along with the mean ice thickness for a nearby sea ice site. The mean dates of freeze-over and first sign of deterioration are indicated by (F) and (D) respectively. (after Maxwell 1980).

3.2 Experimental Site

Small Lake, located in a dolomite basin, covers 0.15 km² and lies within a catchment of 1.5 km² (Fig 3.8). To the north and east of the lake is a steep slope associated with the Airport fault while on the southwestern side of the lake is the Allen Bay anticline (Thorsteinsson 1958). Radiocarbon dating for the Resolute area (Washburn and Stuiver 1985) indicates that the lake separated from the sea between 1500 and 3000 years ago and since then has cut an outlet channel through a low point in the Allen Bay anticline. At present, the lake water level is 5 m above sea level. The soils in the catchment are typical of the Resolute area. Polar soils, lithosols and rock outcrops account for 75 percent of the basin area while the tundra gleys and bog soils represent 13 percent. The remaining area is occupied by the lake and semi-permanent snow patches. Most of the boggy areas are located near the shore, yielding water to the lake throughout the summer.

The permafrost thickness under Small Lake is unknown. Using Resolute ground temperatures, Lachenbruch (1957) calculated that the permafrost thickness should decrease to approximately 200 m near the sea due to the moderating effect of the seawater (at -1.6° C). This is consistent with Judge's (1977) computations for the Truelove Lowland (Devon Island) where the permafrost

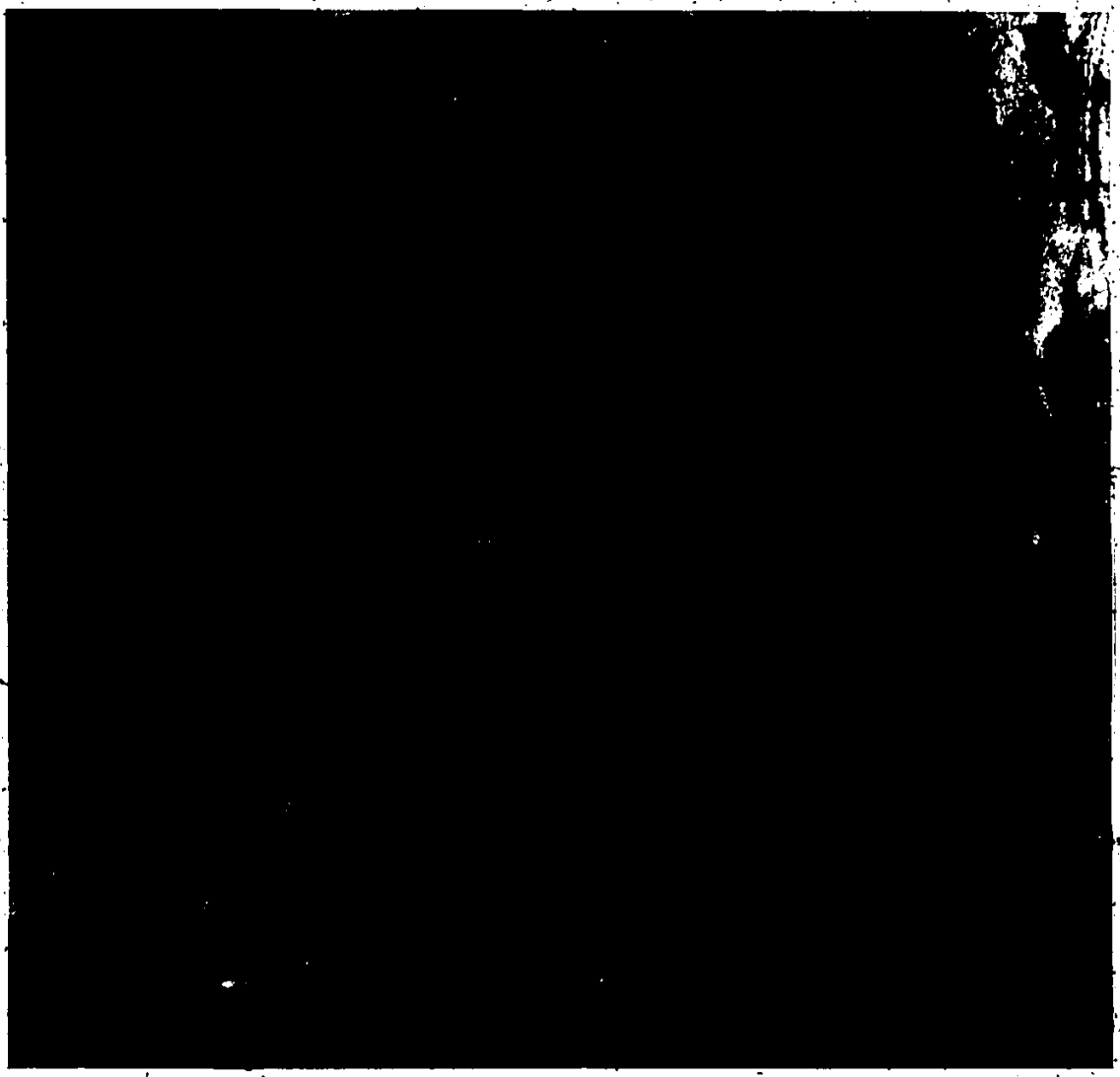

Figure 3.8. Small Lake catchment and topography. The dark areas near the lake and on low angle slopes are bog soils. The steep hill east of the lake is predominately rock with polar soils covering the remainder of the basin. The contour interval is 10 m.

reached 650 m beneath the inland plateau but thinning to approximately 220 m at the edge of the ocean. Isostatic rebound complicates the calculation (Taylor et al 1983) but the exact effect in the Resolute area is unknown.

Several aspects of the hydrology of Small Lake and its catchment have been examined by Woo (1980) and Woo et al (1981). The water balance for the catchment is shown in Fig. 3.9. One prominent feature is the considerable accumulation of snowmelt water in the lake during the melt season. This water is impounded by a snow drift which blocks the narrow outlet channel every year. The lake level usually rises for 3 to 4 weeks and then drains catastrophically (Fig. 3.10). There are no streams in the catchment but surface runoff is prevalent along the eastern shore. Surface flow peaks during snowmelt and declines as the ground thaws and subsurface flow increases (Fig. 3.10).

Small Lake has a maximum depth of 10.0 m (Fig. 3.11). An elongated reef isolates Gauge Bay from the main basin, but the interchange of water is not restricted by ice in the winter. Extensive shallows are found near Tent and Beach Bays but the rest of the lake has a steep shoreline.

3.3 Instrumentation and Methods

Figure 3.12 shows the main sites where measurements

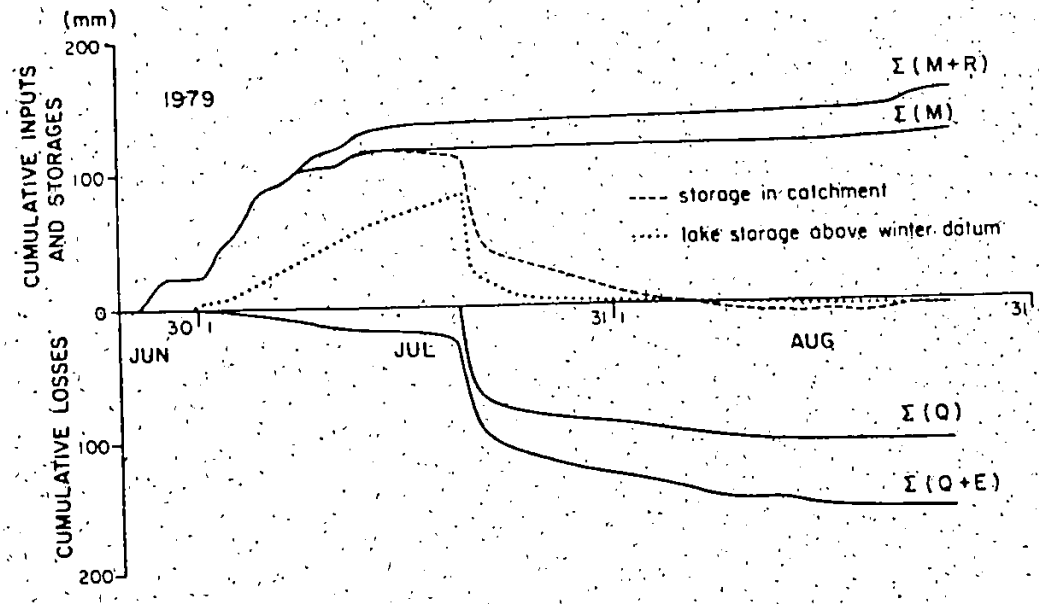

Figure 3.9. Water balance of Small Lake, 1979. M is the snowmelt water, R is precipitation, Q is lake discharge and E is evaporation (after Woo et al 1981).

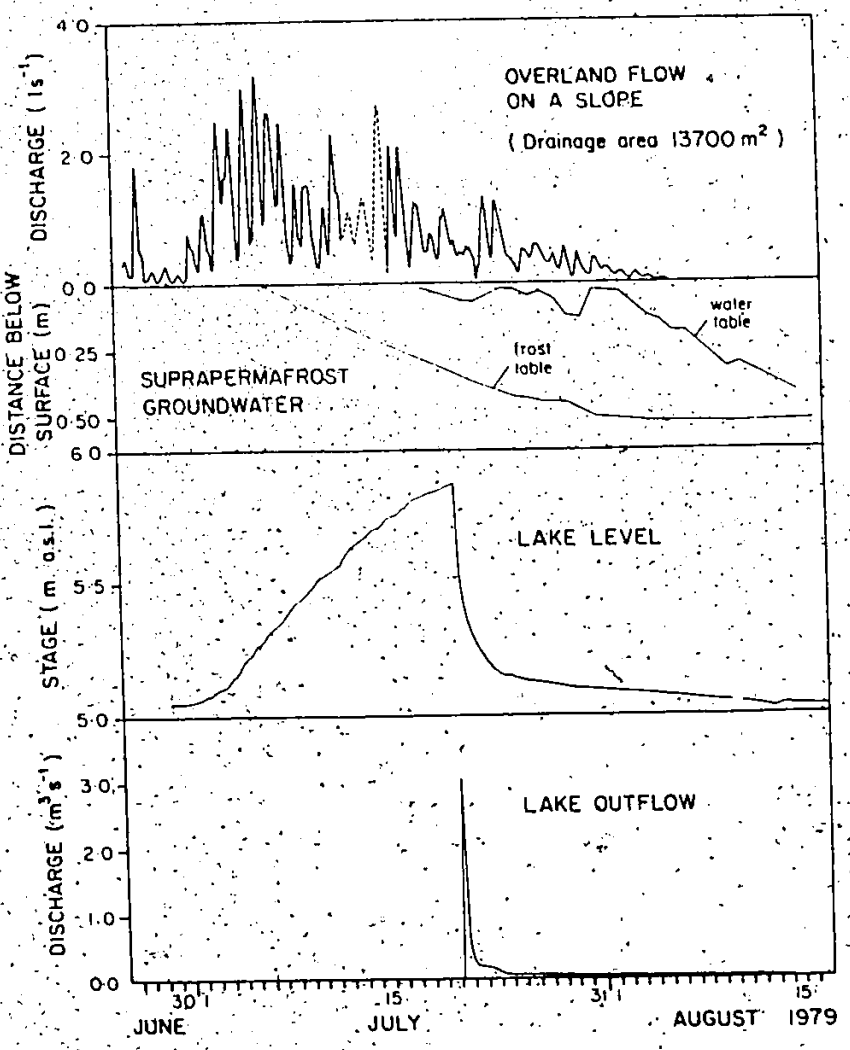

Figure 3.10. Hydrologic behaviour of Small Lake and its drainage basin during the summer (after Woo et al 1981)

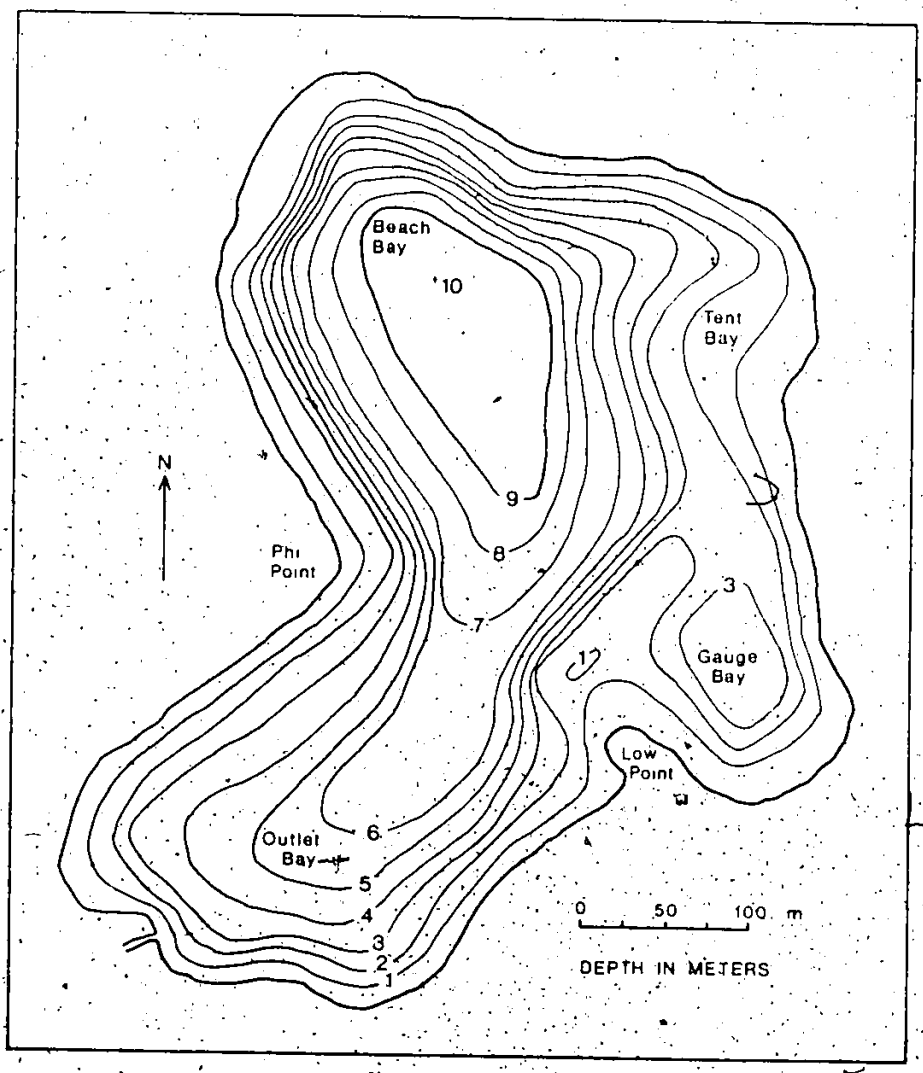

Figure 3.11. Small Lake bathymetry. All names, except Small Lake, are unofficial and are used for descriptive purposes only.

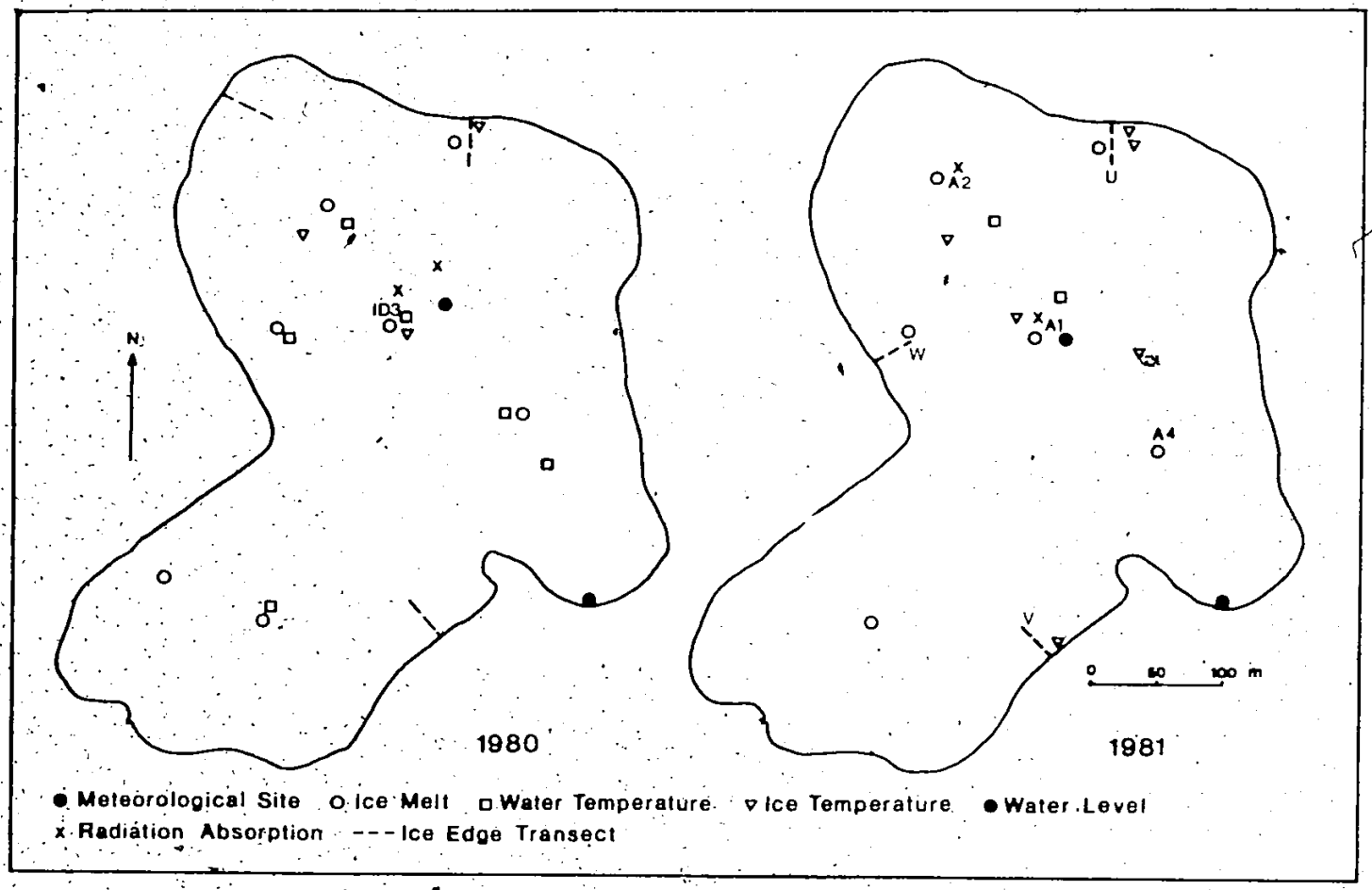

Figure 3.12 Main measurement sites on the Small Lake ice cover, 1980 and 1981. The more minor sites and the edge retreat locations have not been plotted due to short-term use and variable location.

were made at Small Lake for the two major study years. The most comprehensive data were collected at the main meteorological site where several variables were continuously recorded. Other sites were visited once a day for manual observations.

3.3.1 Weather Station Data

Since the Atmospheric Environment Service weather station at the Resolute Airport was close to the research site, many meteorological observations were not duplicated. The station data also provided back-up information to allow missing data for Small Lake to be estimated. The fluxes of total incident shortwave radiation, diffuse shortwave radiation, reflected shortwave radiation and net radiation over a gravel surface that were measured at the weather station are directly transferable to the study site. Other variables that could be used without major adjustments include precipitation, wind direction and cloud cover conditions and air pressure. Missing air temperature and wind speed data for the lake were estimated from the station data using equations derived by linearly regressing the lake and station data for the period when concurrent measurements were made at both sites. All of the above data were available on an hourly basis except precipitation which was six hourly.

3.3.2 Radiation

A Swissteco net radiometer was set up at the meteorological site on the ice and remained there throughout the melt period. A second net radiometer, when available, was moved to different locations on the ice surface to extend the spatial observations. The signals from both instruments were recorded on Rustrak recorders whose charts were coded on an hourly basis. Latimer (1971) suggests that these instruments have an error of 5 percent but given the error in the coding of the charts and the difficulty in keeping the sensors level on the melting ice, a more realistic error is 10 percent.

Shortwave radiation reflected by the ice was obtained by a Kipp and Zonen CM5 pyranometer whose signals were recorded on a Rustrak strip chart recorder. The hourly albedo of the ice surface was obtained using the total incident shortwave radiation from the weather station and the reflected shortwave radiation from the ice. The incoming shortwave radiation received at the lake and at the weather station did not correspond exactly because of the chart timing errors at Small Lake and the slightly different cloud coverage over both sites. A more accurate albedo was obtained once each day when the pyranometer was used to manually measure the incoming and reflected shortwave radiation sequentially. The manual

albedo survey was done near solar noon to minimize levelling errors and a digital multimeter was used to read the output. All the radiometers were strongly affected by low solar elevations that occurred at the early and late hours of the day. The difficulty in maintaining a level sensor compounded the inherent sensor errors at low sun angles (Latimer 1971).

3.3.3 Radiation Attenuation

The attenuation of radiation within the ice cover was measured using Phillips photocells. These sensors have a 180 degree field of view and spectral peak of 615 nm with 60 percent of the absorbed radiation falling between 510 and 710 nm. Sensors were placed under the ice at two ice ablation locations and remained throughout the melt period. Other sensors were installed in the ice above the hydrostatic water level. Coupled with incident radiation measured using a photocell and an albedo measurement, the radiation absorbed in the ice layer can be determined.

3.3.4 Air Temperature and Humidity

Air temperature and relative humidity were obtained using a Weathermeasure hygrothermograph housed in a Stevenson screen located 1 m above the ice. Temperature records were calibrated daily with a mercury thermometer and the resulting error was approximately 0.2° C.

Relative humidity was checked against daily measurements obtained using an Assman psychrometer. The error was approximately 5 percent. From these data, the vapour pressure was obtained using the empirical equations given by Dilley (1968).

3.3.5 Water Temperature and Specific Conductance

The temperature of the lake water was measured by Fenwal thermistors read with a Beckman digital multimeter. These have an accuracy of 0.2° C. In 1979, a single thermistor bead was lowered to different depths to obtain the water temperature profile for Small Lake. This was replaced by a thermistor array with measurement levels of 0, 0.1, 0.25, 1, 2, 3, 4, 6, and 7 m above the lake bottom. In addition, a thermistor array with sensors at 0, 0.01, 0.02, 0.05, 0.2, 0.5, 0.75, 1.0, 1.5, 2.0, 3.0 and 4.0 m below the water interface was lowered through a hole in the ice. Since it is difficult to locate the exact position of the ice-water interface, additional thermistors at -0.01, -0.02, -0.03 and -0.04 m were used to provide detailed temperature data in this interface zone. In 1981, a styrofoam float with thermistors at distances of 0, 0.005, 0.01, 0.02, 0.03, 0.05, 0.10, 0.20, 0.30, and 0.40 m below the ice-water interface were installed under the ice for an extended period to minimize the influence of the hole through the ice. When water

temperature in the open water was required, a float with a submerged thermistor was used.

Specific conductance (electrical conductivity) of the water was measured to gain some knowledge of the structure and movement of the water beneath the ice cover. This was obtained with a YSI plastic probe measured with a Beckman conductivity bridge. The probe was lowered to various depths where the water temperature was known.

3.3.6 Ice, Snow and Soil Temperatures

Ice and soil temperatures were also measured with Fenwal thermistors. For floating ice, thermistors were emplaced at 0, 0.4, 0.8, 1.2, 1.6, and 2.0 m below the ice surface. For bottom-fast ice, five thermistors were set into the ice. These were located near other thermistor arrays that had been set in the lake bed in the previous fall at depths of -0.1, 0, 0.1, 0.2, 0.3 m beneath the interface. All of the thermistor arrays melted out before the ice became isothermal due to the absorption of radiation by the sensors and wire.

Snow temperatures were measured at various depths near the basal ice study site and at some of the other ice temperature sites.

3.3.7 Wind Speed and Direction

Wind speed was measured with a Cassella sensitive

cup anemometer at 1 m above the ice surface and recorded on a Rustrak event recorder. The combined error of the sensor, the recorder and coding is probably less than 10 percent. To obtain the surface roughness of the ice cover, additional non-recording anemometers were periodically set between 0.25 and 2.5 m to obtain a wind speed profile. A set of six Bradley sensitive anemometers was used briefly in 1981 to obtain additional wind speed profiles to calculate the surface roughness. Wind direction was manually observed once each day as a check on the weather station data.

3.3.8 Precipitation

Rainfall was measured at one or more manual gauges in the Small Lake catchment. A more detailed precipitation record was obtained from the weather station.

3.3.9 Snow and Ice Surveys

The premelt snow cover on Small Lake was surveyed each year. In 1979 and 1980, snow depths and densities were obtained along transects that were part of the main catchment snow survey. In 1981, a more detailed survey was conducted along a regular grid on the lake. Snow depths obtained at various ice temperature and ice thickness measurement sites were also incorporated. In addition to measurements on the survey grid, ice thickness was also

determined whenever instruments and sensors were installed in the ice. Other ice thickness measurements were obtained under a wide range of snow depths.

3.3.10 Ice Ablation and Accretion

Basal ice in a snowpack is produced when snowmelt water refreezes on a cold substrate (Marsh and Woo 1984). On Small Lake, its growth was monitored at a site by probing from a reference datum, through the snow until the ice was reached. Its spatial extent was found by removing the snow at many locations and determining the basal ice thickness. Snow ablation was measured at the thermistor and ice ablation sites in 1979 and 1980 and at a more accurate snow ablation site on land using the method described in Heron and Woo (1978).

Ice ablation was measured at about 7 sites on the lake. The measurement device, based on the design of Ramseier and Weaver (1975), consists of a metal tube hung beneath the ice on 2 resistance wires. The wires could be heated (if necessary to release the wires from the ice) from a 12 Volt battery connected to the ends of the wires to complete the circuit. The whole assembly was then raised until the tube reached the ice bottom. A change in ice thickness was determined by noting the change in the distance between the handle and the ice surface. Since the ice surface was uneven at times and there was usually some

local disturbance, the ice surface was taken to be the bottom of a long board (about 2 m) laid on the ice. Measurement accuracy is about +/- 5 mm and is dependent upon the consistent placing of the board and the roughness of the ice.

Surface ablation of the ice cover was obtained using stakes embedded in the ice adjacent to the ice thickness devices. The board again provided the surface reference and ice loss was determined from the change in stake height. In 1979, white wooden stakes (30 mm diameter) were used. These melted out quickly, requiring frequent resetting so that a fixed datum could not be assured. In 1980, plexiglass collars were added to the white stakes with some improvement. In 1981, plexiglass tubes with collars were successfully used. After more than 1 m of surface ablation, the cumulative error was approximately +/- 10 mm. The amount of melt at the ice bottom is computed as the difference between the ice thickness change and the amount of surface ablation. As a residual term, it inherits the errors of the other measurements, and meaningful results could be obtained only from longterm measurements or when melt rates were high.

The hydrostatic water level of the ice cover was also measured at the ice ablation sites. In 1981, it was measured inside the plexiglass tube and before that it was

obtained from a hole near the ablation stake.

3.3.11 Ice Density

A change in ice density within the ice indicates the amount of internal melt. Several methods were attempted to determine ice density. Ice cores were removed from the ice cover with a 3 inch diameter CRREL corer, weighed and the volume determined by measurement. This method has an error of approximately 50 kg/m³. However, the ice fractured into small pieces easily and usable cores were rare. The second method used a wood chisel to chip out a pit in the ice surface measuring approximately 0.1 m X 0.1 m in area. The ice fragments were weighed periodically using a spring balance and the volume of ice determined from the dimensions of the pit. This information permitted an ice density profile to be constructed for the site. This method was practical only after the ice crystal boundaries had melted and while the ice surface was still relatively smooth, thus limiting it to the first few weeks of melt. The profile depths were usually limited to less than 0.2 m, after which the hydrostatic water level was reached and the control of the pit volume deteriorated. The accuracy of this method was also about 50 kg/m³.

3.3.12 Ice Edge Behaviour

The development of a moat along the edge of the lake can be divided into two phases, when the ice edge is frozen to the lake bed and when it floats freely. In the first period, up to 5 transects were set up to monitor the changing moat width and the rate of ice melt (Fig. 3.12). In 1980, the points were surveyed, but in 1981, stakes were used to indicate the measurement points. When the ice edge floated free, reference stakes were set up around the edge of the ice cover and the distance to the edge was measured. At these referente points, the ice edge thickness was also obtained.

The above information, combined with triangulation to obtain the ice movement, and oblique photographs from the top of the hill beside the lake permitted maps of the ice cover extent to be drawn.

3.3.13 Water Level

The level of the lake was measured using a Leupold-Stevens type F recorder resting on a stilling well located in the shallow part of Gauge Bay (Fig. 3.12). Water level was also read daily off a staff and both records were tied to a bench mark.

CHAPTER 4

STUDY PERIOD

The ice decay processes on Small Lake were observed in detail for three years. The data used in this study were obtained almost exclusively from the field seasons of 1980 and 1981, since the data from the reconnaissance year, 1979, were incomplete. The 1979 data, whenever usable, were also included. This chapter describes the meteorological, lake ice and water conditions during the decay period and provides a qualitative discussion decay processes. Information given here will serve as background to the models developed in subsequent chapters.

4.1 Meteorological Conditions

Meteorological variables were measured at Small Lake and by the Resolute Airport weather station. Some data from the weather station, such as solar radiation, could be transferred directly to Small Lake. Other data, such as wind speed and air pressure required adjustment based on regression relationships or physical laws. All the weather station data reported in the following sections have been adjusted and are compatible with the data obtained at Small Lake.

4.1.1 Air Temperature and Relative Humidity

In the weeks before snowmelt began, the air temperature was typically -5 to -10° C. Temperatures rose slowly until the mid-day values exceeded the freezing point for several hours. There was minimal snowmelt at this time since refreezing occurred at night, limiting snowmelt to only a few hours each day. Such conditions lasted only several days. After this, the air temperature tended to remain above 0° C for the rest of the melt period. As Figs. 4.1 and 4.2 indicate, air temperature occasionally fell below freezing during the night, but continuous daylight minimized the nocturnal heat loss and the diurnal temperature range. The only exception observed during the period of study occurred in late July 1980 when the area was under the influence of a cold air mass for several days, leaving a thin veneer of snow on the ice. The air temperature increased after the melt began, partly because of the heating from the ground laid bare by melt. The maximum temperatures rarely exceeded 10° C. Temperature fluctuated considerably during the day depending on whether the wind was blowing onshore from the cold sea ice or from the warmer bare ground.

The relative humidity varied between 60 and 95 percent throughout the study period although 100 percent humidity could be reached on cool, foggy days. The

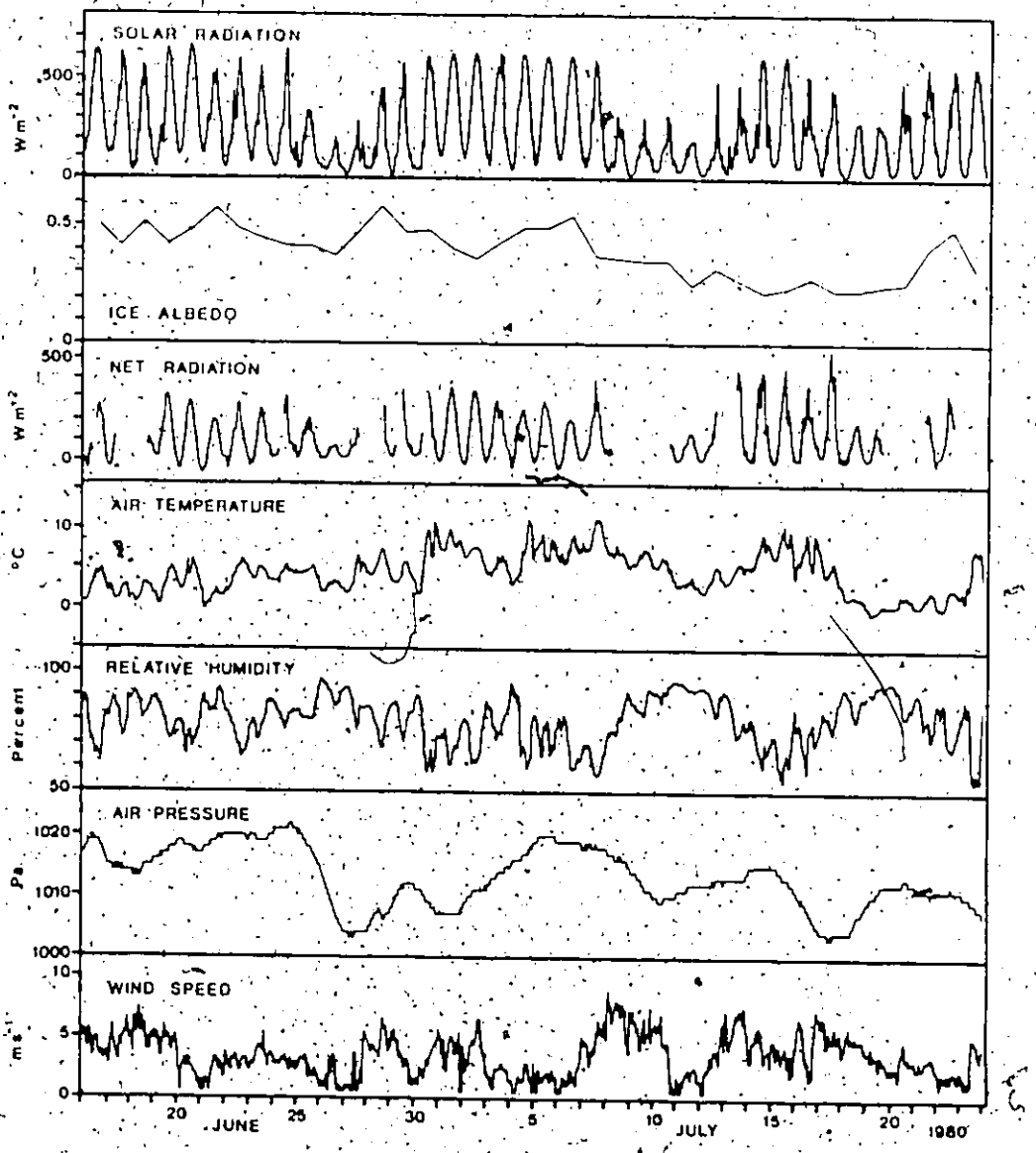

Figure 4.1. Meteorological conditions at Small Lake during ice decay, 1980.

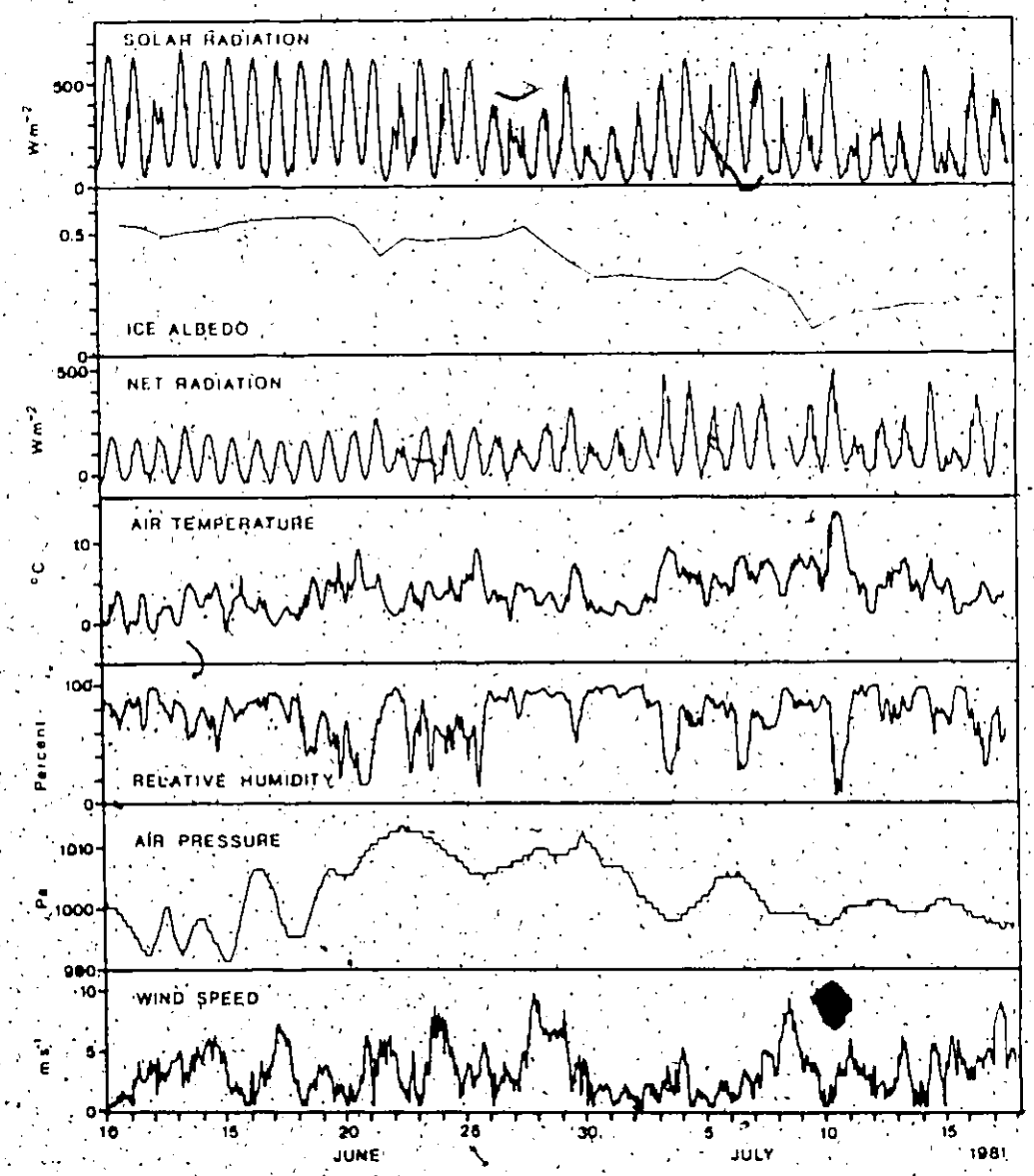

Figure 4.2. Meteorological conditions at Small Lake during ice decay, 1981.

fluctuations in relative humidity showed an inverse pattern with air temperature.

4.1.2 Radiation

The radiation balance of the ice surface (Figs. 4.1 and 4.2) is controlled primarily by the incident solar radiation and hence displays a diurnal cycle. The size of these diurnal cycles tended to increase thoughout the melt season relative to the shortwave radiation. This was due to the decrease in ice albedo which resulted in more absorbed shortwave radiation despite a decrease in incident solar radiation after the summer solstice. Occasionally, the net radiation exceeded the incident solar radiation when the ice albedo was very low. This phenomenon was rare, but indicated that the net longwave radiation was a radiation source during this period. Such events were limited to warm, foggy days. At the beginning of the melt season, net radiation fell below zero for only a short period each day when the solar elevation was low. As melt advanced, the net radiation was usually positive for all 24 hours.

4.1.3 Wind Speed

Longterm variations in wind speed observed at Small Lake were related to the movement of air masses in the region. Diurnal cycles in wind speed were also evident on

a number of days (Figs. 4.1 and 4.2). Wind speed averaged 5 m/s, but peak wind speeds of 10 m/s were reached on several occasions. Periods of dead calm were not common and were short lived.

4.1.4 Precipitation

Precipitation throughout the study period was minimal, with 24 mm in 1980 and 22 mm in 1981. Most of this occurred as rain, but a trace amount of snow fell late in 1980. Maximum daily rainfall was 8 mm, but there were many foggy days that produced trace precipitation events.

4.2 Lake Water Conditions

4.2.1 Lake Water Levels

Like many other lakes in the Resolute area, the outlet of Small Lake was snow-dammed for part of the melt season. Drifting snow during the winter filled in the outflow channel as indicated in Fig. 4.3. This prevented discharge of the lake water, causing the lake level to rise. As shown on Fig. 4.3, the pattern of water level change was similar each year, though the maximum water level attained was different. The water input was from snowmelt in the drainage basin and the diurnal variation was reflected in the rising limb of the lake hydrograph (Fig. 3.10). The maximum level of the lake was determined

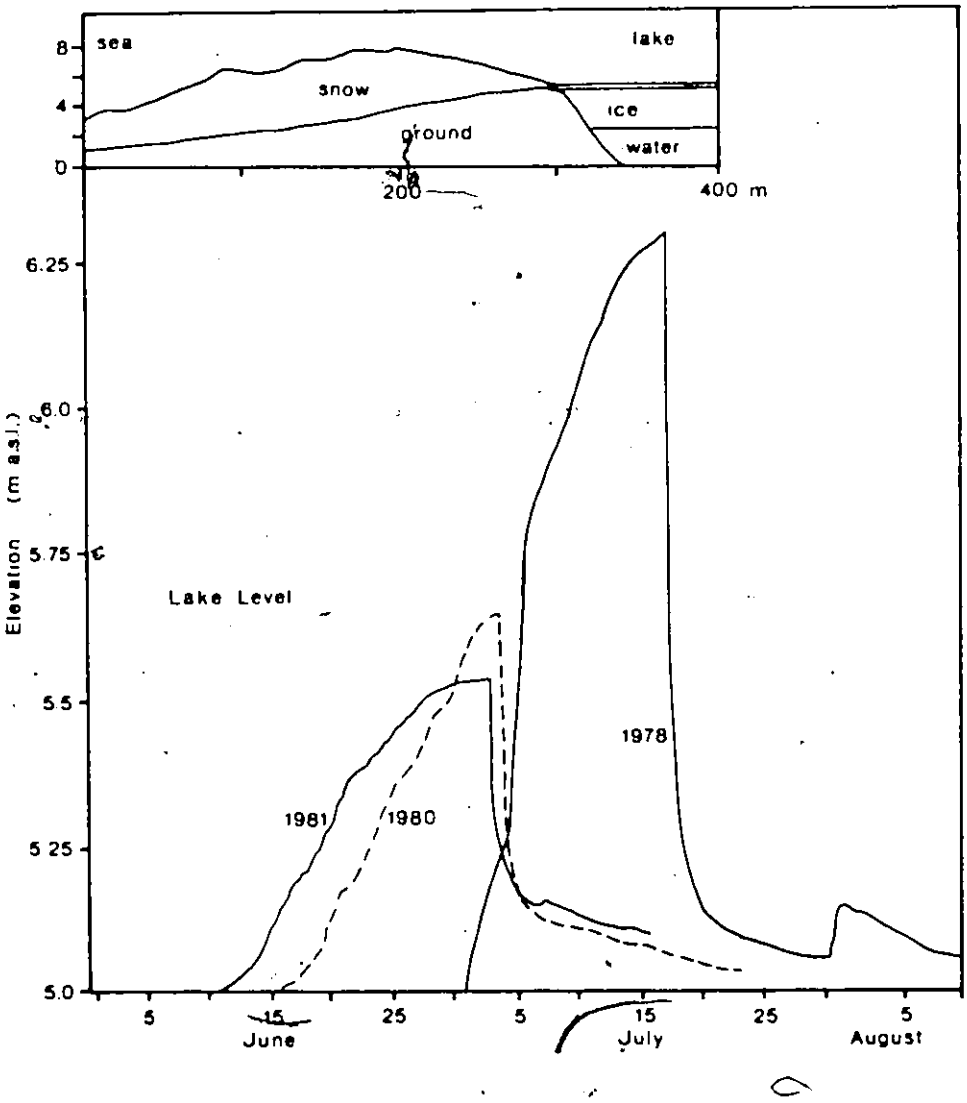

Figure 4.3. Small Lake water levels for the study periods in 1980 and 1981. The 1978 peak was the highest lake level recorded from 1977 to 1981. The inset is a cross section down the outlet channel from Small Lake to Allen Bay indicating the height and extent of the snow blocking the channel.

by the rate of snowmelt, the amount of snow in the catchment and the height of the snow dam. In 1978, a heavy snowcover combined with a rapid melt produced the largest known lake level rise of 1.3 m. In 1981, one of the smallest lake level increases of 0.5 m occurred due to a lack of snow (Fig. 4.3). When the water level reached the top of the snow dam, drainage of the ponded water was rapid and the lake water level dropped quickly toward the summer level (Fig. 3.10). The lake level remained relatively low for the rest of the summer.

4.2.2 Lake Water Temperature and Specific Conductance

The annual water temperature regime for High Arctic lakes has been described by Schindler et al (1974). The thermal conditions and specific conductance observed in Small Lake during the melt period (Fig. 4.4) are similar to those for Char Lake. Before any melt began, the water column was warmed by radiant energy penetrating through the partially snow covered ice. When melt began, the bulk of the lake water was above 3° C. Between depths of 3 to 8 m, the water was both isothermal and isoconductive due to the active vertical mixing. A layer of cool, stable water was located immediately under the ice cover and a second layer of warmer water was found above the lake bottom.

The melting of snow and ice yielded a layer of low

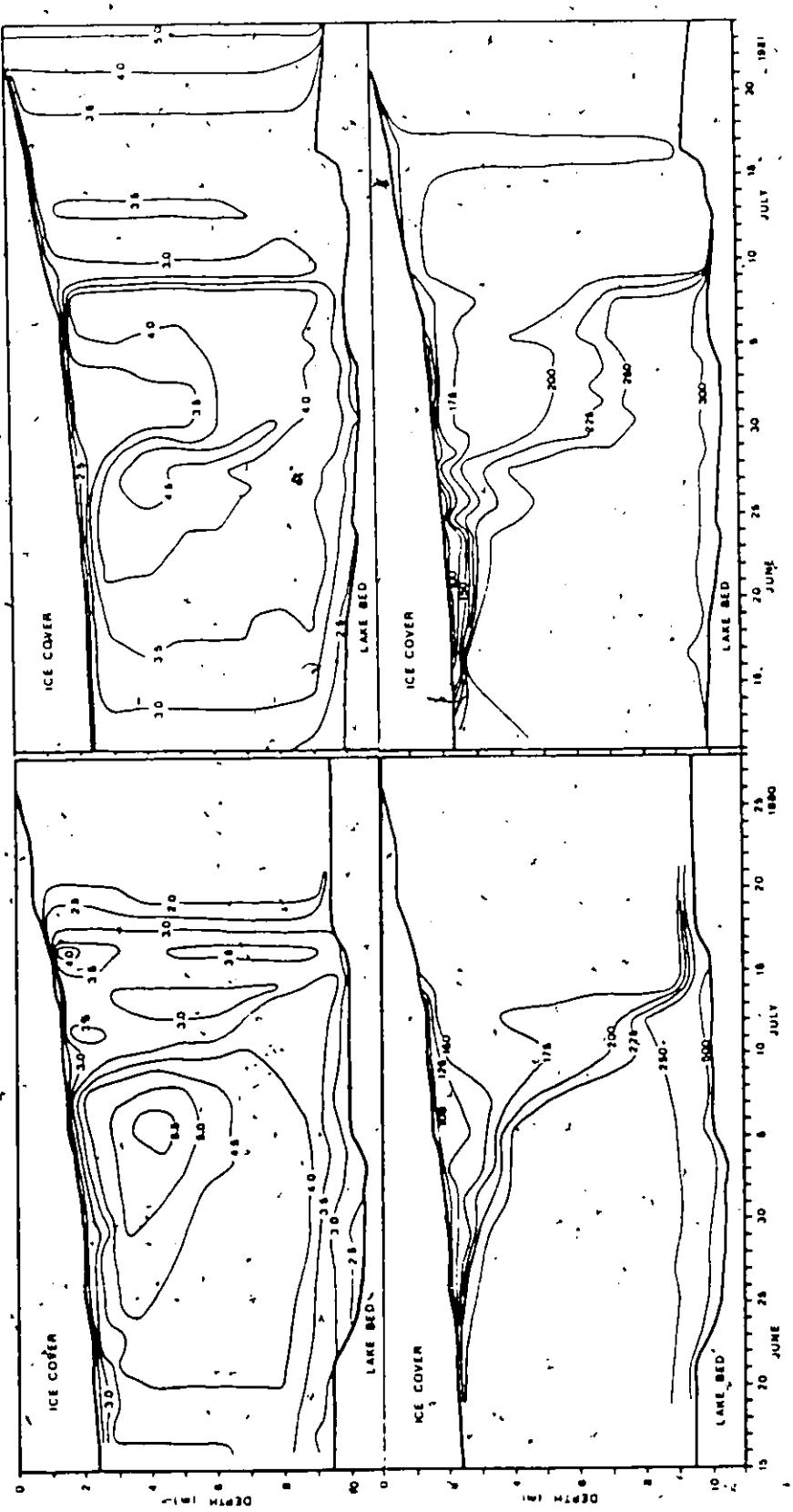

Figure 4.4. Small Lake water temperature (C) (upper) and specific conductance ($\mu S/cm^{-1}$ at 25 C) (lower) in 1980 and 1981. The uneven lake bottom is a result of the changing lake levels combined with ice drift.

specific conductance water immediately beneath the ice cover. This layer was even more stable due the lack of dissolved solids and continued to thicken as melt continued. The presence of this stable layer profoundly influenced the subsequent development of the water temperature profile. As radiant heating of the water intensified and as more inflow of warm, low specific conductance water entered the lake from basin snowmelt, a wedge of warm water with temperatures above 4.0° C developed at the boundary of the cold water beneath the ice and the warmer isothermal water. The zone of maximum water temperature then extended downward gradually after vertical mixing began. More thorough mixing occurred toward the end of the melt period when the wind-induced circulation in the open water around the floating ice cover eliminated the specific conductance and temperature stratification. A layer of cool water remained under the ice until the ice cover was melted completely. The lake water temperatures then rose above 4° C due to radiant heating and wind-induced mixing in all parts of the profile except near the lake bottom where heat was being conducted from the water into the lake bed.

Of particular importance to the melting of the ice cover is the temperature of the layer of water immediately beneath the ice. As shown in Fig. 4.5, there was a large water temperature gradient within 0.05 m beneath the ice.

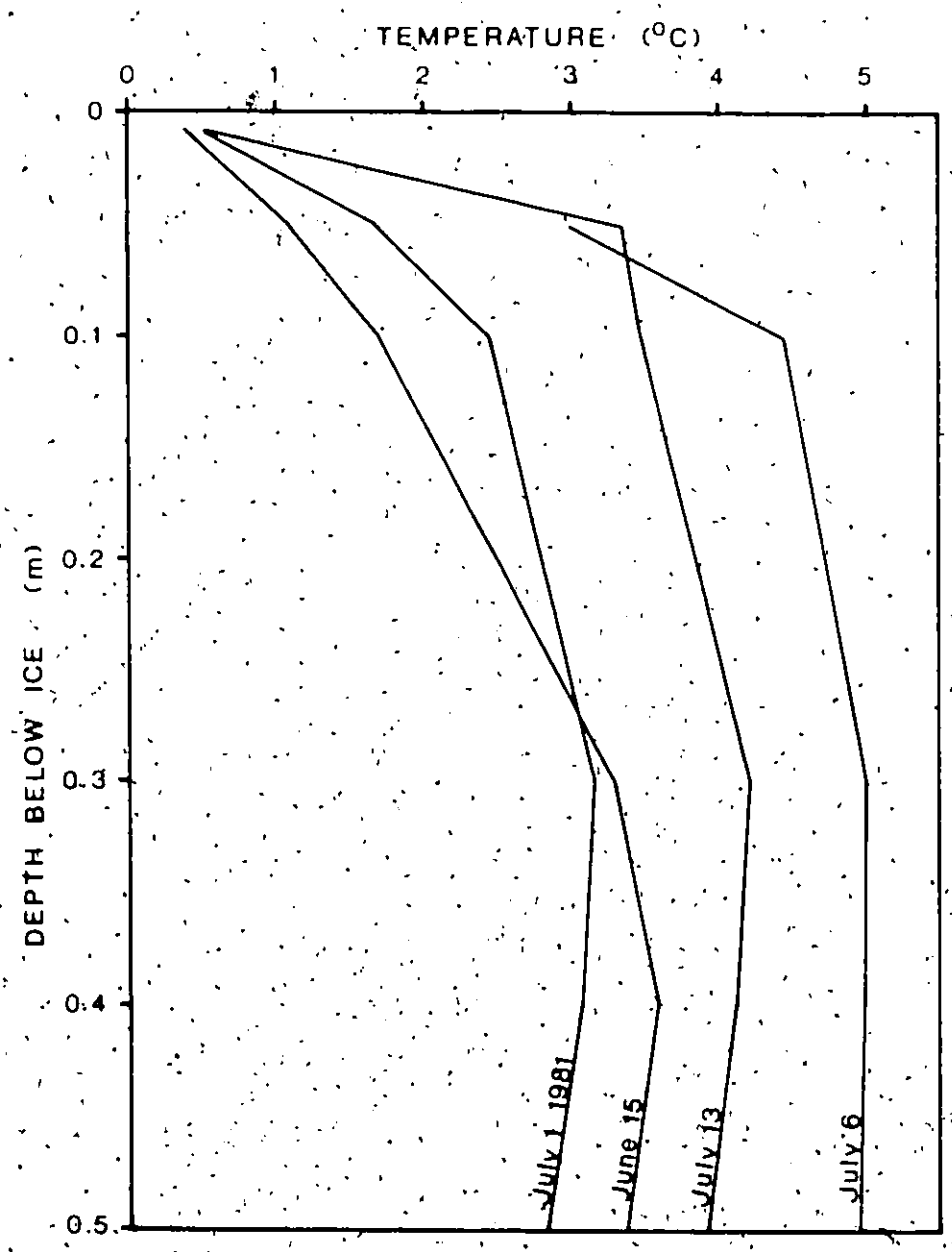

Figure 4.5. Selected water temperature profiles from immediately beneath the ice cover, 1981.

It was not possible to obtain a water temperature of 0° C at the ice-water interface due to 1) radiant heating of the sensors in spite of attempts to shield them and 2) the large size of the thermistor relative to the thermal gradient. When a string of thermistors was lowered through a hole in the ice, this problem was further complicated by the effect of the hole on the thermal structure. As a result, the temperatures close to the ice are probably overestimated (Swinzow 1961). The water temperatures at a depth of 0.05 m are not as severely affected by the above problems and they were used to compute the water heat flux.

The variation of the water temperature 0.05 m below the ice in 1980 and 1981 is indicated in Fig. 4.6. Temperature fluctuated between 0.5 and 3.3° C. The marked increase in water temperature that occurred midway through the melt period in both years can be attributed the increased radiant energy that penetrated the ice and warmed the water as the ice thickness diminished.

4.3 Lake Ice Cover Conditions

4.3.1 Premelt Conditions

4.3.1.1 Snowcover

Surveys of the snow cover in the Small Lake catchment and on the lake ice cover were carried out immediately before the beginning of melt. The results of

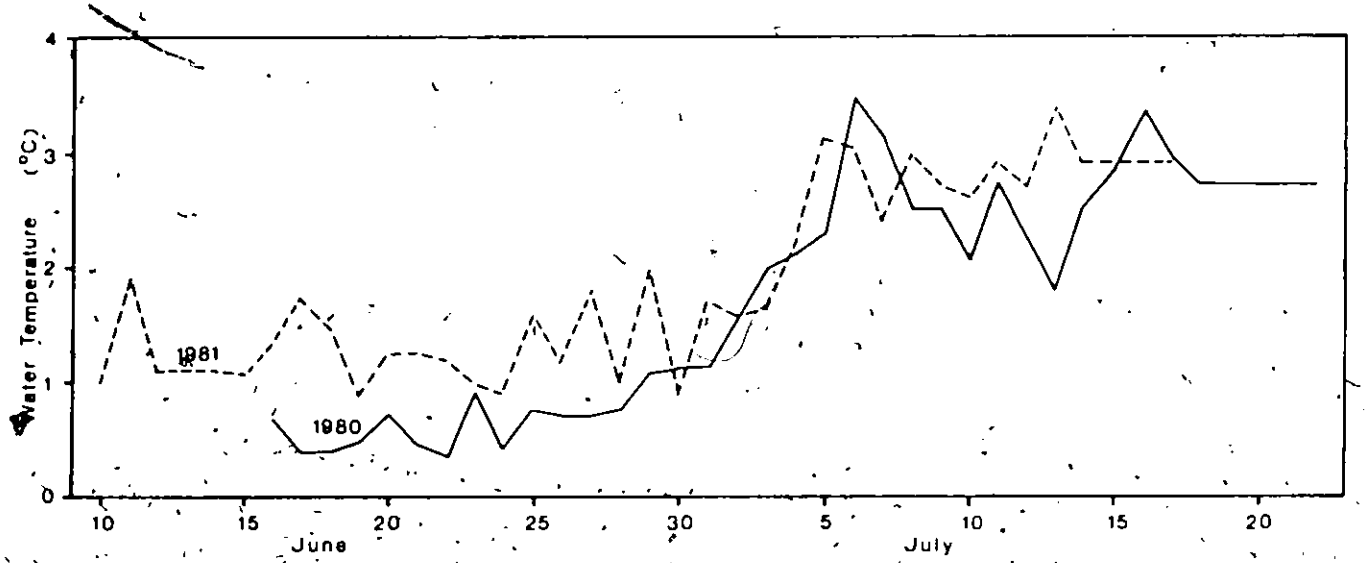

Figure 4.6. Water temperature at a depth of 0.05 m below the bottom of the ice cover for 1980 and 1981.

these surveys for 1980 and 1981, shown in Figs. 4.7 and 4.8 are typical of all the years in which the snow cover was examined. The central part of the lake usually had a thin cover of 0.1 m or less while the edges of the lake maintained a deep snowpack of up to 1.5 m. This distribution of snow was produced by wind scour and subsequent deposition. Scouring action was most evident on those lakes in the Resolute area with a large hill along one side of the lake (eg. Small, North, Tern, and Char Lakes). Lakes found in basins of relatively uniform topography (eg. Resolute and Meretta Lakes) had a deeper, more uniform snowcover of approximately 0.5 m. The large drifts at the edge of Small Lake are due to steep shorelines, especially along the western shore, which trap and hold drifting snow. Minimal edge effect was found along the southeast shore which is low. While Fig. 4.7 and 4.8 indicate a complete snowcover, in detail, this is not the case. In 1980, the central part of the lake where the ice was wind scoured was 25 percent snow-free and in 1981 the corresponding value was 10 percent. However, in 1978, there was no bare ice. These snow-free patches were irregular and too small to be mapped at the scale of the maps shown in Figs. 4.7 and 4.8.

4.3.1.2 Ice Thickness

Ice thickness was measured for two to four weeks at

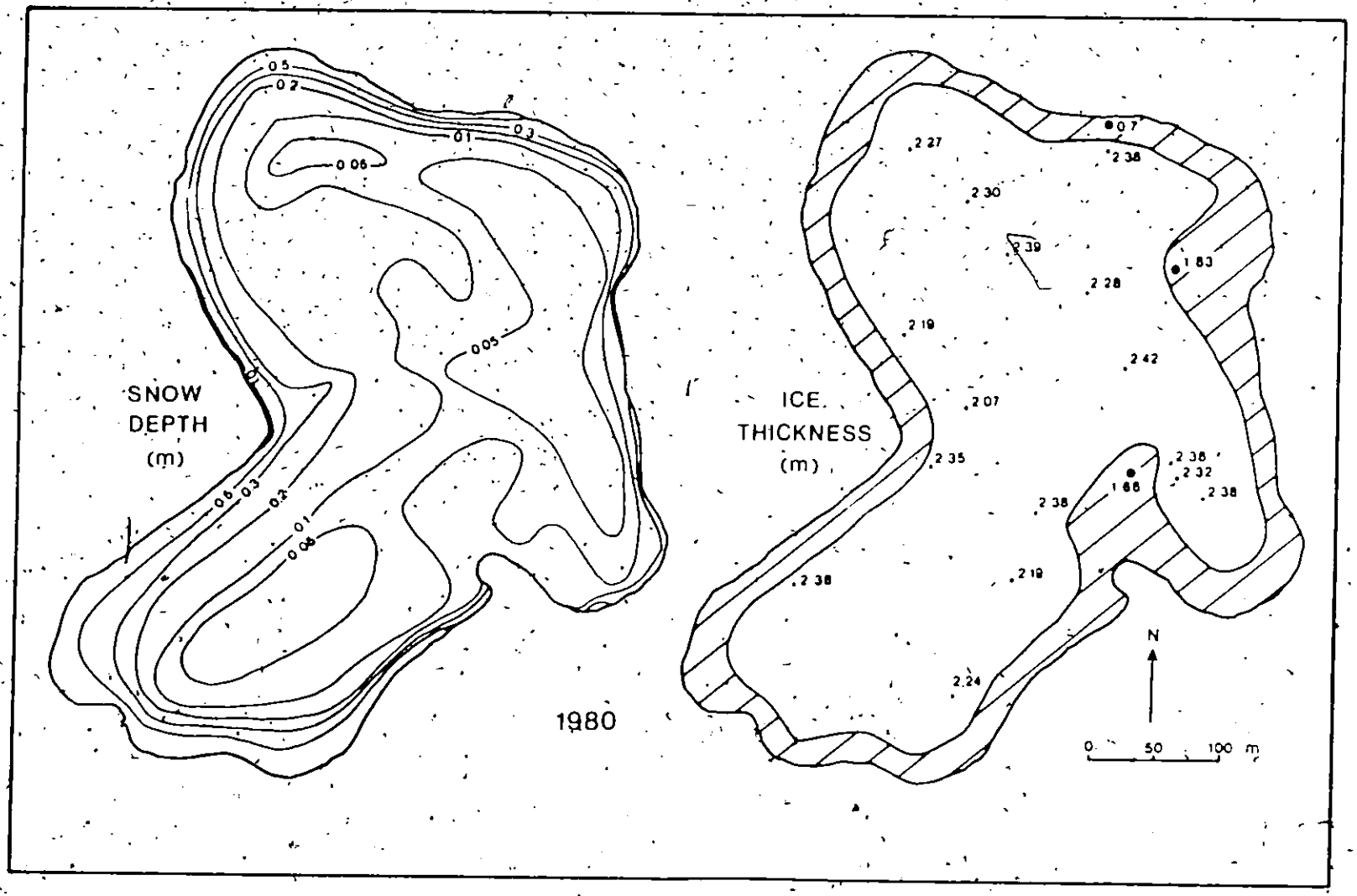

Figure 4.7. Snowcover depth and ice thickness for Small Lake, 1980. The hatched area indicates where the ice is frozen to the lake bottom.

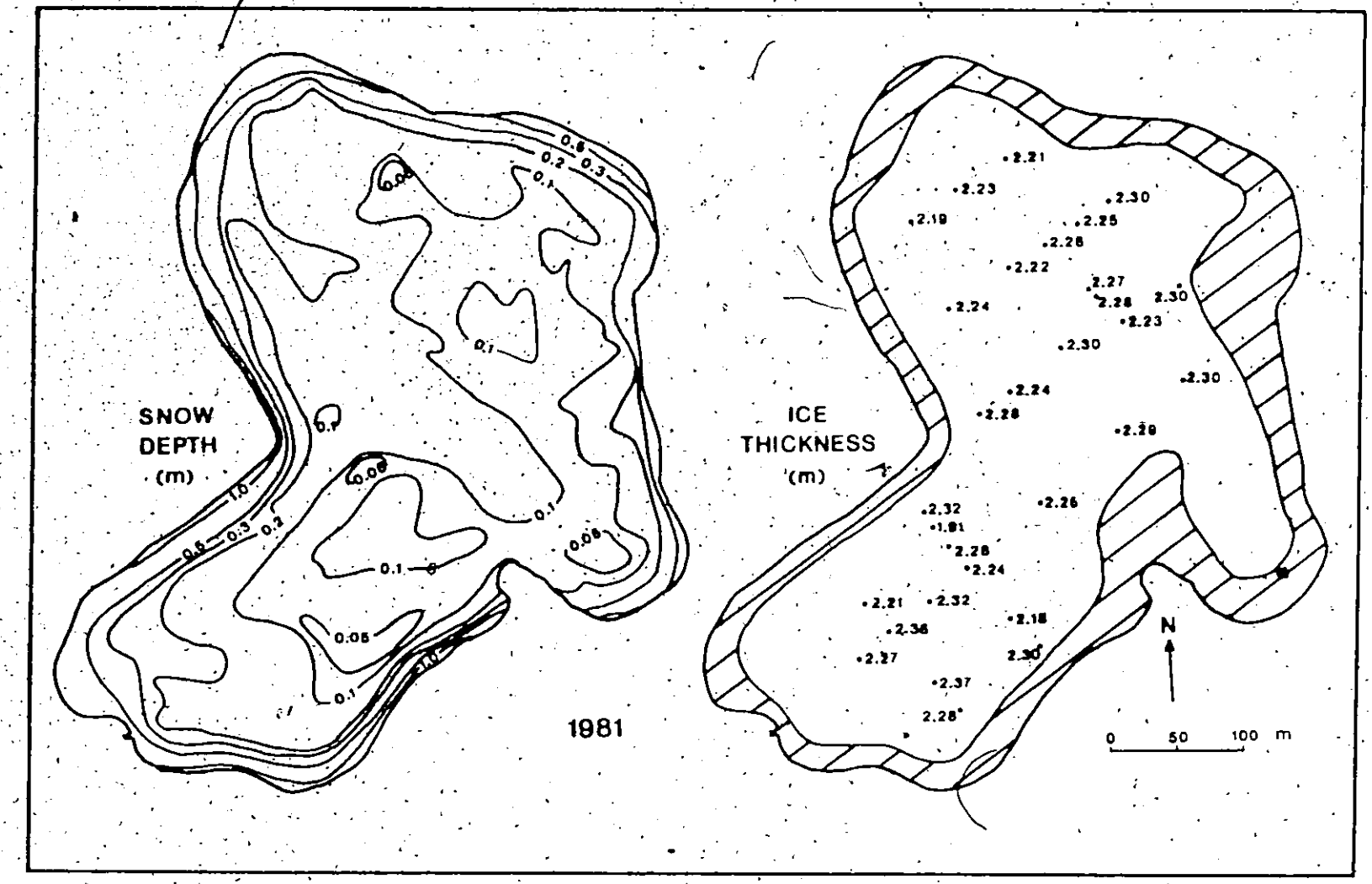

Figure 4.8. Snowcover depth and ice thickness for Small Lake, 1981. The hatched area indicates where the ice is frozen to the lake bottom.

the end of the ice growth season except in 1981 when equipment problems delayed the survey to the first few days of melt. Although not ideal, there was little loss of ice thickness within that period. The results of these surveys are shown in Figs. 4.7 and 4.8.

The greatest thickness of ice was found where the snow was scoured and remained thin throughout the winter. In 1980, the maximum thickness was 2.42 m in the north-central section of the lake while in 1981 the maximum observed was 2.37 m in the southwest. The spatial variation in ice thickness was usually less than 0.1 m over much of the lake surface. Where the snow depth varied greatly and where large drifts remained for much of the winter, abrupt ice thickness changes of 0.3 m could occur.

The thinnest floating ice observed in 1980 was 2.18 m and in 1981 it was 1.91 m. Floating ice could be thinner since a minimum ice thickness of 1.60 m was observed in 1979. However, thin floating ice was usually found under thick drifts near the shore and the possibility of damaging the ice drill on the frozen lake bottom was too great to risk drilling there.

All the ice thickness data obtained from floating ice survey were plotted against snow depth at each site to produce Fig. 4.9. This diagram demonstrates the insulating effect of snow upon the growing ice sheet. There is considerable scatter due to the effect of drifting snow.

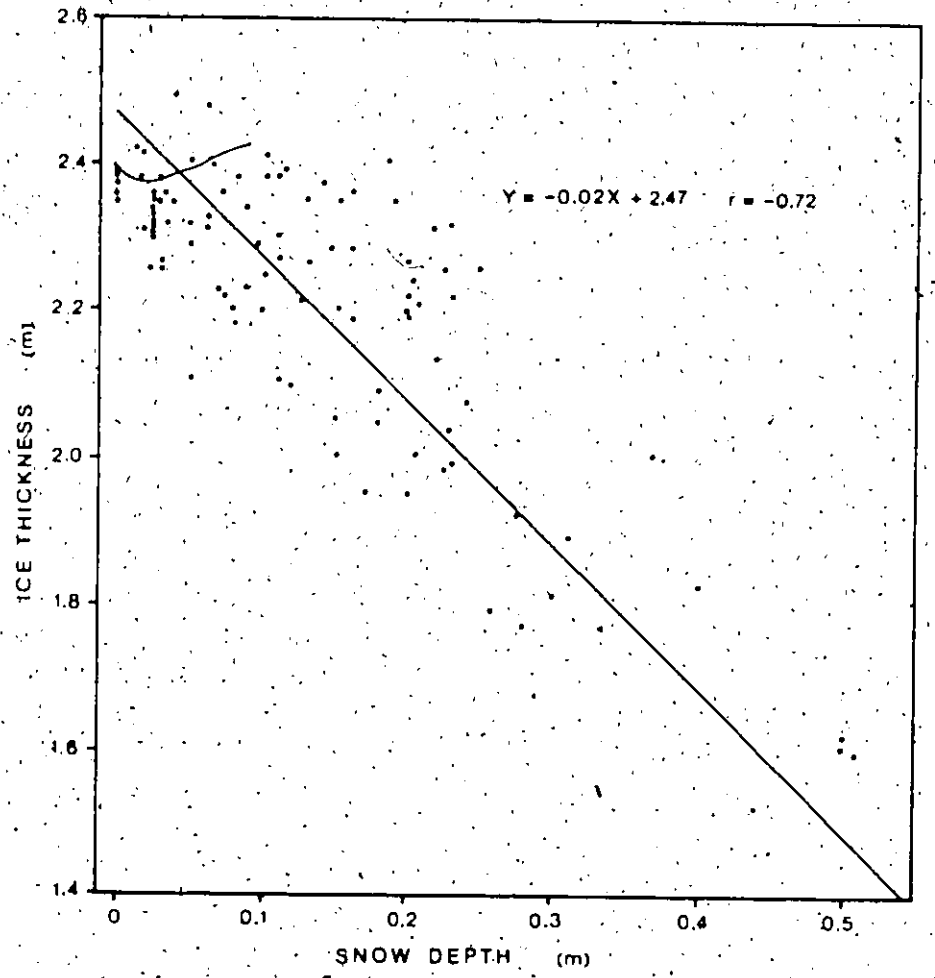

Figure 4.9. Relationship between the depth of snow on the ice cover and the thickness of the underlying ice for lakes in the Resolute area. Ice surveys from 1977 to 1982 provided the data.

but the inverse relationship is evident. It was not possible to precisely locate the boundary between the ice frozen to the lake bottom and the ice that was floating for the entire lake due to the limited number of samples obtained(ranging from 22 to 40). Instead, the boundary was approximated using the snow depth to estimate the ice thickness from Fig. 4.9 and comparing that value to the lake bathymetry. The ice thickness maps (Figs. 4.7 and 4.8) indicate that about 25 percent of the ice cover was frozen to the lake bottom, the largest area was found along the shallow shoreline at the southeastern side of the lake.

4.3.1.3 Ice Characteristics

Ice cores and blocks removed during other routine work were inspected for air bubbles and ice structure. A few cores were examined under crossed polarized filters to determine the crystallography but only a few crystals were present and the necessary laboratory facilities were lacking for a more detailed analysis. Thus, most observations were made in the field both before and during the melt period.

Michel and Ramseier (1970) classified freshwater ice into groups based on crystallography and mode of formation. While detailed observations on the ice crystallography were not possible, the ice characteristics

of the Small Lake ice cover was classified using the scheme of the above authors.

The initial or primary ice layer on Small Lake is usually lost to sublimation over the winter. In 1978-79 15 mm of surface ice was lost in this manner. As a result it is often difficult to determine the nature of the initial ice skim. While clear, transparent ice commonly forms the primary ice layer, nucleation due to snow and possibly frazil were also observed. Although the nature of the primary ice layer may not be determined, it exerts a strong influence on the ice that forms later in the winter.

The Small Lake ice cover was composed of two types of transparent secondary ice that cannot be visually separated prior to melt. Both contained columnar crystals, but the grain size and the orientation of the optical axis differed. The spatial variation of these crystal types can be attributed to events occurring during the freeze-up which resulted in different types of primary ice (Michel 1978). Once melt commenced, internal melting of individual ice crystals allowed them to be classified visually. Fine grained ice appeared darker than the coarse grained ice. The initial size of the fine grained ice was approximately 1 mm in diameter at the ice cover surface. The size increased slowly until the diameter reached 50 mm at a

depth of 1.5 m below the ice surface. The coarse grained ice was whiter and had an initial ice crystal diameter of about 10 mm which grew to 800 mm or more near the bottom of the ice sheet. The fine grained ice has a horizontal optical, or c-axis, for the entire ice thickness. The coarse grained ice is more complex. Initially, the c-axis is vertical at the ice surface and for a depth of 0.3 to 0.5 m. As a result of the wedging-out processes described by Perey and Pounder (1958), the c-axis vertical crystals are gradually replaced by c-axis horizontal crystals. This orientation remains unchanged for the rest of the ice thickness. The horizontal c-axes showed no preferred horizontal alignment in either ice type. Ice from lakes in the Truelove Lowland (Devon Island) has been observed by Koerner (1963) to behave in the same manner.

4.3.1.4 Ice Temperature

Measurements of ice temperature were made using arrays of thermistors frozen into the ice cover. Observations commenced up to one month prior to melt and continued until the thermistors were free of the ice. The measurement sites included a variety of ice thickness and snow depth conditions. The generalized thermal conditions are depicted by Fig. 4.10 for an ice cover frozen to the bottom, and by Fig. 4.11 for floating ice.

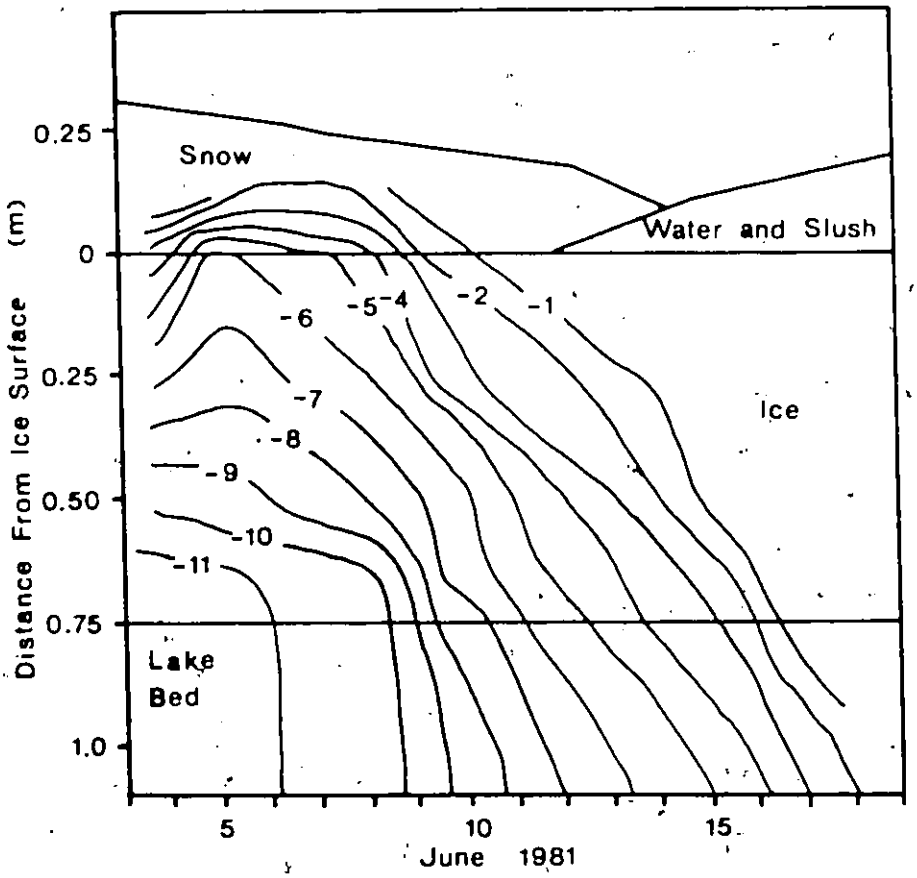

Figure 4.10. Temperature of ice frozen to the lake bed at the beginning of the ice decay period.

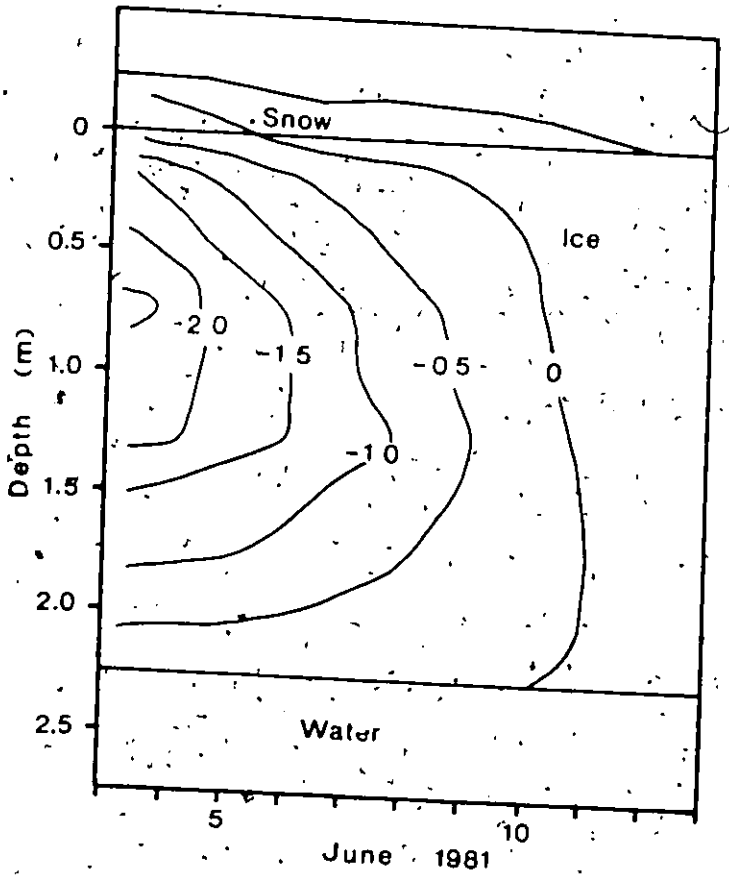

Figure 4.11. Temperature of a floating ice cover at the beginning of the ice decay period.

The floating ice cover was relatively warm in comparison to the ice frozen to the lake bottom. Considerable warming had occurred by the time the thermistor array was installed and the lowest temperature of -2.5° C was located at the central part of the ice sheet. At the bottom of the ice, there were two sources of heat, including the heat flux from the water conducted upward to the ice and the latent heat released as a small amount of ice continued to grow. At the upper surface, heat was conducted downward through the snowcover. When the snowcover was thin or absent, the ice was much warmer because shortwave radiation could be absorbed by the ice. In 1981, for example, the bare ice was already near 0° C on June 3 and the thermistor array never froze in place. Under thick snow, the absorption of radiant energy is limited by the reflectivity and opacity of the snow (Giddings and LaChapelle 1961, Warren 1982). As shown in Fig. 4.11, the influence of absorbed radiation was small due to the snowcover.

Where the ice was frozen to the lake bottom, energy was conducted downward to warm both the ice and the lake sediment. Warming was underway when the sensors were installed. When the snowmelt water reached the snow-ice interface, a layer of basal ice was formed (Woo and Heron 1981) releasing latent heat which was conducted downward

to warm the ice. The frozen sediment continued to draw heat from the ice until around June 18 when the bottom of the ice cover approached 0° C. However, the ice remained frozen to the lake bottom for 5 more days. This period of prolonged attachment to the lake bottom was facilitated by the presence of basal ice which limited the radiant heating of the lake ice, and by the conduction of a small amount of heat to the lake bottom.

4.3.2 Melt Period

4.3.2.1 Ice Melt

The loss of ice from lake cover can be partitioned into four sections, melting at the upper and lower surfaces, internal melt within the ice as well as the loss of ice along the edge of the ice cover. The melt at the upper and lower surfaces can be determined by direct measurement of the change in ice thickness at a site with reference to a datum fixed in the ice. Internal melt results from the absorption of radiant energy by the ice cover to cause a change in the density of the ice. If the ice temperature is below freezing, the energy is used to warm the ice and no melting occurs. While the ice temperature is easily obtained, the ice density of a melting ice cover is difficult to measure due to fragile ice conditions. Finally, the loss of ice along the edge of the ice cover can be measured directly. This component

involves some ice loss by mechanical processes but the ice removed from the main ice cover quickly melts in the moat.

4.3.2.1.1 Internal Melt

Internal ice melt in the Small Lake ice cover did not usually occur until the overlying snow was gone. The first indication of this phenomenon was melting along crystal boundaries of the surface layers. Below the surface, the ice cover remained frozen for several days, allowing water to pond in surface depressions. This water eventually drained through the ice along the edge of the pond when internal melt had established interconnected passages for vertical drainage. Ice density profiles were taken at several sites in 1981, shortly after internal melt had started and the ponds had drained. Three examples of these are shown in Fig. 4.12 which suggest that most of internal melt occurred near the ice surface and decreased exponentially with depth. At the surface, the ice density was comparable to that of snow but increased rapidly with depth. Below the hydrostatic water level, the ice density was relatively constant at more than 800 kg/m^3. The density profiles of the fine and coarse grained ice were similar. Ice density profiles obtained two weeks later did not differ substantially from the last one in Fig. 4.12. After this, no additional ice density profiles were obtained but visual observation indicated that the ice

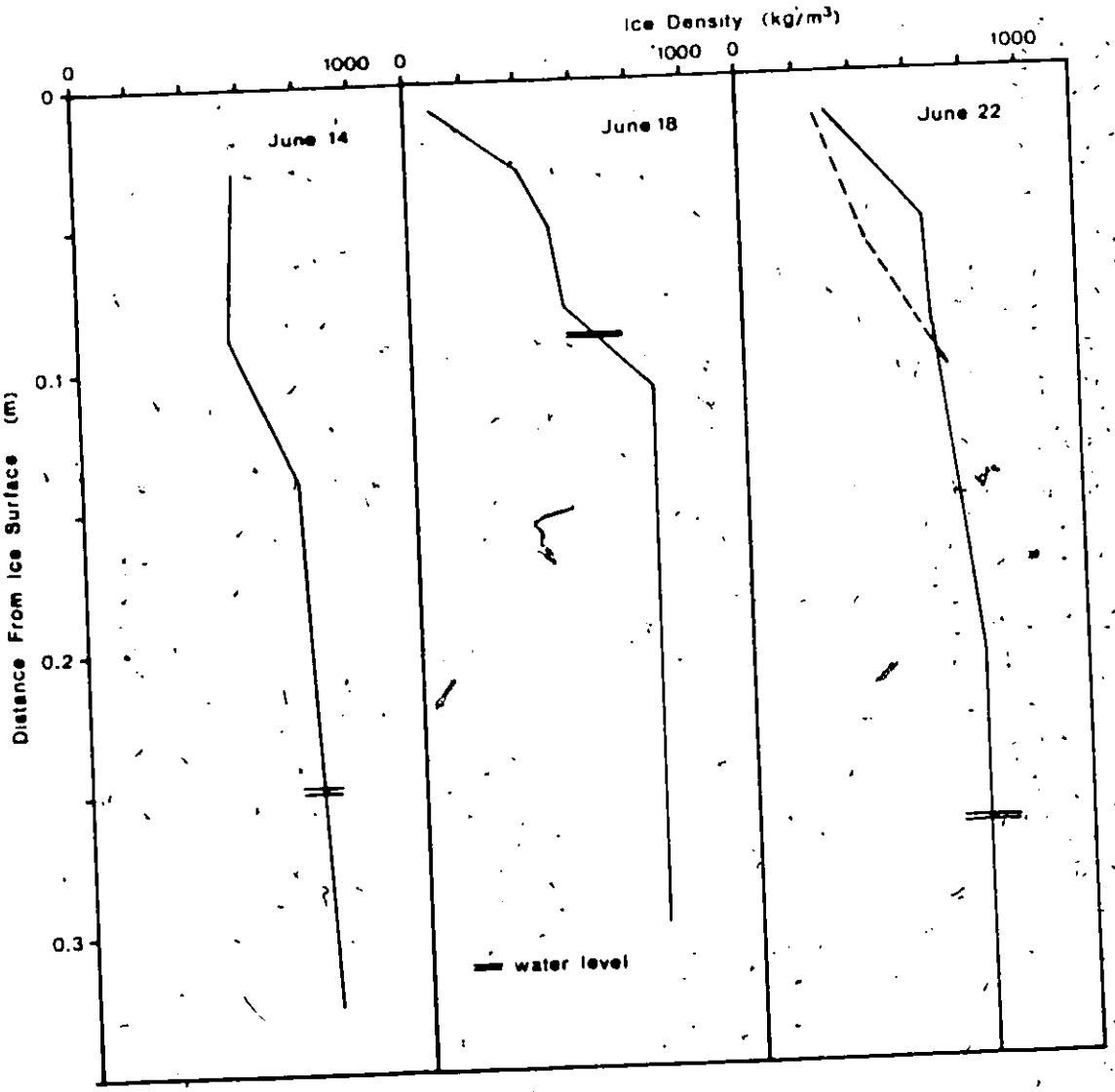

Figure 4.12: Ice density profiles in the upper 0.4 m of the melting ice cover in the vicinity of the meteorological site, 1981.

density still increased with depth. Individual ice density values were also obtained from incomplete cores removed from below the hydrostatic water level late in the melt season. These densities ranged from 620 to 810 kg/m³ and had a mean of 750 kg/m³. This value indicates that most internal melt was concentrated in the upper ice layers.

4.3.2.1.2. Surface Ice Melt

The melt at the upper ice surface was measured with stakes set across Small Lake in 1980 and 1981. In 1980, white wooden stakes (initially with plexiglass collars) were used. These stakes were reset every second or third day but they were often loosened as the ice melted around them. Thus their accuracy is suspect. In 1981, all-plexiglass stakes with collars were employed. Four weeks after the beginning of melt, the vertical movement was limited to 10 mm. Hence, the 1981 ice ablation data are more reliable.

The 1981 ice ablation observations for three of the sites are shown in Fig. 4.13. The initial lowering of the ice surface was slow because of the high densities of the surface ice layers and low melt energy. Once the surface density was reduced by internal melt, the rate of surface lowering increased, and continued throughout the melt period. The peak ablation rate of 106 mm/d was produced on

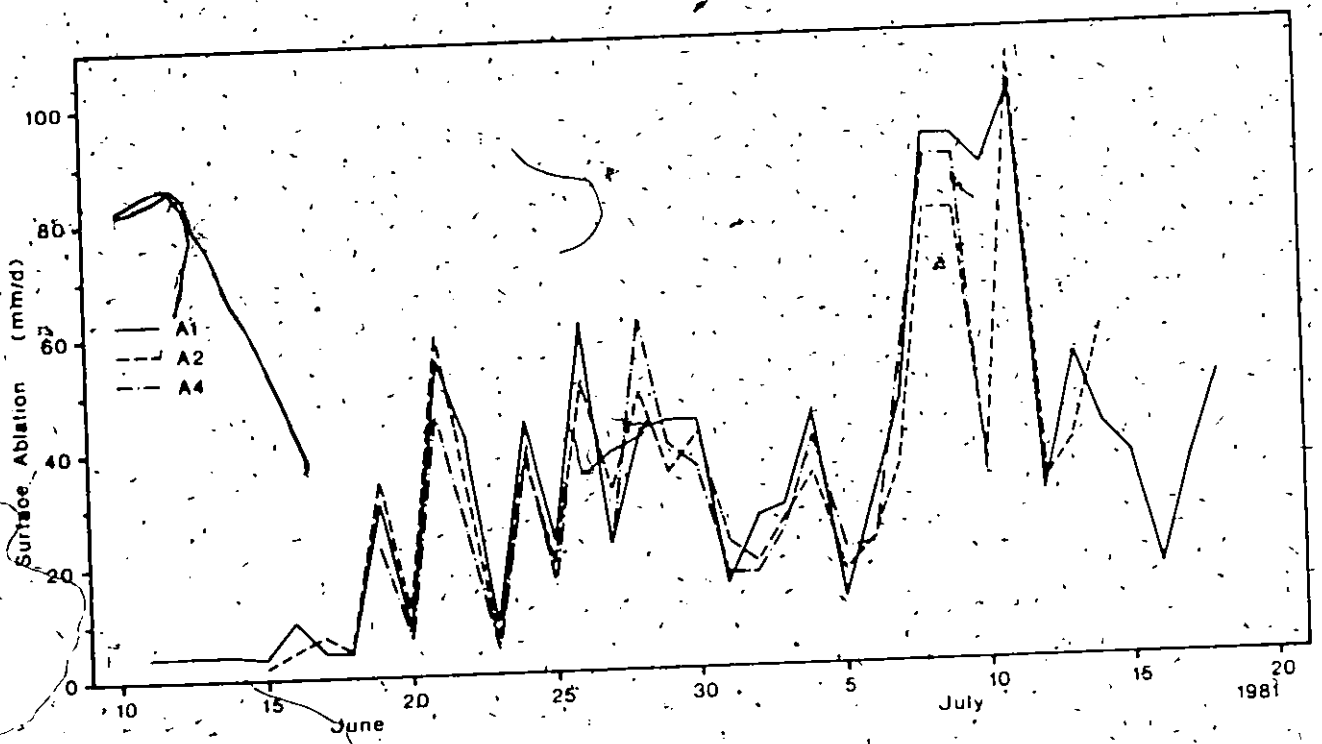

Figure 4.13. Ice ablation rate from the upper ice surface for three sites in 1981.

a warm, windy day when abundant melt energy was available. The ablation rates for three widely separated sites on different types of ice (Fig. 4.13) differed by less than 30 percent for individual measurements, most of which can be explained by measurement error. Over the melt period, the cumulative ablation for these three sites was only 5 percent different from the mean value, suggesting that the surface ice ablation was similar across the ice cover.

The 1980 ablation results for the main measurement site (Fig. 4.14) were similar to those observed in 1981. The primary differences lie in the generally lower ice ablation rates, especially the peak values, and the very low melt at the end of the melt period. The former may be real but is probably an artifact of the poor instrumentation in 1980, while the latter was enhanced by cool temperatures.

The surface ablation accounted for the largest change in ice thickness. Using the two sites near the centre of the lake, A1 in 1981 and ID3 in 1980 (Figs. 4.15 and 4.16) the upper surface ablation was 74 percent of the total change in ice thickness in 1981 and 60 percent in 1980.

4.3.2.1.3 Bottom Ice Melt

The melt at the bottom of the ice was relatively small and was determined as the difference between the

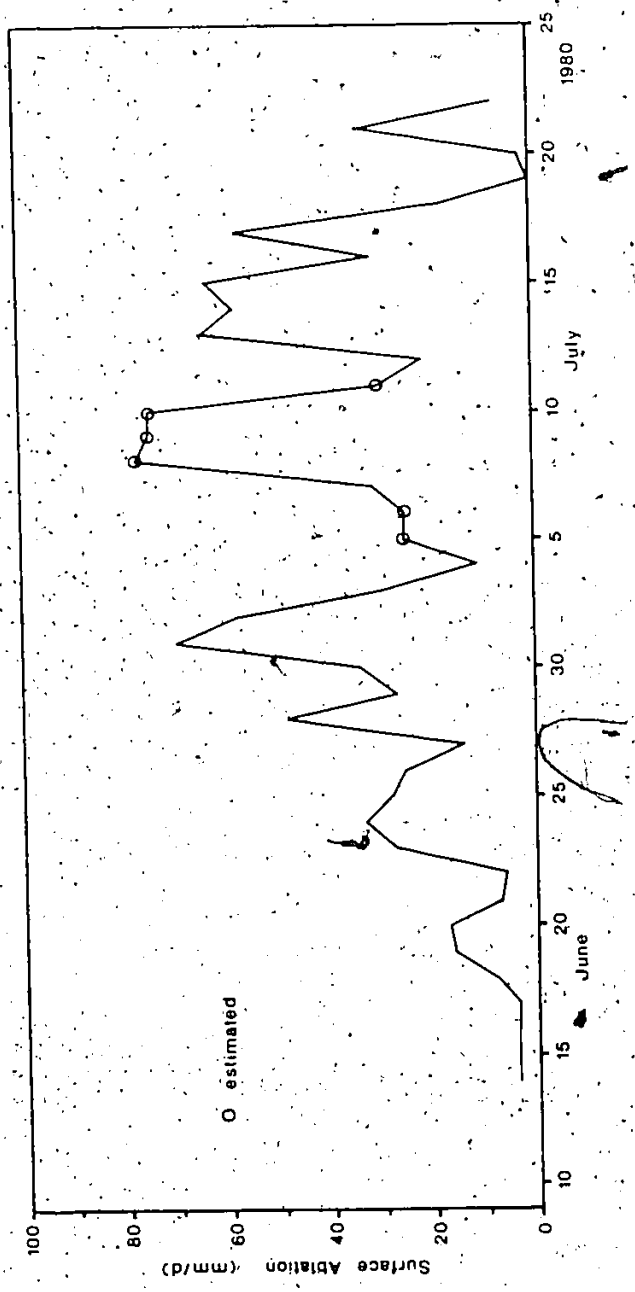

Figure 4.14: Ice ablation rate from the upper ice surface, 1980.

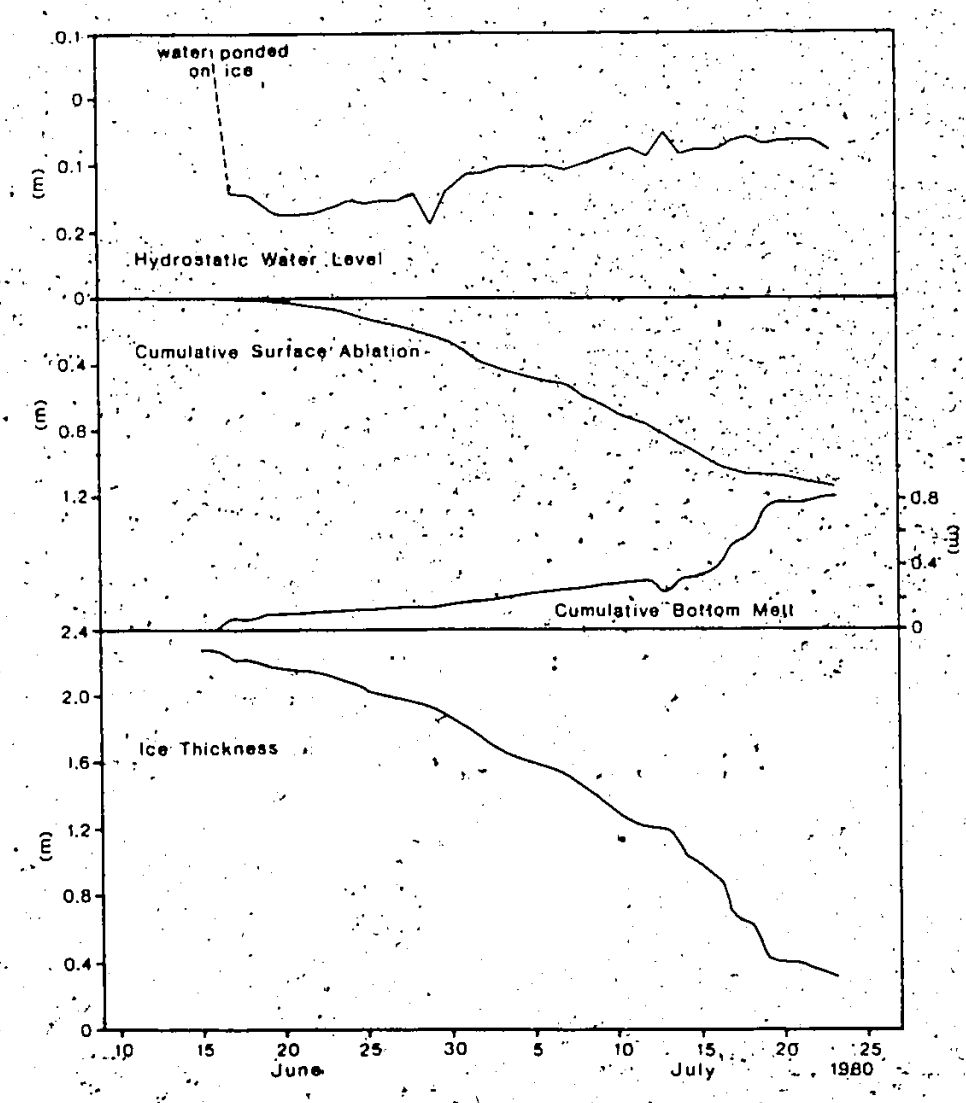

Figure 4.15. Ice thickness, cumulative surface ablation and bottom melt, and the hydrostatic water level for site ID3, 1980.

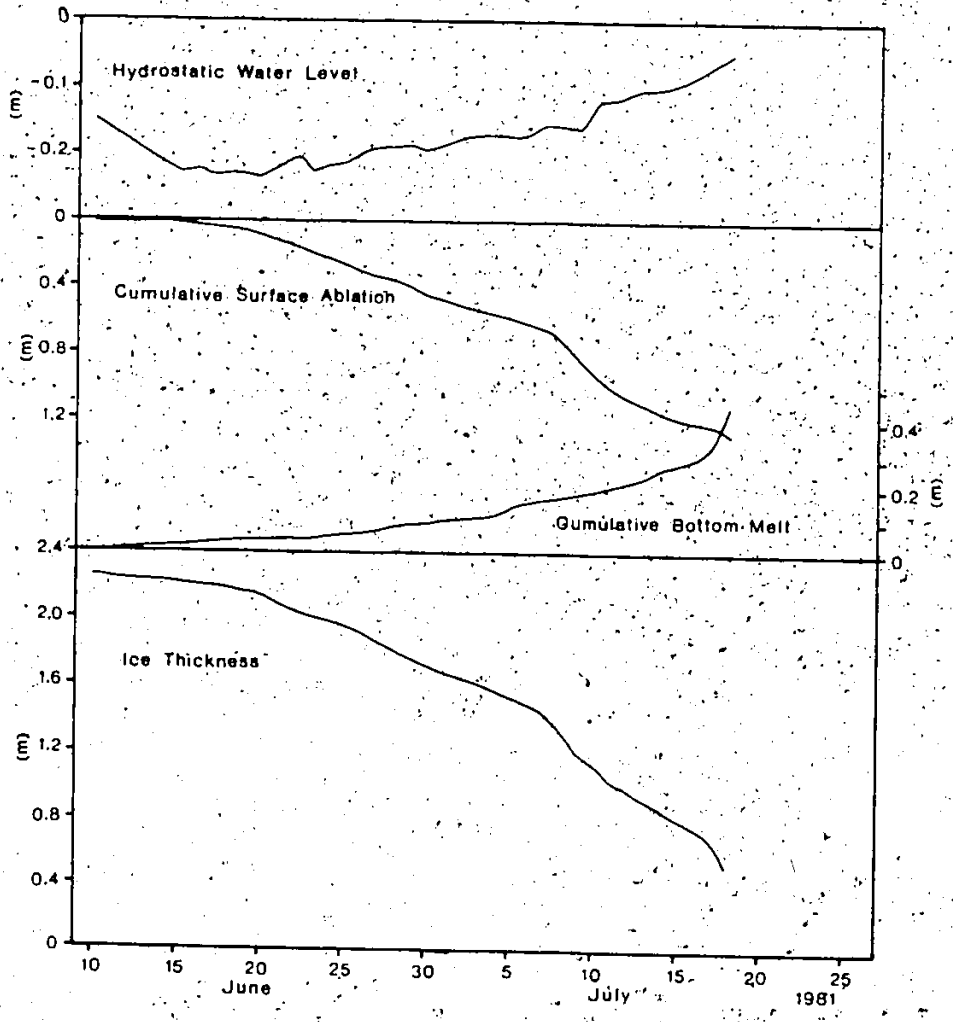

Figure 4.16. Ice thickness, cumulative surface ablation and bottom melt, and the hydrostatic water level at site A1, 1981.

change in ice thickness and the surface ablation. Since it is a residual term, the cumulative measurement error of the two other values can be larger than the bottom melt itself. This is well illustrated by Fig. 4.17 for the main melt site in 1981. In the first half of the melt period the bottom melt rate fluctuated greatly, indicating that individual values were poorly estimated. The error was probably random. In the second half of the melt period, the values became more consistent, suggesting that the random error was reduced.

The cumulative bottom melt in 1980 (Fig. 4.16) showed a similar pattern to that of 1981. Despite almost twice as much bottom melt in 1980 than 1981, the water temperatures remained similar in both years. This result again suggests that in 1980, melt caused the ablation stakes to sink, thus underestimating the surface ablation and overestimating the bottom melt.

4.3.2.1.4 Moat Formation and Development

The development of a moat can be divided into two phases. The formation of the moat begins when water ponds on the ice surface near the edge of the lake and is in equilibrium with the lake level. Establishing the date at which the first moat segments formed was difficult for many areas of the lake. In 1980, the initial snowmelt was rapid and up to 70 percent of the ice cover was quickly

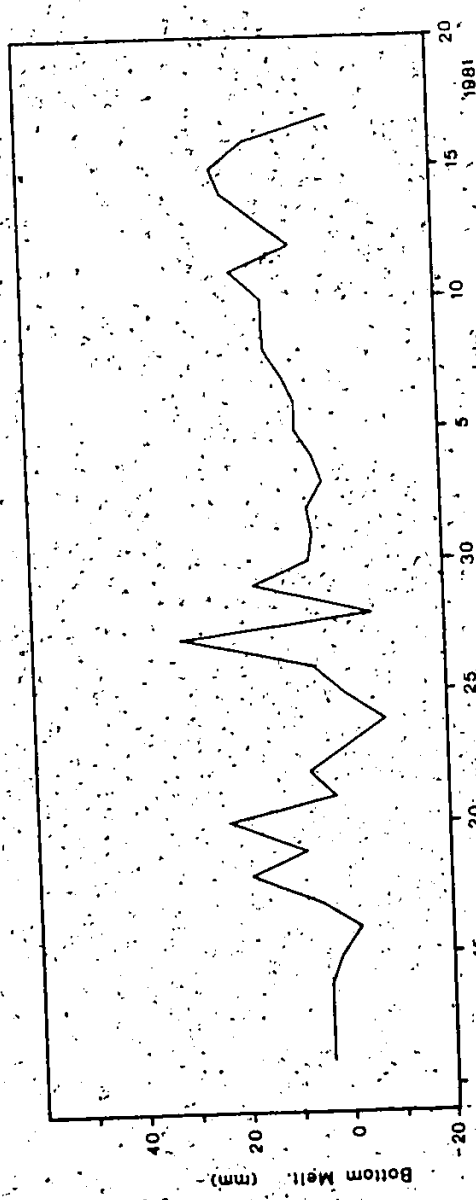

Figure 4.17. Daily melt at the bottom of the ice cover at site A1, 1981.

covered by melt water ponds. These ponds were raised above the lake level and drained over the next 2 days when the ice around them candled and the water percolated through the ice. Those near the edge of the lake survived and by June 18th, 4 days after the beginning of melt, a moat was established around the lake near the edge. The beginning of melt in 1981 was more gradual and the ice cover candled before large amounts of water reached the ice surface. There was some slushing, but the only ponds formed were along the lake shore. The water seeped through the ice elsewhere and no ponds formed. In 1981, the moat was complete, 5 days after the beginning of melt, on June 15th.

Figure 4.18 shows the behaviour of the ice cover along a transect from the shore toward the centre of the lake. The lake level rose steadily throughout the initial phase of moat formation and the ice cover rose as well except where it was frozen to the lake bed. The location of the frozen zone coincided with the presence of basal ice which limited the warming of the lake bed by minimizing the shortwave radiation reaching it. If all the basal ice melted, as in the case of Fig. 4.18, the ice edge floated to the surface shortly thereafter and was free of the shore. While many sites with a thin initial snowcover melted free of the shoreline, other sites developed large cracks in the ice at the edge of the zone

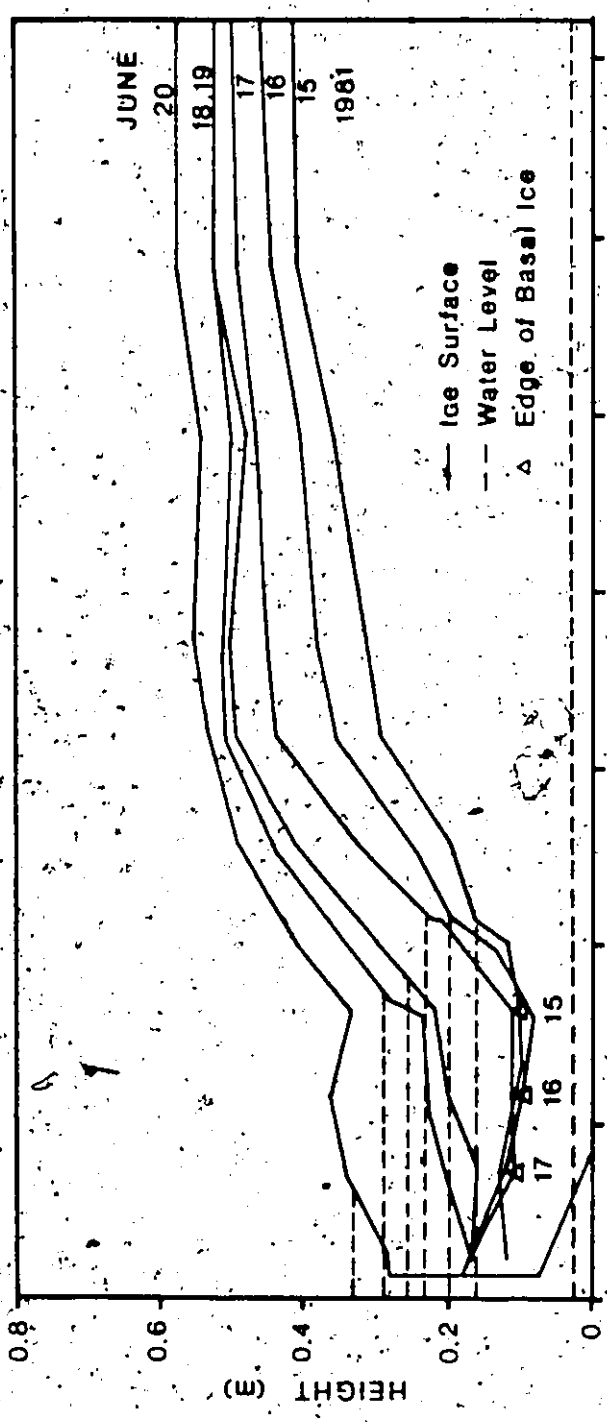

Figure 4.18. Moat development at transect U during the rise in lake level, 1981.

where the ice was frozen to the lake bed and at the lake side edge of the moat (Table 6.2). The ice between them then floated to the surface and usually moved down the moat. These fragments melted completely within days. The initial phase of moat development ended when the ice either fractured or melted free of the shore at a site. In 1980, the first moat phase lasted only 2 days near Low Point where the ice melted free of the shore. At a site with a deep initial snow depth near Phi Point, this initial phase lasted 14 days, until July 1st. In 1981, the results were similar with the first site completing phase one of moat development by June 13th, after 3 days of melt and the last location by June 25th after 14 days.

The second phase of moat development occurred when the ice has broken free of the shore. Even before the entire ice cover is free to move about the lake, the ice edge at a site retreats from the shore due to a combination of thermal and mechanical processes. These include the transfer of heat to the ice from the water, the mechanical removal of ice crystals and ice fragments by waves and the radiation-induced release of crystal fragments from submerged sections of the ice (also known as ice rams (U.S. Navy 1952)). Wind, and the resulting waves and water circulation in the moat accelerates the rate of ice loss from the edge of the ice cover. Additional factors influencing the rate of ice edge

retreat are ice thickness, ice crystal size and location on the ice edge with respect to the direction of the waves. A small and irregular source of ice loss occurs as a result of interactions between the shore and the ice cover as the latter drifts about the lake. This is determined by the ice strength and the nature of the ice movement.

The cumulative edge retreat for several transects perpendicular to the ice edge are given in Fig. 4.19. During the 25 days of measurement in 1981, approximately 45 m of ice was lost from from the edges at a mean rate of 1.8 m/d. Daily rates for 1980 and 1981 are shown in Fig. 4.19. The initial edge retreat rates in 1981 were typically 1.3 m/d and these values decreased as the ice edge thickness increased (Fig. 6.15). The minimum rates of ice loss from the edge of 0.1 m/d coincided with peak ice edge thickness in the middle of the decay period. Following this, the rate of ice loss increased, with a peak value of 12 m/d, as the ice thinned and became weakened by internal melt. The loss of reference markers from the ice edge early in 1980 during periods of high ice loss has reduced the number of observations. Had these been included in Fig. 4.19, the seasonal changes in ice edge retreat rates would be similar for both study years.

The loss of ice along the edge reduced the area of lake ice cover (Fig. 4.20). The initial decrease in the

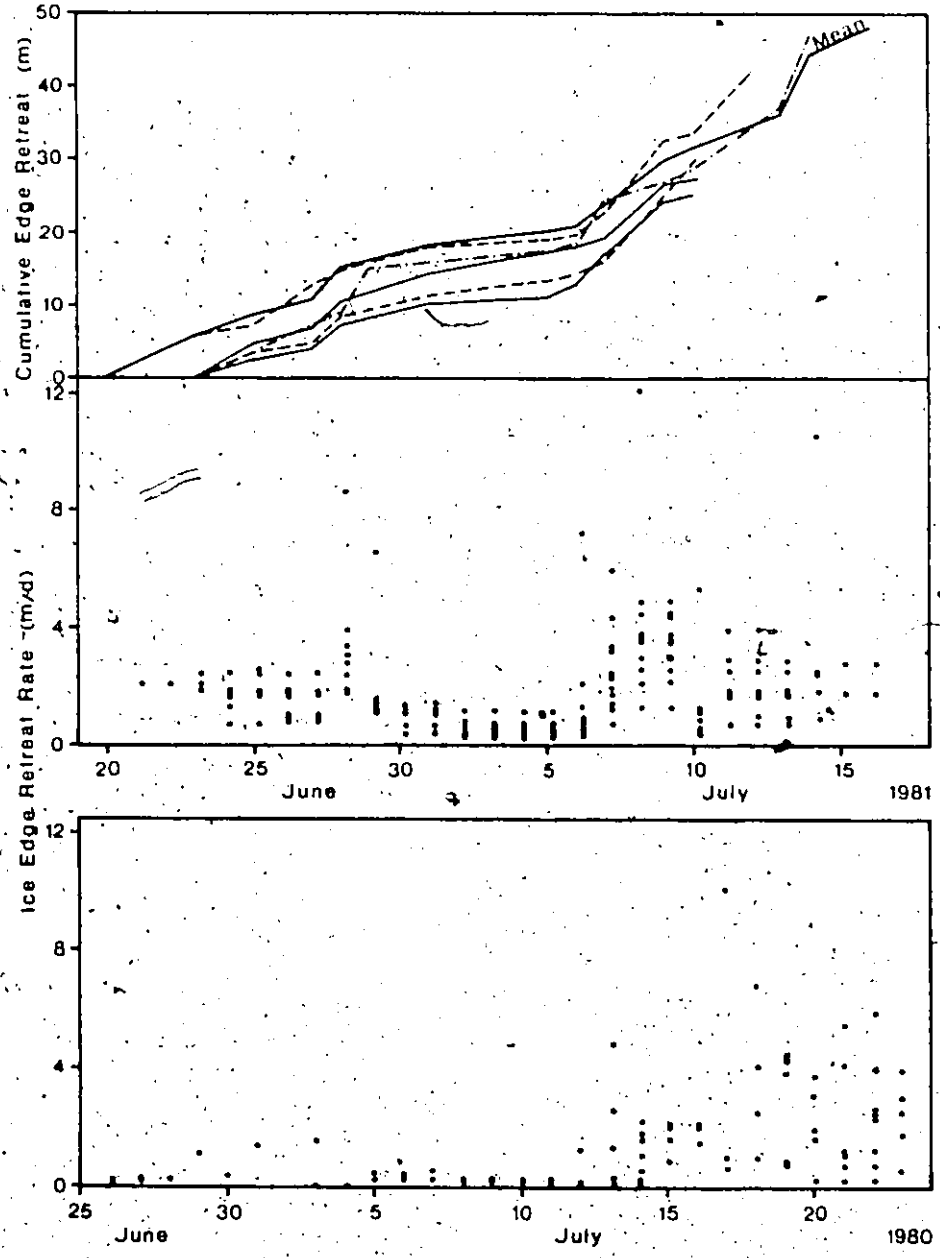

Figure 4.19. Ice edge retreat rate and cumulative ice edge retreat, 1980 and 1981.

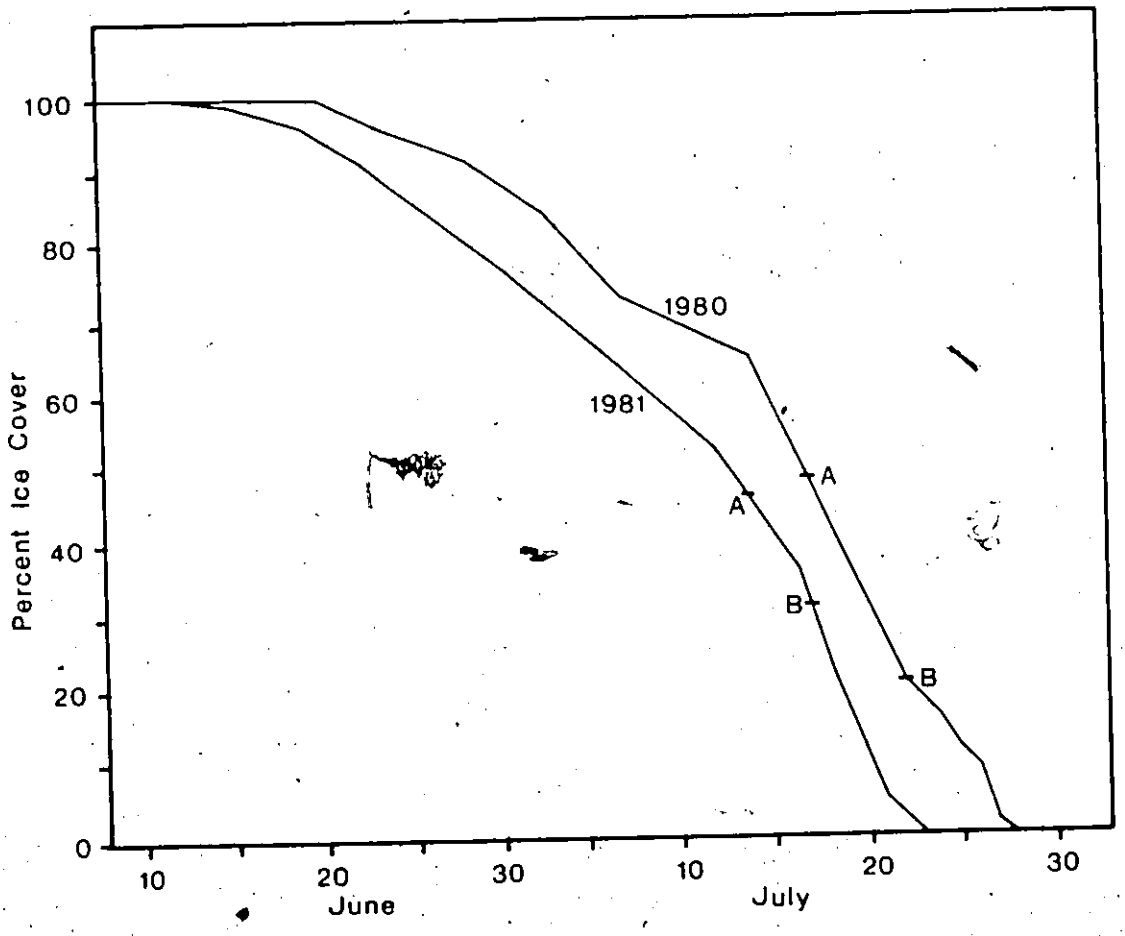

Figure 4.20 Small Lake ice cover area, 1980 and 1981. The date at which the ice cover broke into two pieces is indicated by (A) while major fragmentation occurred at (B).

percentage of ice cover was small and results from the limited length of ice edge capable of losing ice. This increased as the entire ice edge began to retreat and the rate of retreat became larger. After approximately 30 days of melt, internal ice melt had reduced the ice strength sufficiently that the ice cover could no longer resist the stresses imposed upon it during its interaction with the shore. The ice cover fractured in two, with the dividing line between Low and Phi Points. Within 3 days, additional fragmentation occurred and the area of the ice cover decreased even more rapidly due to the increased ice cover perimenter and thinner, weaker ice. Once the ice cover area reached less than 5 percent, the fragmentated ice mass melted quickly. In 1980, complete clearance of the ice cover required 42 days, 1 day less than in 1981.

CHAPTER 5

ICE MELT AT A SITE

5.1 Theory of Lake Ice Cover Decay

The growth, thermal regime and decay of a lake ice cover are controlled by the energy balance of the ice cover

$$(5.1) \quad dS/dt = Q^*_{ic} + Q_H + Q_E + Q_P + Q_W$$

where Q^*_{ic} is the radiation balance of the ice, Q_H and Q_E are the sensible and latent heat fluxes at the upper ice surface, Q_p is the heat added by precipitation and Q_W is the heat flux from the lake water to the bottom surface of the ice and dS/dt is the change in heat storage in the ice due to temperature changes as well as the gain or loss of mass. The change of mass occurring during ice growth (dH/dt) can be easily approximated by Stefan's Equation

$$(5.2) \quad dH/dt = -k_i (T_a - T_0) / H \rho_{pi} L_f$$

where k_i is the thermal conductivity of ice, ρ_{pi} is the density of pure ice, L_f is the latent heat of fusion, H is the ice thickness and T_a and T_0 are the air temperature and temperature at the ice-water interface. For ice decay, the energy balances must be determined for the zones where

melt occurs, including 1) the air-ice interface, 2) the ice-water interface and 3) the ice interior. In the discussion that follows, a positive flux is considered to be directed towards the ice.

5.1.1 Melt at the Air-Ice Interface

The energy balance at the upper ice surface is

$$(5.3) \quad L^*_i + Q_H + Q_E + Q_p - Q_{mu} - Q_I = 0$$

where L^*_i is the longwave radiation balance, Q_{mu} is the energy involved in surface melt and Q_I is the heat flux into the ice. The net longwave radiation can be considered as part of the surface energy balance since the incident longwave raadiation is rapidly absorbed by the ice. However, it is necessaary to conceive of the ice surface as an infinitely thin ice layer. There is no heat flux into the ice when the ice temperature is at 0°C because no temperature gradient exists. Thus, during the melt period, Eq. 5.3 can be rewritten to yield the surface melt rate $(dh/dt)_{us}$.

$$(5.4) \quad (dh/dt)_{us} = Q_{mu}/\rho_{pi} L_f = (L^*_i + Q_H + Q_E + Q_p)/\rho_{pi} L_f$$

The longwave radiation balance may be obtained from the radiation balance of the ice surface

$$(5.5) \quad L^*_i = Q^*_i - (1 - \alpha_i) K\downarrow$$

where α_i is the shortwave albedo of the ice and K↓ is the incident shortwave radiation.

Since the surface of the ice cover is fixed at 0°C and 100 percent relative humidity during the melt period, the bulk transfer approach can be used to compute the fluxes of sensible and latent heat.

$$(5.6) \quad Q_H = \rho_a C_a D_H u_z (T_z - T_s)$$

$$(5.7) \quad Q_E = \rho_a L_v (\varepsilon/P) D_E (q_z - q_s)$$

Here, ρ_a is air density, C_a is the heat capacity of the air, L_f is the latent heat of vapourization, ε is the ratio of the molecular weights of air and water, u_z is the wind speed at height z, T_z and T_s are the temperature at height z and at the surface while q_z and q_s are the vapour pressures at the same locations. The drag coefficients, D_H and D_E are assumed equal and are obtainable from

$$(5.8) \quad D_H = D_E = D = K^2/(\ln(z/z_0))^2$$

where K is von Karman's constant. The surface roughness, z_0, can be estimated from the following equation under neutral atmospheric conditions

$$(5.9) \quad z_0 = \exp((u_2 \ln z_1 - u_1 \ln z_2)/(u_2 - u_1))$$

where z_1 and z_2 refer to the heights at which the wind speeds, u_1 and u_2 were obtained.

The bulk transfer equations should be modified for use in the stable boundary layers which overlie melting ice. This can be accomplished by modifying the drag coefficient using the Richardson number (Ri), defined as

$$(5.10) \quad Ri = g\, z\, (T_z - T_s) / T_z\, (u_z - u_s)^2$$

where g is the acceleration due to gravity. For stable conditions when Ri>0 , Price et al (1976) give the drag coefficient as

$$(5.11) \quad D_S = D / (1 + b\, Ri)$$

and for unstable boundary layers (Ri<0)

$$(5.12) \quad D_S = D / (1 - b\, Ri)$$

where b is a coefficient with a value of 10 (Price et al 1976).

The final term to be estimated in Eq. 2.4 is the heat brought to the surface by rainfall.

$$(5.13) \quad Q_p = \rho_w\, C_w\, R\, (T_p - T_s)$$

where ρ_w is water density, C_w is the specific heat of water, T_p is the temperature of the rain which can be approximated by the wet bulb temperature and R is the rainfall intensity.

5.1.2 Melt at the Ice-Water Interface

The energy balance at the bottom of the ice cover

is

$$(5.14) \quad Q_{ml} = Q_W - Q_I$$

where Q_I is the heat conducted up into the ice and Q_{ml} is the heat used in bottom ice melt. During the melt period, the ice is isothermal at 0°C so that Q =0. Thus the melting at the lower ice surface $(dh/dt)_{ls}$ is

$$(5.15) \quad (dh/dt)_{ls} = Q_W / \rho_{pi} L_f$$

The heat flux from the water is

$$(5.16) \quad Q_W = k_w (dT_w/dzw)$$

where k_w is the thermal conductivity of water and dT_w/dzw is the temperature gradient at the ice-water interface. For operational purposes, this can be approximated by

$$(5.17) \quad Q_W = k_w (T_{zw} - T_o) / zw$$

where T_{zw} is the water temperature at a distance zw from the ice-water interface. In a water column that has stable stratification and is free of currents, the thermal conductivity is 0.586 W/m/K. Such conditions are normally observed in Small Lake with a melting ice cover.

5.1.3 Internal Melting in the Ice Cover

The general heat conduction equation for clear, snow-free ice (Greene 1981) is

$$(5.18) \quad dT_i/dt = k_i/C_i \; (d^2T_i/dz_i^2) + (e/C_i) \; (1 - \alpha_i) \; K\downarrow \exp(-e \; z_i)$$

where dT_i/dt is the change in temperature with time, C_i is the heat capacity of ice, d^2T_i/dz_i^2 is the rate of change of the ice temperature gradient with depth, and $(e/C_i)(1-\alpha_i)$ $K\downarrow \exp(-e\ zi)$ is rate of heating at depth zi in the ice cover due to the absorption of shortwave radiation. In a melting ice cover, the ice is isothermal at 0°C, thus eliminating thermal conduction. Internal melting is due to the absorption of solar radiation.

The Bouguer-Lambert Law describes the manner in which monochromatic radiation is attenuated as it penetrates any medium.

$$(5.19) \quad I_{zi} = I_s \exp(-e \; zi)$$

Here, I_s and I_{zi} are the irradiances at the surface and at depth zi while e is a coefficient describing the nature of the attenuation. It is called the absorption coefficent when applied to pure ice where the only loss is due to absorption. The term extinction coefficent is used when scattering is also attenuating the radiation. Following Eq. 5.19, the amount of radiation absorbed in a layer of ice (Q_R) of thickness zi is

$$(5.20) \quad Q_R = (1 - \alpha_i) \; K\downarrow \; (1 - \exp(-e \; zi))$$

The equivalent internal melt for the ice

cover $(dh/dt)_{in}$ is

$$(5.21) \quad (dh/dt)_{in} = (1 - \alpha_i)\, K\downarrow\, (1 - \exp(-e\, H) / \rho_{pi}\, L_f$$

where H is the ice cover thickness.

In the one dimensional case, the total ice melt rate in water, in water equivalent (WE) units is

$$(5.22) \quad dh/dt = (dh/dt)_{us} + (dh/dt)_{ls} + (dh/dt)_{in}$$

where the subscritps us, ls and in denote the upper and lower ice surfaces and the ice interior.

5.2 Computational Proceedures

The computational procedure necessary to calculate lake ice melt at a site is summarized by the flow chart in Fig. 5.1. A detailed description of the model and its main components follows.

5.2.1 Model Input

The information required by the model is listed in Table 5.1. The parameters required by the calculations and some initial ice property values are entered at the beginning of the model. Other physical constants were set in the model. All but three meteorological variables were input hourly. The water temperature was manually observed

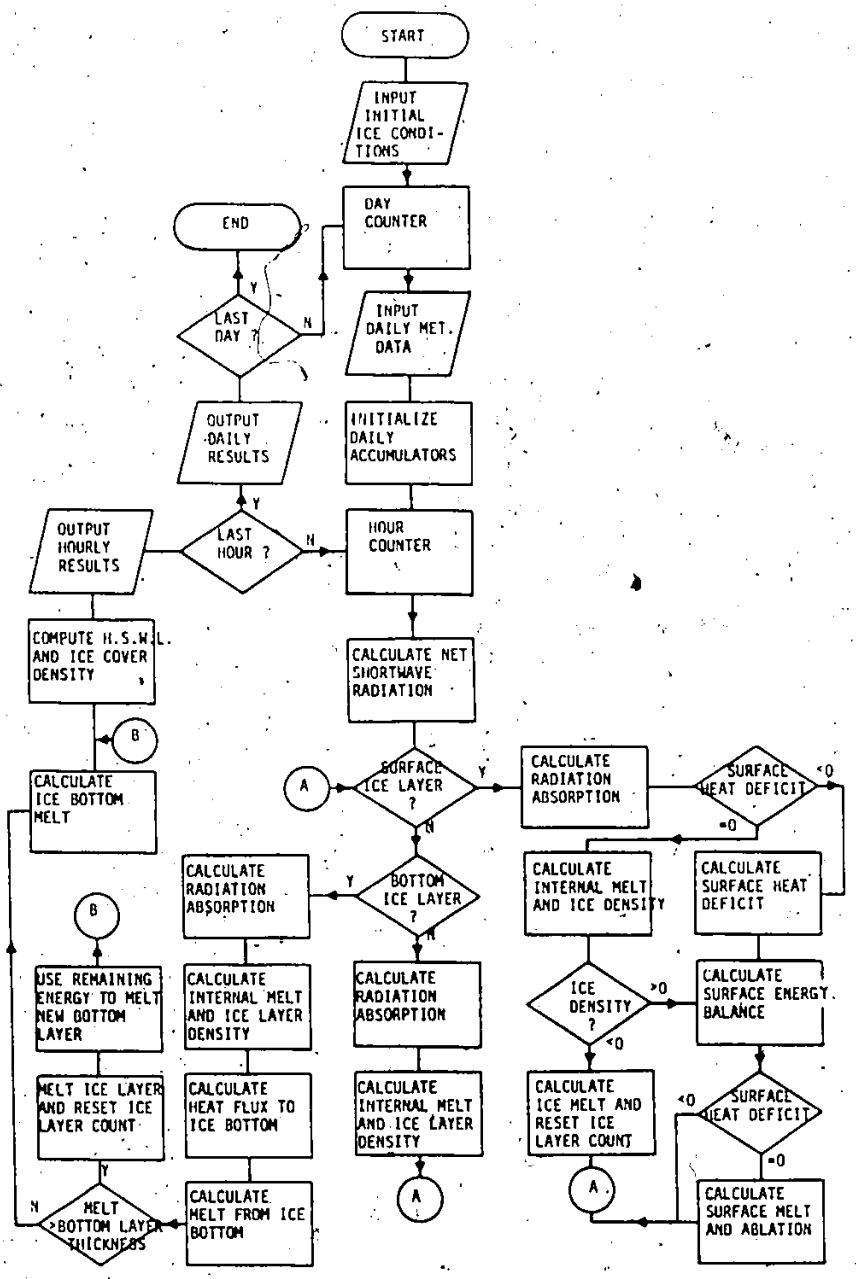

Figure 5.1. Simplified flow chart of the one-dimensional ice melt model.

Table 5.1

Input and Output Variables for the One-Dimensional Model

Input

Variable	Frequency	Symbol
Number of computation days	Once	T
Ice layer thickness	Once	Δz_i
Initial ice thickness	Once	H
Height of meteorological measurements	Once	z
Distance of water temperature below bottom of ice cover	Once	zw
Ice albedo	Daily	α_i
Net longwave radiation of ice surface	Daily	L^*_i
Water temperature	Daily	T_w
Air temperature	Hourly	T_z
Vapour pressure	Hourly	q_z
Incident shortwave radiation	Hourly	$K_\downarrow$
Wind speed	Hourly	u_z
Air pressure	Hourly	p^z
Rainfall	Hourly	R

Ouput

Variable	Frequency	Symbol
Sensible heat flux	Hourly, daily	Q_H
Latent heat flux	Hourly, daily	Q_E
Absorbed shortwave radiation flux	Hourly, daily	Q_R
Water heat flux	Hourly, daily	Q_W
Heat flux from precipitation	Hourly, daily	Q_P
Upper ice surface melt (WE)	Hourly, daily	$(dh/dt)_{us}$
Internal ice melt (WE)	Hourly, daily	$(dh/dt)_{in}$
Lower ice surface melt (WE)	Hourly, daily	$(dh/dt)_{ls}$
Upper ice surface ablation	Hourly	$(dH/dt)_{us}$
Lower ice surface melt	Hourly	$(dH/dt)_{ls}$
Ice thickness	Hourly	H
Hydrostatic water level	Hourly	h_{wl}
Ice density profile	Daily	ρ_i
Total melt energy	Daily	
Total melt (WE)	Daily	

once each day and this was assumed to represent the mean daily water temperature. The longwave radiation balance was computed using Eq. 5.5, but, being calculated as the residual of the other three radiation terms, substantial error may exist for short periods. Such error diminishes when the values are averaged over daily intervals. Similarly, the shortwave albedo becomes more reliable when daily values are used.

5.2.2 Initialization

The ice cover model used for these calculations consists of many layers, the number of which depended upon the initial ice thickness and the layer thickness. For example, given an ice cover of 2.4 m, a layer thickness of 0.02 m was considered to be a reasonable compromise between computational accuracy and computing time. Each layer was assigned an upper and a lower boundary, an initial ice skeleton density equal to the density of pure ice and an accumulator for the amount of absorbed radiation since the beginning of melt.

At this time, all the other accumulating variables were set to zero and the physical constants were specified. Accumulating variables required for daily calculations were reset before the daily computations commenced.

5.2.3 Internal Ice Melt

The internal melt of the ice cover was calculated sequentially for each layer, based on Eq. 5.19 to 5.21. To determine the extinction coefficient, Eq. 5.19 is rewritten as

$$e = -\ln (I_s / I_{zi}) / zi \qquad (5.23)$$

When applied to monochromatic light, e is known as a spectral absorption coefficient and is constant with depth in a medium. The spectral absorption coefficients for water and ice in the shortwave spectrum are shown in Fig. 5.2. The summary diagram of Goodrich (1970) is nearly identical. The practical use of spectral absorption coefficients is limited since the spectral distribution shortwave radiation varies with atmospheric conditons and is rarely recorded continuously. If integrated irradiances are used in Eq. 5.23 then e becomes a bulk extinction coefficient and loses its independence of material thickness. The attenuation of the radiation in growing and melting sea ice and in growing freshwater ice has been examined extensively (Maguire 1975, Grenfell and Maykut 1977). In contrast, the coefficient for melting lake ice is little known. This study therefore examines the extinction coefficient during the melt period. Surface irradiance is obtained with

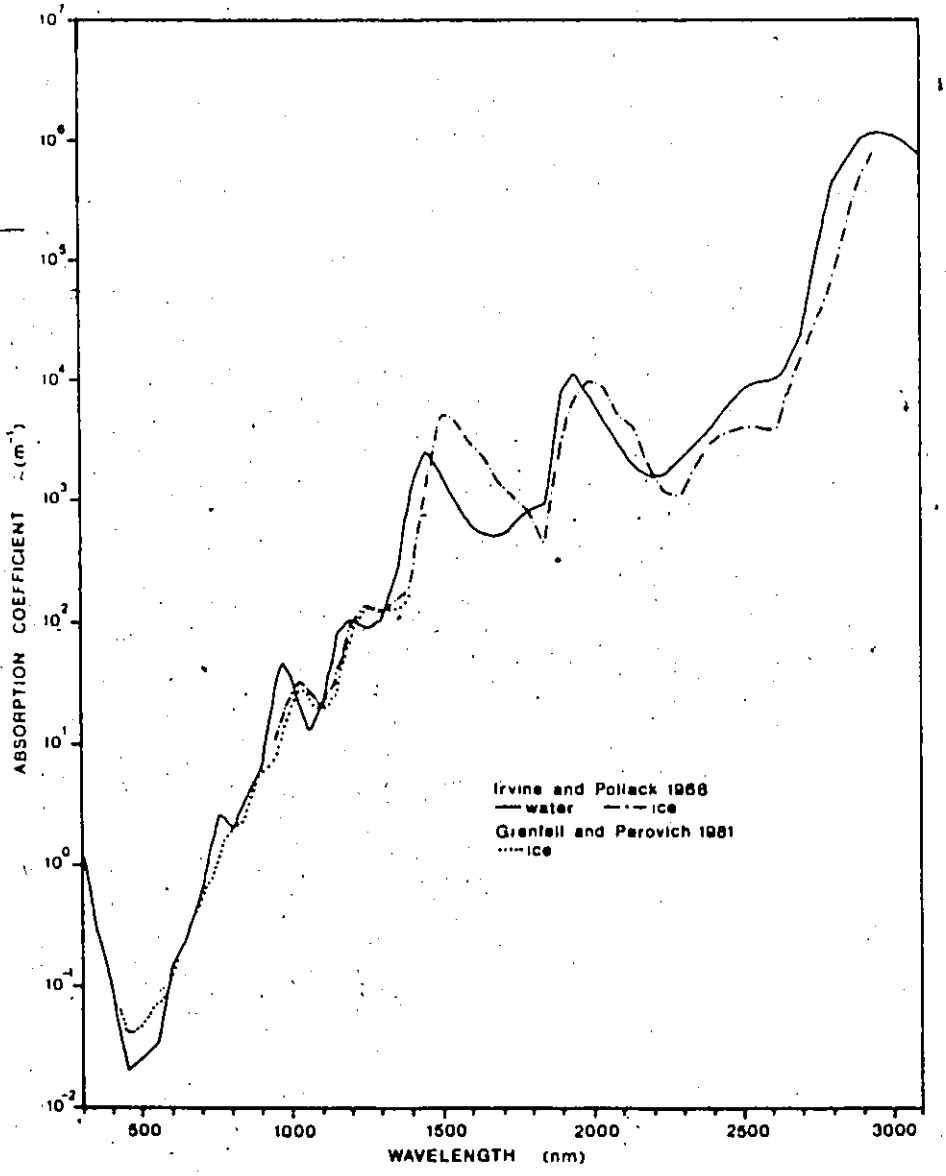

Figure 5.2. Shortwave radiation absorption coefficients for pure ice and water.

(5.24) $I_s = (1 - \alpha_i) K\downarrow$

The bulk extinction coefficient for the entire thickness of the Small Lake ice cover, ranged from 0.65 to almost 1.0 m^{-1} with 0.8 m^{-1} being a typical value. The values obtained in other studies are given in Table 5.2. The extinction coefficients found in this study are consistent with those of Hobbie (1973), Bolsenga (1980) and Roulet (1982) but not with Gorelkin (1980). It is possible that some white ice may have been included in the last study.

The bulk extinction coefficient for the entire ice cover is not particularly useful because melting lake and sea ice have an upper layer of approximately 0.15 m of porous ice above the hydrostatic water level that greatly attenuates radiation. The absorption coefficient for this layer averaged 4 m^{-1} for the Small Lake ice cover in 1981. Thus the remaining ice below the hydrostatic water level must have averaged 0.3 m^{-1}. The latter value is consistent with Fig. 5.3 for the spectral region of the photocells used in this study (peak wavelength 615 nm) and suggests that the lower portion of the lake ice cover behaves like pure ice.

Grenfell and Maykut (1977) examined the attenuation of shortwave radiation in melting sea ice and present both bulk and spectral extinction coefficients in the wavelength range from 400 to 750 nm. The bulk extinction

Table 5.2

Extinction Coefficients in Various Types of Ice

Authors	Absorption Coefficient (m^{-1})	Ice Conditions
Goldman et al (1967)	0.4-0.55	melting lake ice
Hobbie (1973)	0.52-1.2	calculated from diagram for melting lake ice
Maguire (1975b)	1.5-2.0	clear, cold ice
	20.0	cloudy ice
Bolsenga (1978,1980)	0.6-0.8	melting black lake ice with some surface water
	4.8-5.2	frozen brash ice
Gorelkin et al (1980)	5.2	Saturated, transparent, loose lake ice
Roulet (1981)	5.0-12.0	snow-ice in spectral range 400-700 nm
This Study	0.65-1.0	melting lake ice
	4.0	porous surface layer
Untersteiner (1961)	1.5	calculated from sea ice thermal profile
Weller (1969)	1.1	sea ice
	0.7	blue ice
Adams (1975)	1.2	melting sea ice
Grenfell and Maykut (1977)	10.5	white surface layer of melting sea ice on cloudy day, bulk value
	17.1	bulk value on a clear day
	1.4-1.5	sea ice interior
	3.0-20.0	spectral range 400-750 for surface layer

coefficients were very large near the surface of the porous ice layer (nearly 100 m^{-1}) but decreased rapidly, reaching 2 m^{-1} at a depth of 0.2 m. In the interior of the sea ice, the bulk extinction coefficient averaged 1.5 m^{-1}. Vertically averaged bulk extinction coefficients for the upper 0.1 m of white, porous surface layer were found to be 10.5 m^{-1} under cloudy skies while for clear conditions, a value of 17.1 m^{-1} applied. Spectral extinction coefficients ranged from 3 to 14.5 m^{-1} at wavelengths of 400 and 700 nm. The spectral extinction coefficients were extrapolated to 1400 nm by Grenfell (1979) where the value reached 10 m^{-1}. The bulk extinction coefficient obtained in this study for the surface ice layer applies to a 200 nm band centred on 615 nm and this too narrow to be considered representative of bulk extinction coefficient for the wavelengths (400 to 1400 nm) containing most of the shortwave radiation. Since data, similar to the sea ice results described above, does not exist for melting freshwater ice, these findings were used to estimate the appropriate vertically-averaged bulk extinction coefficient for the porous lake ice layer above the hydrostatic water level in the manner outlined below.

Grenfell and Perovich (1984) measured the incident spectral irradiance under a number of sky conditions near Barrow, Alaska. The peak irradiance was found to be in the

vicinity of 700 nm. The extinction coefficient obtained with the photocell will be most comparable to spectral extinction coefficients in the wavelength range from about 600 to 700 nm since the irradiance and photocell sensitivity peak in this band. From the data of Grenfell and Maykut (1977), the spectral extinction coefficients for the surface sea ice layer range from about 5.5 to 14 m^{-1}, with an average roughly twice as large as the bulk extinction coefficient obtained for the surface lake ice layer. An estimate of the bulk extinction coefficient valid for a larger wavelength range was obtained by dividing the mean of the two bulk extinction coefficients for the surface sea ice layer mentioned above (10.5 and 17.1 m^{-1}) in half. The resulting value of 7 m^{-1} was used to describe the shortwave extinction in the white, porous lake ice above the hydrostatic water level. This approximation procedure is based upon the assumption that the surface layers of the sea and lake ice behave in a consistent manner with respect the attenuation of shortwave radiation.

The surface bulk extinction coefficient was varied linearly with time to mimic the development of the porous surface layer at the beginning of the melt period. The initial value for the surface layer was set at 0.3 m^{-1}. The porous surface layer extended down to the hydrostatic water level. On a number of occasions the reflective

surface layer was melted faster than it could be regenerated and the ice surface became dark, with an albedo decreasing to less than 0.2. At this time the extinction coefficient was set to 0.3 m^{-1} to account for the elimination of the white, porous surface layer.

The bulk extinction coefficient for the ice below the hydrostatic water level was estimated using the spectral absorption coefficients (Grenfell and Perovich 1981) and spectral irradiances and albedos (Grenfell and Perovich 1984) for the wavelengths 400 to 1400 nm which contain most of the shortwave radiation. The bulk absorption coefficient (a), was weighted with respect to the irradiances

$$(5.25) \qquad a = \sum_{400}^{1400} a_\lambda \, (1 - \alpha_\lambda) \, K\downarrow_\lambda \, \Delta\lambda \; / \sum_{400}^{1400} (1 - \alpha_\lambda) \, K\downarrow_\lambda \, \Delta\lambda$$

Here, λ is the wavelength and a_λ, α_λ, $K\downarrow_\lambda$ are the spectral absorption coefficient, albedo and irradiance respectively. The bulk absorption coefficient calculated in this manner varied from 0.5 m^{-1} near the ice surface to 0.14 m^{-1} at a depth of 2.4 m. The mean value of 0.3 m^{-1} coincided with the measured extinction coefficient so this value was used to describe the extinction of shortwave radiation in the ice below the hydrostatic water level

Using the extinction coefficients thus computed,

the amount of energy absorbed by a given layer is

$$(5.26) \quad Q_R = I_s \, (1 - \exp(-e \, zi))$$

where I_s is the irradiance at the top of each layer and the internal melt is

$$(5.27) \quad (dh/dt)_{in} = \sum_{zi=0}^{H} Q_R \, \Delta zi$$

The skeletal density for each layer of ice is computed from

$$(5.28) \quad \rho_i = \rho_{pi} \, (\sum_{0}^{t} Q_{R(n)} \, \Delta t \, / \, J_n$$

where $Q_R(n)$ is the accumulated internal melt energy of a layer and J_n is the energy required to melt the entire layer.

The hydrostatic water level is required to determine when an ice layer becomes part of the porous surface layer. This is computed by balancing the accumulated buoyancy of lower ice layers with the weight of the layers of the surface layers. The buoyancy of an ice layer of unit cross-sectional area (F_n) is

$$(5.29) \quad F_n = \Delta zi \, (\rho_w - (\rho_i + (\rho_{pi} - \rho_i) \, / \, \rho_{pi} \, \rho_w))$$

where Δzi is the layer thickness and ρ_w is the water density. The weight of the layer of unit area (W_n) is

(5.30) $W_n = \Delta z_i \rho_i$

The hydrostatic water level is located at a depth where the weight of the ice above this level is balanced by the buoyancy below it. The ice layer containing the hydrostatic water level is located by comparing these two values for each layer, commencing at the surface. The first layer in which the accumulated weight is greater than the buoyancy contains the hydrostatic water level. Its position within the layer is determined by assuming that the gradients of both weight and buoyancy are constant in the layer.

(5.31) $$n_w = \left(\sum_{N}^{n-1} F_n \Delta n + \sum_{n-1}^{N} W_n \Delta n\right) / (W_n + B_n)$$

Here, n is the layer number, N is the total number of layers; n_w is the distance of the hydrostatic water level below the top of the layer.

5.2.4 Surface Melt

The surface ice melt energy can be calculated using Eq. 5.5 to 5.13. To obtain a value for the surface roughness from Eq. 5.9, several measurements of wind speed were made over periods of 5 to 15 minutes at Small Lake. The resultant mean value was 4.5 mm with a standard deviation of 1.5 mm.

The calculated surface melt energy could be negative if the longwave radiation loss from the surface offset the other energy components in Figs. 5.5 and 5.6 or

if the air temperature fell below 0°C. In such cases, this energy deficit was accumulated and no surface melt was permitted. The radiation absorbed by the top ice layer and positive surface melt energy were used to satisfy the energy deficit and any surplus energy was used to melt the ice.

The amount of ice melt (in W.E. units) is obtained by Eq. 5.4, but the amount of surface lowering $(dH/dt)_{us}$ is given by

$$(dH/dt)_{us} = Q_{mu} / \rho_i L_f \qquad (5.32)$$

Using ρ_i instead of ρ_{pi} allows the computation of the change in ice cover thickness. Eq. 5.29 was incorporated in the model structure to calculate the change in ice thickness in the following manner. The radiation absorbed during the hour is first used to determine the internal melting and to compute the new ice density profile. If the absorbed energy melted all the ice in the top layer (ρ_i <0) then the ice surface level is reset and the remaining energy is used to melt the new top layer. The surface ablation is obtained from Eq. 5.29 using the new ice density and the ice surface level is reset. The change in ice thickness is the difference between the old and the new ice surface levels.

5.2.5 Bottom Melt

The amount of melt (in W.E. units) at the bottom of the ice cover is calculated from Eq. 5.15 and like surface ablation, the change in the ice-water interface is

$$(5.33) \quad (dH/dt)_{ls} = Q_{ml} / \rho_i L_f$$

The computed ice melt is removed from the bottom ice layer and the ice bottom level reset. If there is more melt than the layer thickness, the remaining energy is used to melt the new bottom layer. Again, the change in ice thickness is the difference between the new and old ice bottom levels.

5.2.6 Output

The output variables are indicated in Table 5.1. The melt energy and resulting melt for each component are printed hourly. A summary is printed at the end of each day. The other output variables describing the ice characteristics are also listed hourly. In addition, the ice density profile of the ice cover at 2400h is plotted at the end of the day.

5.3 Computed Results

5.3.1 Radiation Fluxes

Net radiation, incident and reflected solar radiation and albedo were measured in the field and used

with Eq. 5.5 to determine the net longwave balance of the ice surface. Fig. 5.3 and 5.4 indicate the variation of the daily totals for each of these radiation components.

The incident shortwave radiation ranged from 8 to 32 MJ/m² in both years. In 1981, a gradual decrease in radiation was caused by a general increase in the amount of cloud cover during the study period. In 1980, no trend was obvious. The albedo of the ice surface in both years declined with time, but was more noticeable in 1981, reaching a minimum of 0.1 at the end of the melt period.

In 1981, the net radiation showed an increase with time despite decreasing solar radiation while in 1980, net radiation tended to vary with solar radiation. This was due primarily to the more extreme change in albedo during the 1981 melt season.

The net longwave radiation component displayed a similar behaviour in both years of study. In 1981, the net longwave radiation increased throughout the melt period, the inverse of shortwave radiation. Although the pattern was still present in 1980, it was not as clear. During periods of heavy cloud cover, the net longwave radiation became a heat source (positive flux) rather than the usual heat loss. This phenomenon occurred as a result of the ice surface temperature being constrained to 0°C. At the Resolute Airport weather station with similar

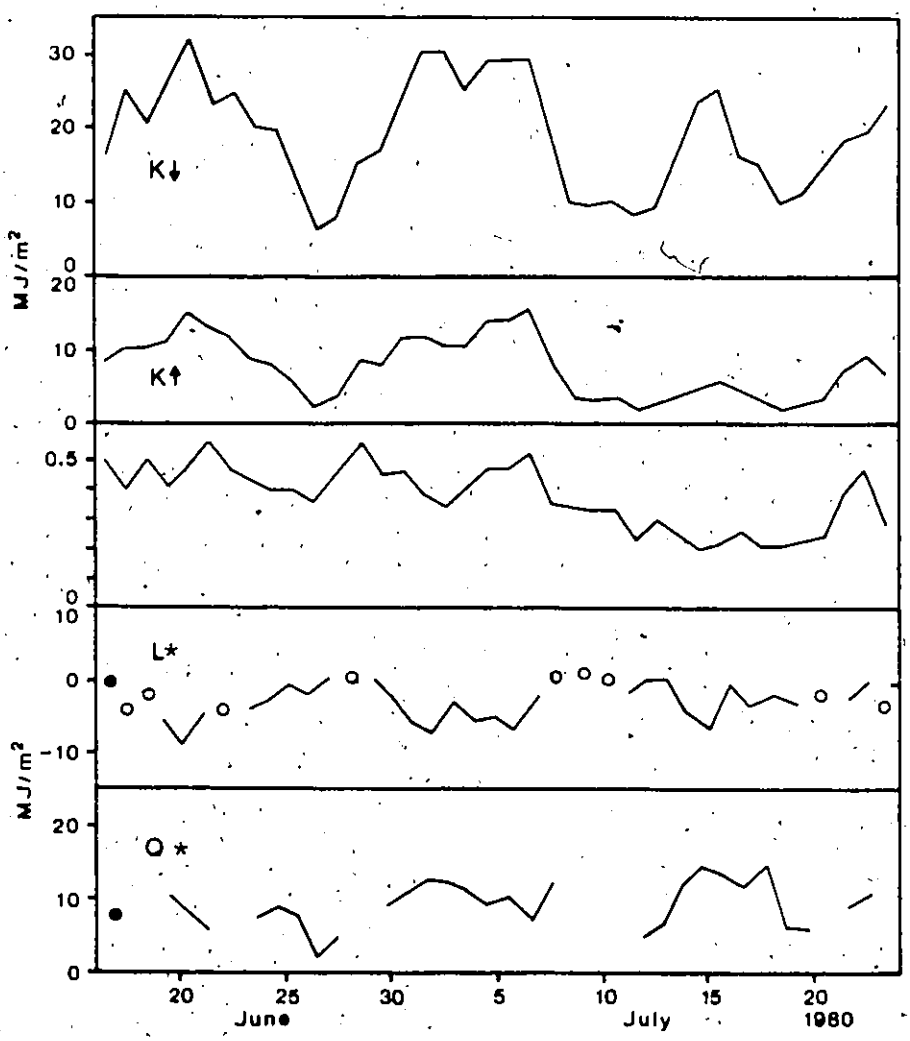

Figure 5.3. Daily ice surface radiation balance for Small Lake, 1980. The solid circles represent single values while open circles represent estimated values. Missing data for Q* have not been estimated.

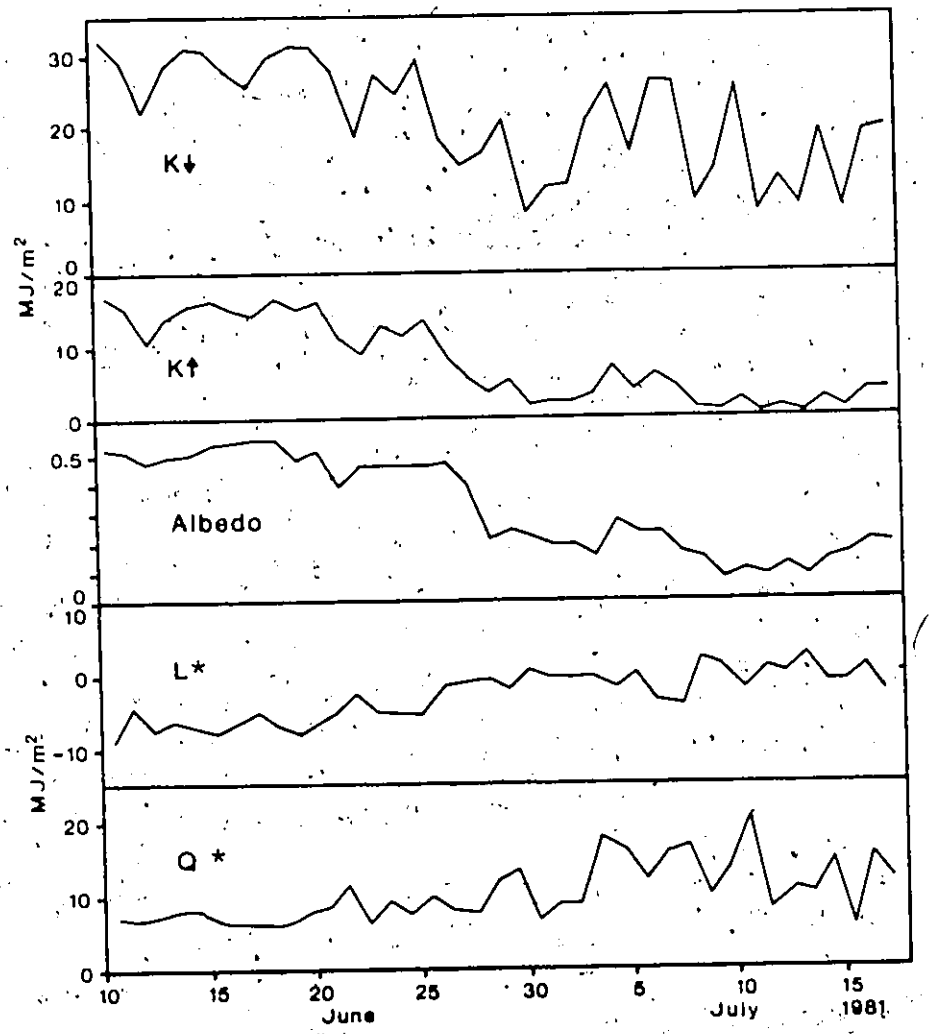

Figure 5.4. Daily ice surface radiation balance for Small Lake, 1981.

atmospheric conditions, the temperature of the gravel surface was not constrained and may reach 10°C or more. Throughout the melt period, the longwave radiation balance at Small Lake was consistently 1 to 2 MJ/m² higher than at the Resolute Bay airport site and the flux was positive for 20 percent of the time. In 1980, net longwave radiation was missing for more than half of a day on several occasions. The missing net longwave radiation was estimated from the net longwave radiation at the Resolute Airport weather station using the Stefan-Boltzman Law

$$(5.34) \quad L^*_g = E\ B\ T_{sg}^4$$

where $L\uparrow_g$ is the longwave flux emitted from a surface with a temperature T_{sg} , B is the Stefan-Boltzman constant and E is the surface emissivity. The emitted longwave flux was calculated for the land and ice surface using the following assumptions: 1) the ice surface temperature was 0°C. while the mean daily air temperature of the weather station was a reasonable approximation of the mean daily land surface temperature and 2) the surface emisivities of both surfaces were 0.95. The estimated net longwave balance for the ice (L^*_i) was

$$(5.35) \quad L^*_i = L^*_g + (L\uparrow_i - L\uparrow_g)$$

where L^*_g is the net longwave radiation for the land while

$L\uparrow_i$ and $L\uparrow_g$ are the emitted longwave fluxes for the ice and for the land. The values estimated in this manner are indicated in Fig. 5.4 by discrete points.

5.3.2 Turbulent Heat Fluxes

The turbulent heat fluxes for 1980 and 1981 are plotted in Figs. 5.5 and 5.6. Sensible heat fluxes ranged from slightly negative values to more than 20 $MJ/m^2/d$. There was a general increase with time as the air temperature rose, with peak values attained during periods of high wind. The latent heat flux followed a trend similar to sensible heat since it was also strongly influenced by the wind speed. Early in the melt season, the latent heat flux was negative as sublimation occurred. As the air warmed and the humidity increased vapour condensed on the ice to release latent heat. The maximum latent heat fluxes for 1980 and 1981 were with values of 11 and 9.8 $MJ/m^2/d$. However, in 1980, the minimum values were much smaller and of longer duration. This can be attributed to a drier atmosphere at the beginning of melt and in the cool period near the end. In 1980, 86 percent of the surface melt energy was supplied by the sensible heat flux and the latent heat flux provided he remainder. In 1981, the equivalent values were 76 and 24 percent respectively.

The heat added to the ice surface by rain was

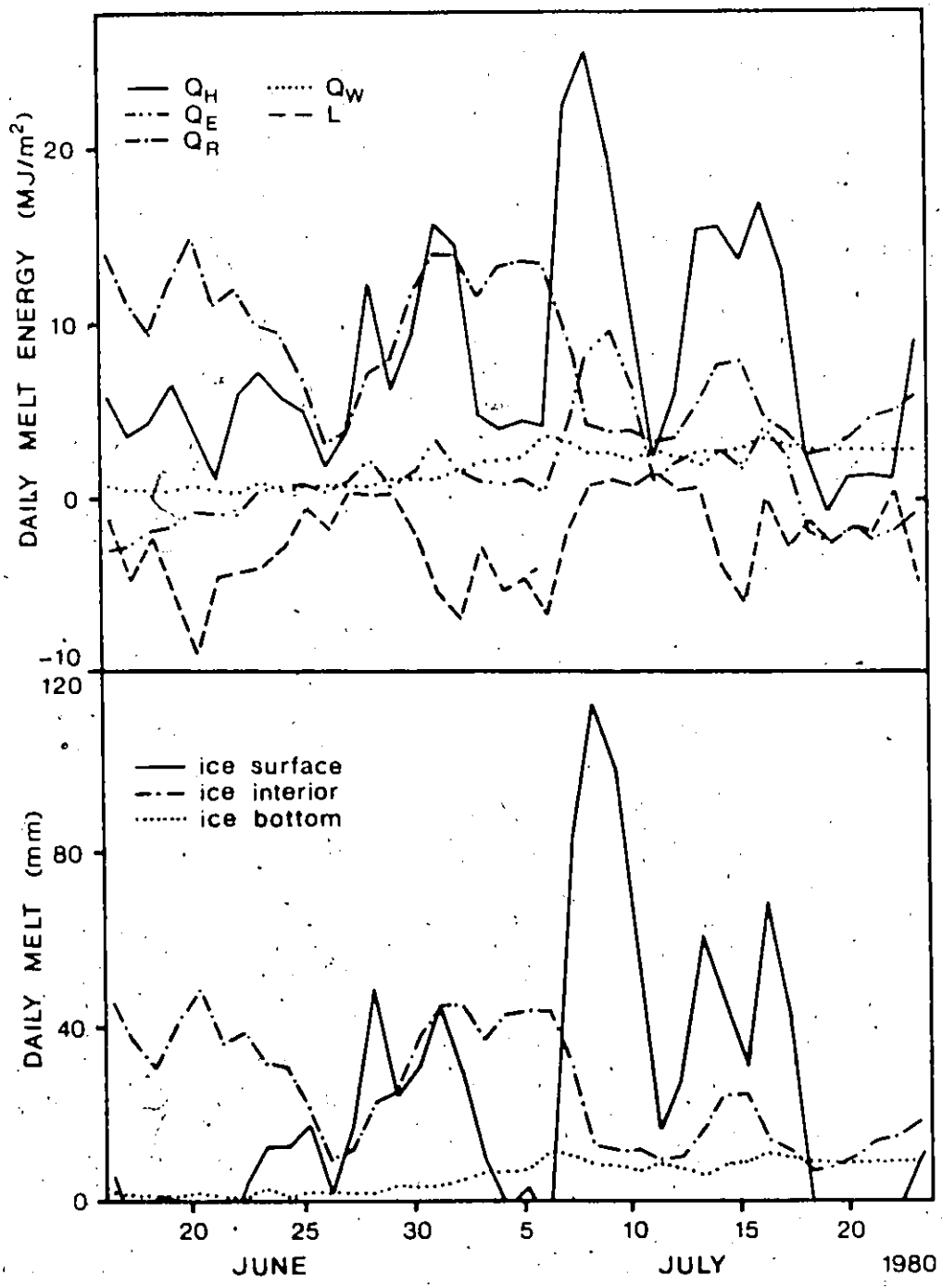

Figure 5.5. Daily energy balance totals for the Small Lake ice cover, 1980. The energy inputs are plotted in the upper section while the resultant melt components are displayed in mm of water equivalent in the lower section.

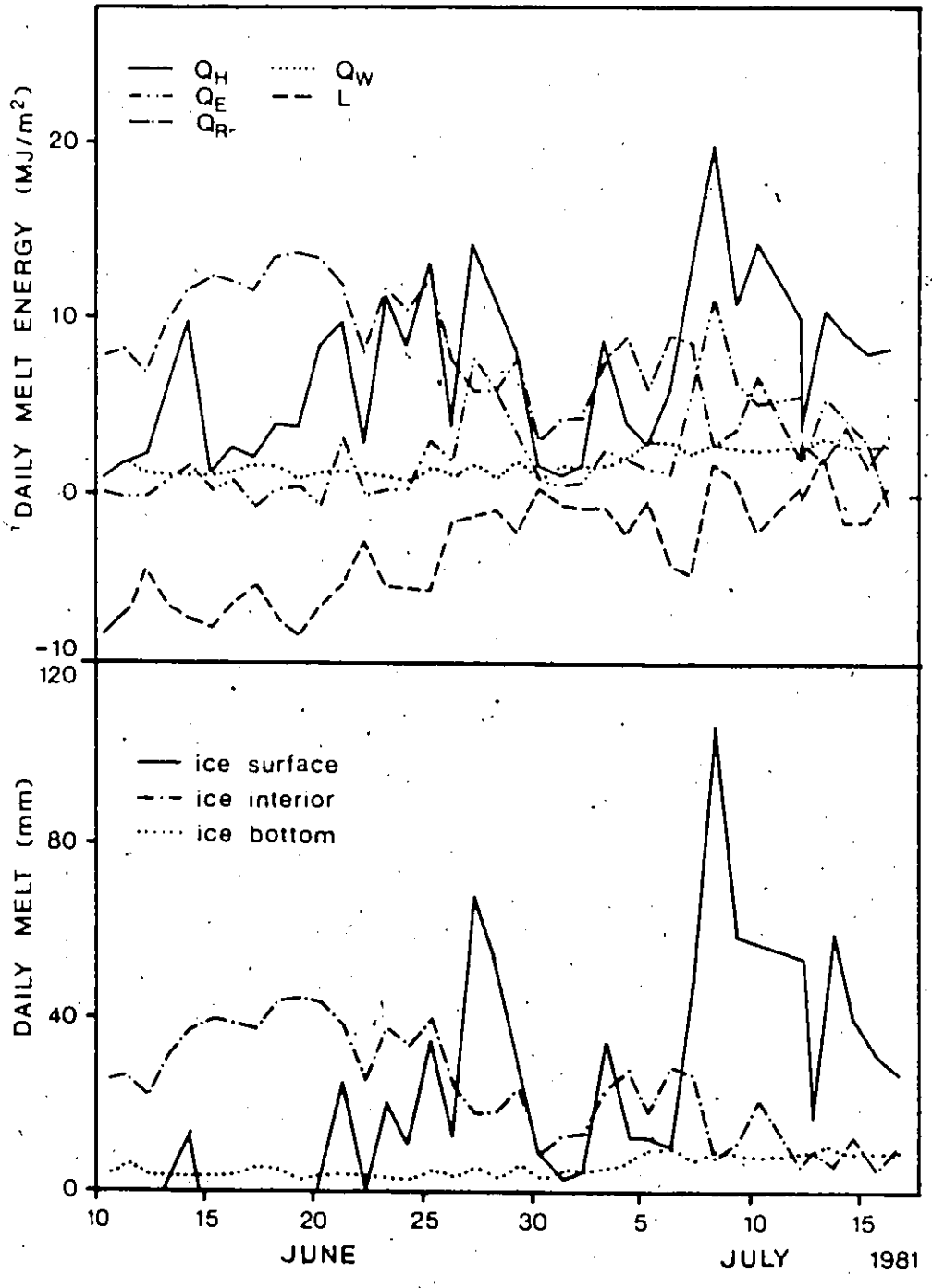

Figure 5.6. Daily energy balance totals for the Small Lake ice cover, 1981. The energy inputs are plotted in the upper section while the resultant melt components are displayed in mm of water equivalent in the lower section.

insignificant.

5.3.3 Water Heat Flux

The heat flux from the water to the ice bottom was computed daily using Eq. 5.17 and the water temperature measured at 0.05 m beneath the ice. In 1980 and 1981, The maximum heat flux was 3.5 and 4.2 $MJ/m^2/d$ respectively. The minimum values for these years were 0.4 and 0.8 $MJ/m^2/d$. In both years, the water heat flux increased gradually throughout the melt period as the water temperature increased.

5.3.4 Melt Components

The heat fluxes were partitioned to determine the melt on the ice surface, at the ice bottom and inside the ice cover. The melt on the upper ice surface was the sum of sensible and latent heat, net longwave radiation and the heat added by rain. The bottom ice melt was the result of the water heat flux while the internal melt was determined by the amount of absorbed radiation. These three components of the total ice melt are plotted in Fig. 5.5 and 5.6

The surface melt accounted for 39 percent of the melt in 1980 and 40 percent in 1981. No melt occurred when the combined heat flux was negative, but once the energy lost by the net longwave radiation was offset by the other

energy terms, the surface melt increased rapidly. The temporal pattern of the surface melt was similar to that for the sensible heat flux since it is the dominant energy component. In 1980, the maximum daily surface melt was 113 mm (water equivalent, WE) which is similar to the 108 mm (WE) peak value of 1981.

Internal melt was the largest melt component, contributing 49 percent of the melt in both years. The variation in internal melt closely follows the shortwave radiation. However, internal melt decreased throughout the melt period due to a thinning of the ice and hence a decrease in the amount of radiation that could be absorbed. The maximum internal melt rates were 49 mm/d (WE) in 1980 and 45 mm/d (WE) in 1981. By the end of the melt period, the internal melt had declined to approximately 15 mm/d (WE).

Ice bottom melt was the smallest in magnitude, accounting for 10 and 12 percent of the total melt in 1980 and 1981.

5.4 Comparison of Observed and Computed Results

5.4.1 Internal Melt

Changes in ice skeleton density reflect the amount of internal melt. Ice density was computed for each ice layer and the model printed an ice density profile daily. The ice density plot for 1981 is given in Fig. 5.7. The

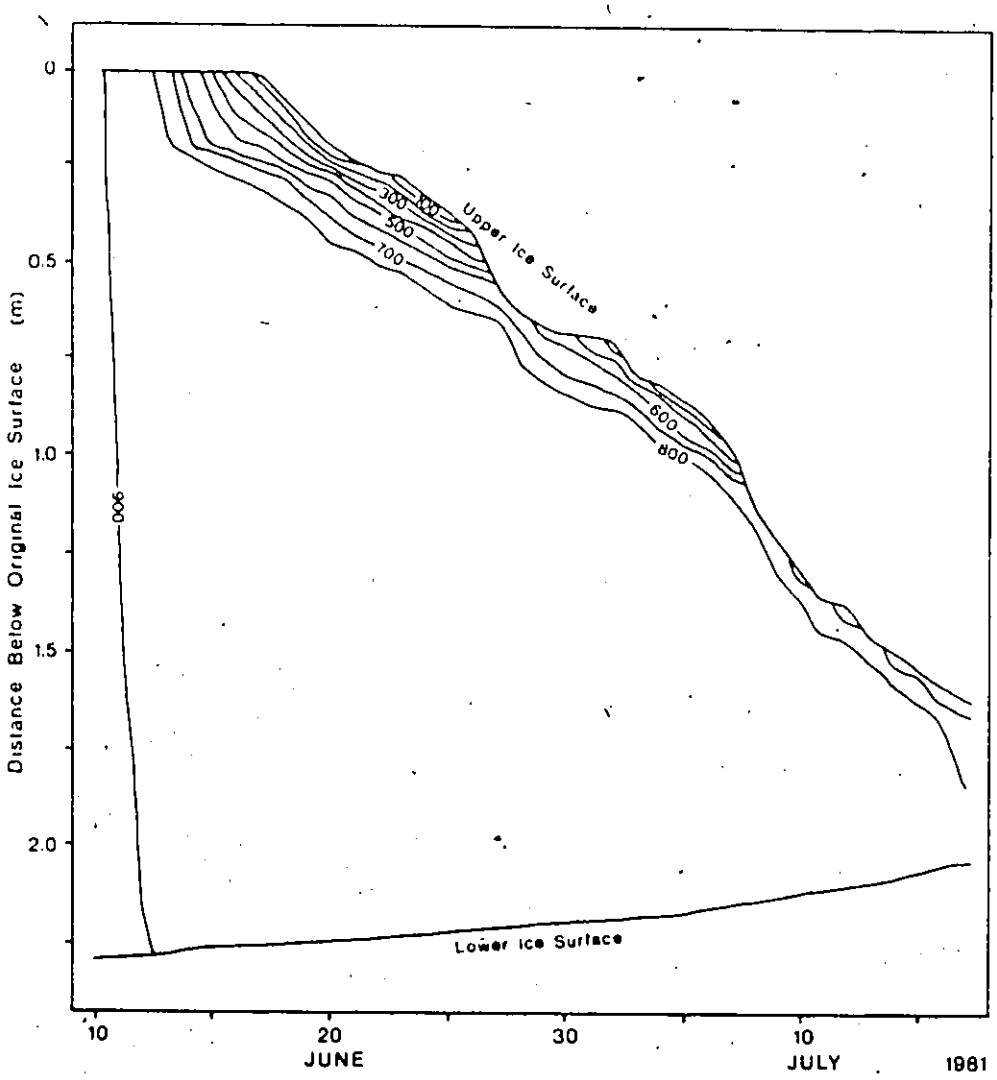

Figure 5.7. Calculated ice density isopleths for the Small Lake ice cover, 1981. Note that the reference datum for the y-axis is the original ice surface.

observed ice density data for 1980 is limited, so only the results from 1981 will be examined here.

An initial ice density of 917 kg/m³ was used for all layers on the first day of computation. This is possibly an overestimate due to the presence of air bubbles trapped in the ice and some earlier internal melt along triple ice crystal boundaries as the ice warmed, but since an accurate density profile is not available, this is a reasonable starting point. For the first week of melt, the computed ice density in the upper layers of the ice cover decreased rapidly as internal melt was concentrated there. The observed density profiles in Fig. 5.8 show the development of the low density surface layers and the general density increase with depth. Also plotted are the computed values for the same layers. On June 18th, the computed values correctly estimated the surface layer density and the density at depth (0.3 m). In the central section of the density profile on this date, the computed values underestimate the ice density by as much as 50 percent. However, the observed hydrostatic water level was 0.2 m closer to the surface than modelled. This resulted in increased model internal melt since a larger extinction coefficient was being used. On June 22nd, the fit has improved substantially and is close to or within the expected accuracy of the observed values. On both of these dates, the surface densities, which are crucial in

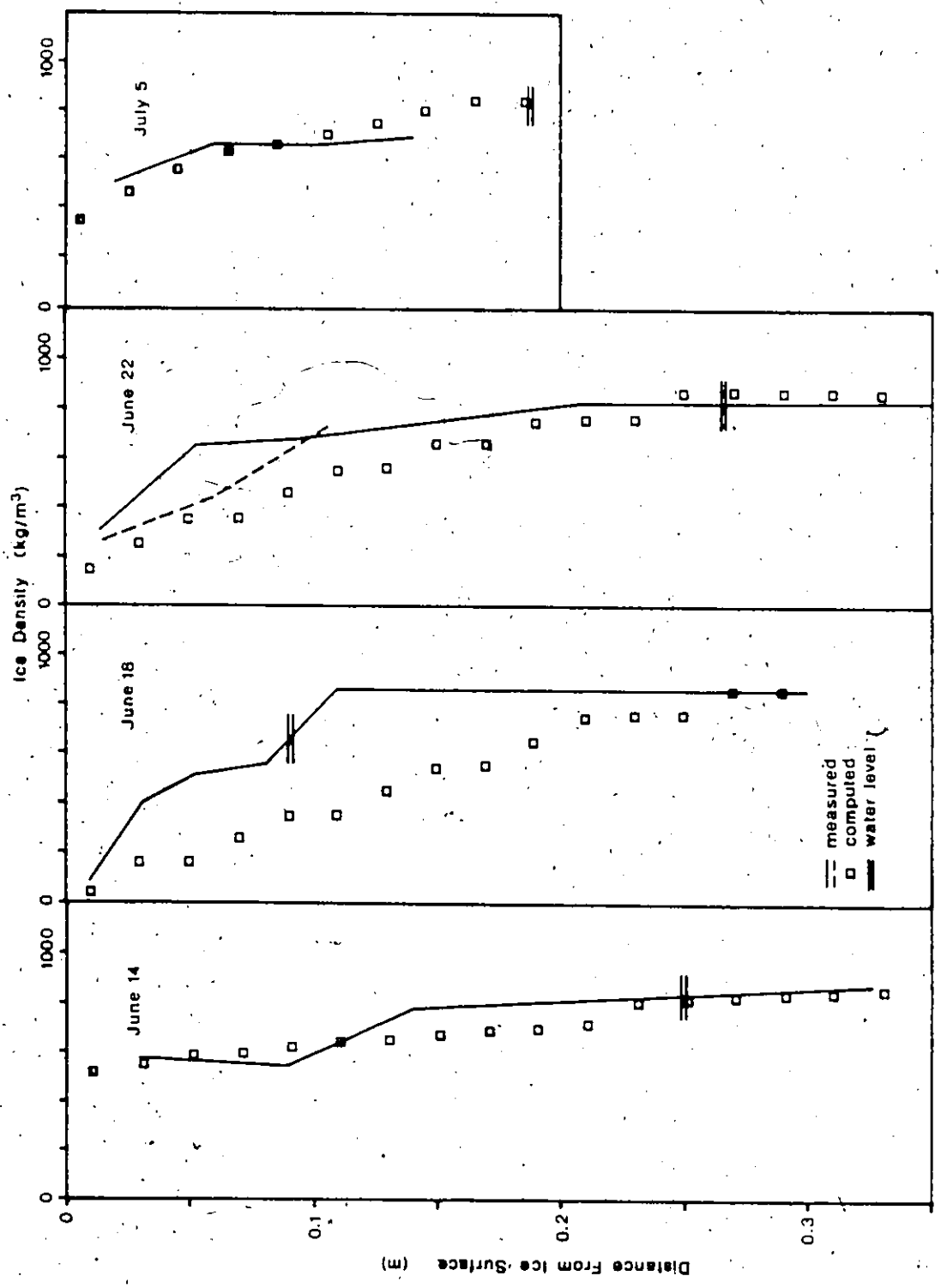

Figure 5.8. Observed and calculated ice density profiles from Small Lake on four dates in 1981.

computing the surface ablation, are close to the observed values. The measured and computed density profiles on June 14 and on July 5 are almost identical.

At the end of the melt period when only about 0.5 m of ice remained, the computed results suggest that the mean ice density was approximately 780 to 800 kg/m³. Density determined from cores taken from the ice cover yielded a mean value of 720 kg/m³ with a range of 190 kg/m³. This relatively high ice density indicated that little radiation has been absorbed in the lower ice layers which is supported by the computed results.

5.4.2 Ice Thickness

Once the ice densities in the upper and lower ice layers are calculated, the melt energy computed for these surfaces (Fig. 5.6 and 5.7) can be converted into a change in ice thickness. The computed and observed ice thicknesses for 1980 are shown in Fig. 5.9. The computed results compare favourably for two periods: 1) June 29 to July 6 and 2) July 19 to July 23. Significant departures occur from the beginning of melt to June 29 when the ice thickness is overestimated. This period of error is caused by a negative surface energy balance due to a large negative net longwave balance for the first 6 days, halting surface ablation but permitting internal melt. The

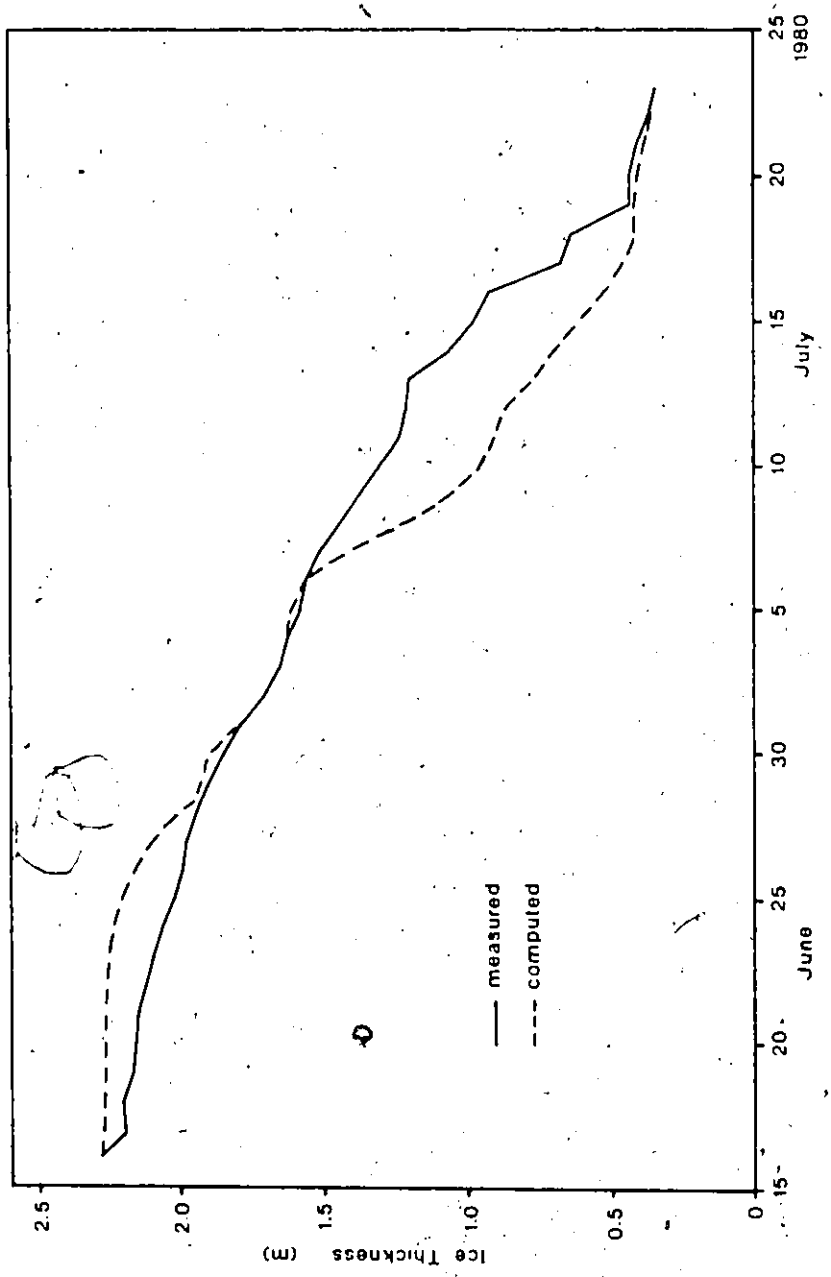

Figure 5.9. Measured and computed ice cover thickness during decay on Small Lake, 1980.

model compensated for the initial underestimation by rapidly melting the surface ice layers whose density had been greatly decreased during the period of halted surface melt. From July 7 to July 9 melt was overestimated because it coincided with a major wind storm when much data were lost and had to be estimated. For July 17 to July 19, the thickness change was underestimated, but for the remaining period, the daily thickness changes could be determined satisfactorily.

For 1981, the computed and observed ice thicknesses do not seem comparable at first glance (Fig. 5.10). The final computed thickness is 0.44 m compared to a measured value of 0.68 m and the predicted ice thickness is consistently thinner than observed. However, most of this overestimation of the ice thickness occurs during 3 periods, each lasting two days. The discrepancies are the result of surface melt errors which will be examined below. Each time a major deviation occurred (Fig. 5.10), plotting of the computed curve was discontinued, and a new curve then started with the initial value set to that ice thickness observation.

Overall, the model predicts reasonably, the daily ice thickness changes for most of the days. However, substantial errors arising in the prediction for any one day can strongly bias the ice thickness estimates for the subsequent period.

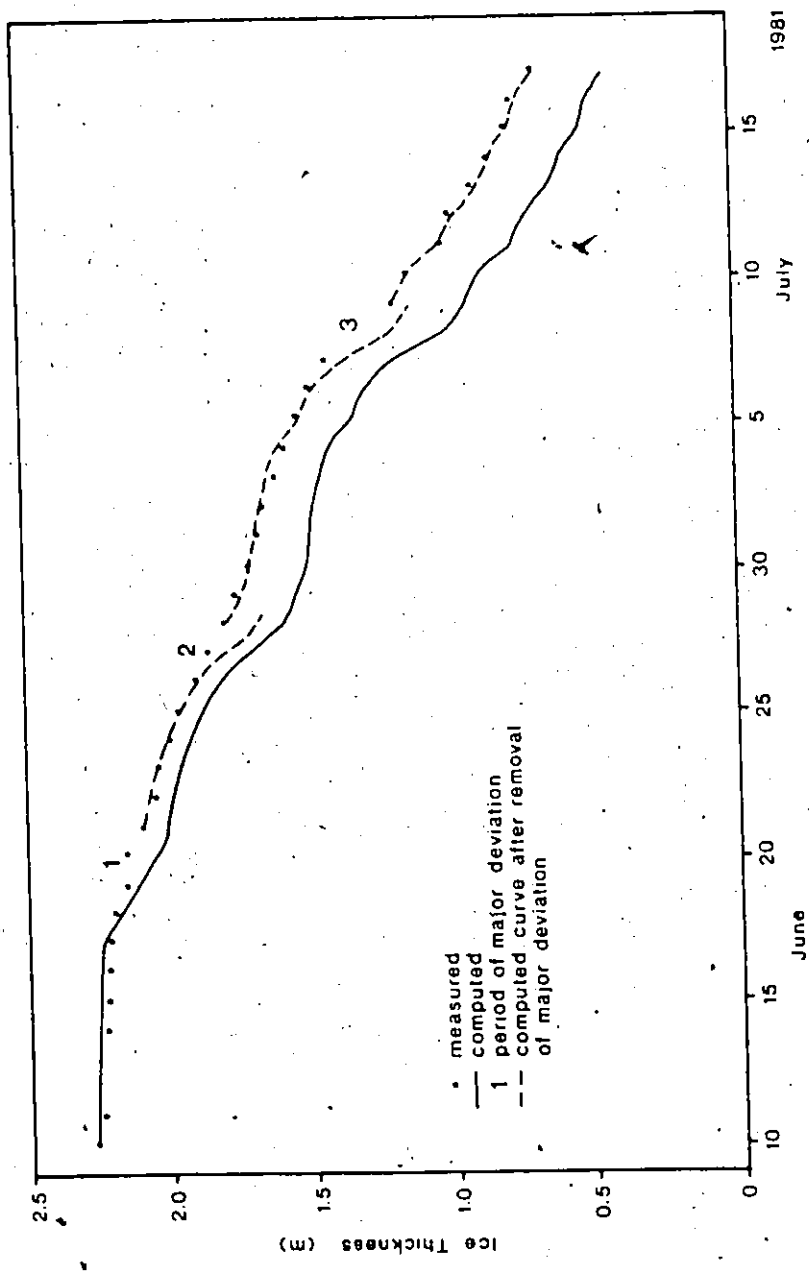

Figure 5.10. Measured and computed ice cover thickness during decay on Small Lake, 1981. After each period of deviation from the observed thickness, the computed curve was offset and restarted from the measured value on that date.

5.4.3 Surface Melt

It is not possible to separate the observed ice thickness change in 1980 into a surface melt and a bottom melt component since the ice ablation stakes appear to have not remained stationary and hence are unreliable. Thus, this section will discuss only the 1981 results.

A scatter plot of the computed and observed ice ablation for the upper surface shown in Fig 5.11. A 48 hour period (2 daily measurements) was chosen for the points in this plot to minimize the error the measured daily ablation values. More than half of the points lie outside the 20 percent error limits. A comparison of the calculated and observed surface values on a cumulative basis (Fig. 5.12), shows that most of the error came from three periods. In the first period, June 18 to June 22, ice density was underestimated (Fig. 5.8), resulting in an overestimate of ablation. The reason for the error in the second period, June 26 and June 27, is not clear. In the third period, July 9 and July 10, a major storm led to some loss of data. As in the case of the large storm late in the 1980 melt period, the model performs poorly when the windspeeds are large. During such times of rapid melt, the surface of the ice changes markedly in terms of albedo, light extinction and surface roughness. Only the changes in albedo but not the other parameters were taken

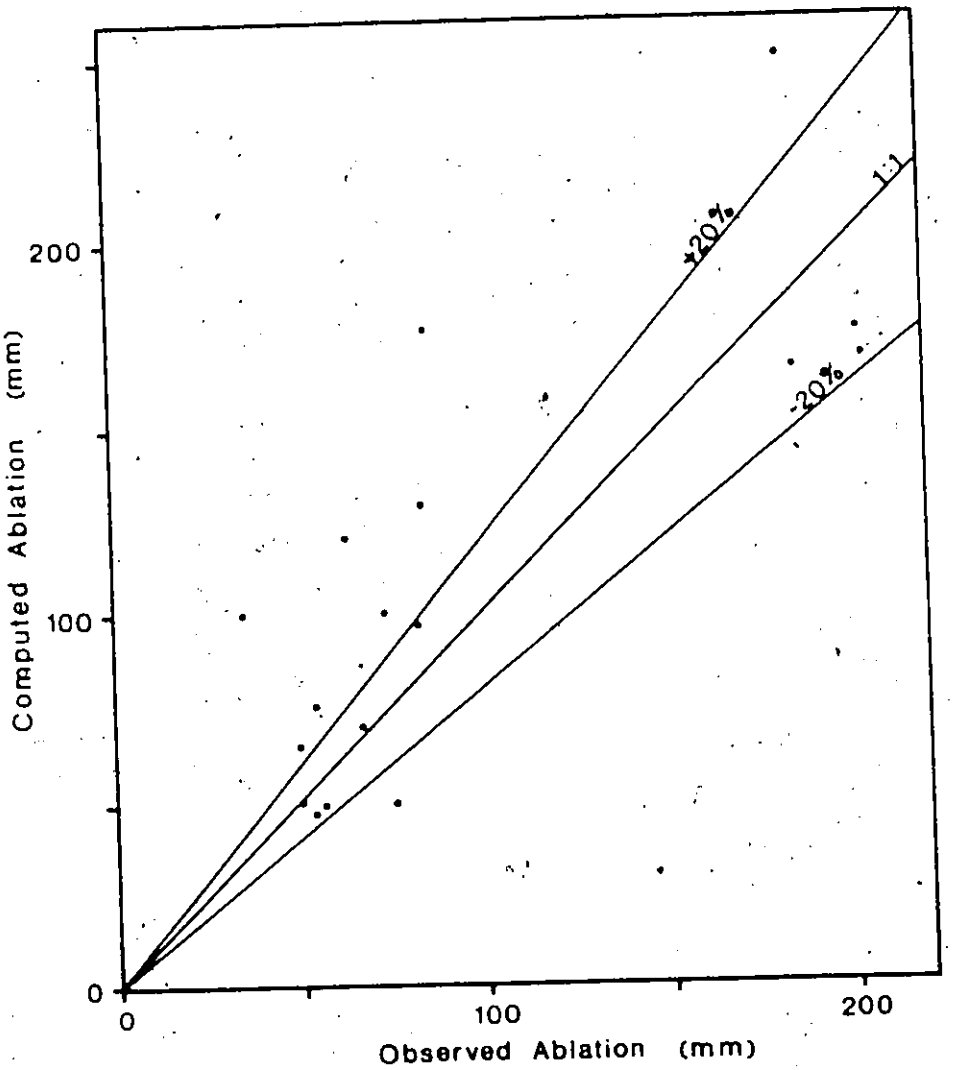

Figure 5.11. Comparison of measured and computed upper surface ice ablation, 1981. Each point is a two day total.

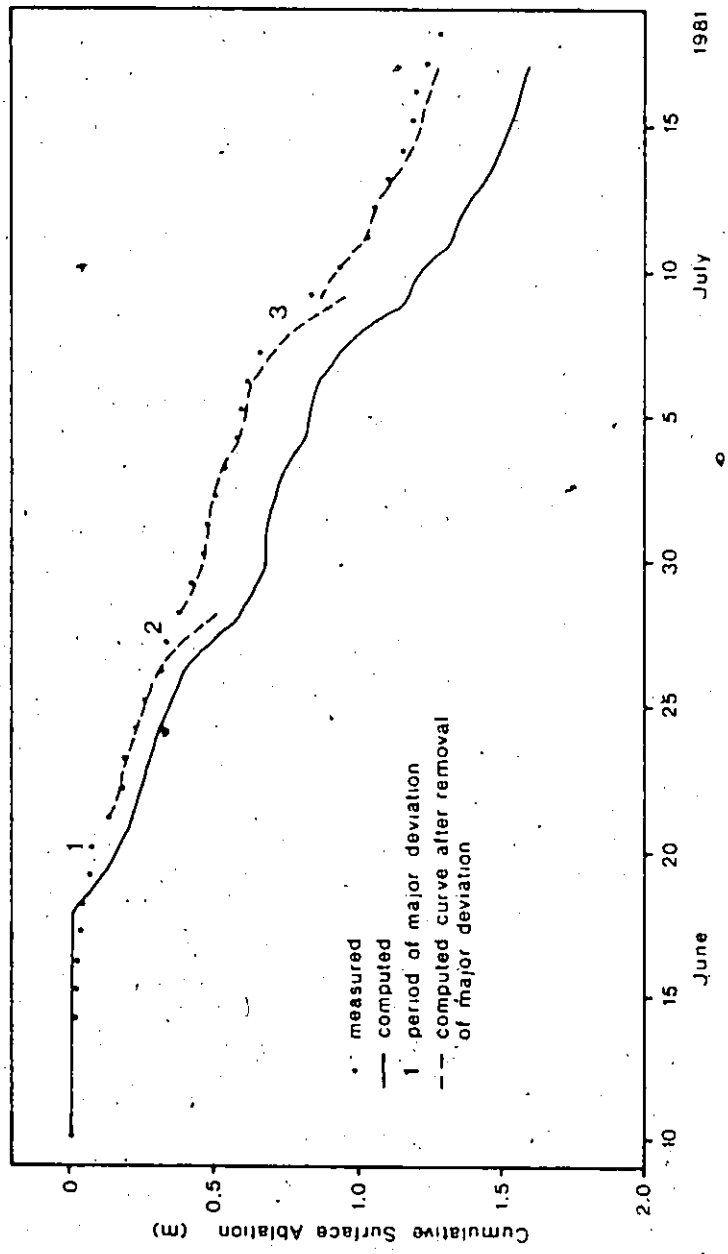

Figure 5.12. Measured and computed cumulative ablation at the upper surface, 1981. After each period of deviation from the observed thickness, the computed curve was offset and restarted from the measured value on that date.

into consideration by the model and this may accoun for the poor results.

5.4.4 Bottom Melt

The melt at the bottom of the ice cover is the least significant of the three melt components. The cumulative melt and the calculated melt for 1981 compare favourably (Fig. 5.13), with the differences rarely exceeding 20 mm until July 12. Beyond that point the model underestimates systematically. This is due to circulation of the lake water and the movement of the ice cover about the lake. These conditions invalidate the assumption of still water used in the model resulting in a total underestimate of 60 mm for the season. To model ice melt with moving water, an apparent thermal conductivity coefficient with a value greater than that for still water must be used.

5.5 Summary

The one-dimensional ice melt model described in this chapter satisfactorily predicts the ice thickness during the ice decay period. For both of the study years, energy absorbed in the ice produced 49 percent of the melt while energy received by the upper ice surface provided 40 percent and the remaining heat flux was to the lower ice surface.

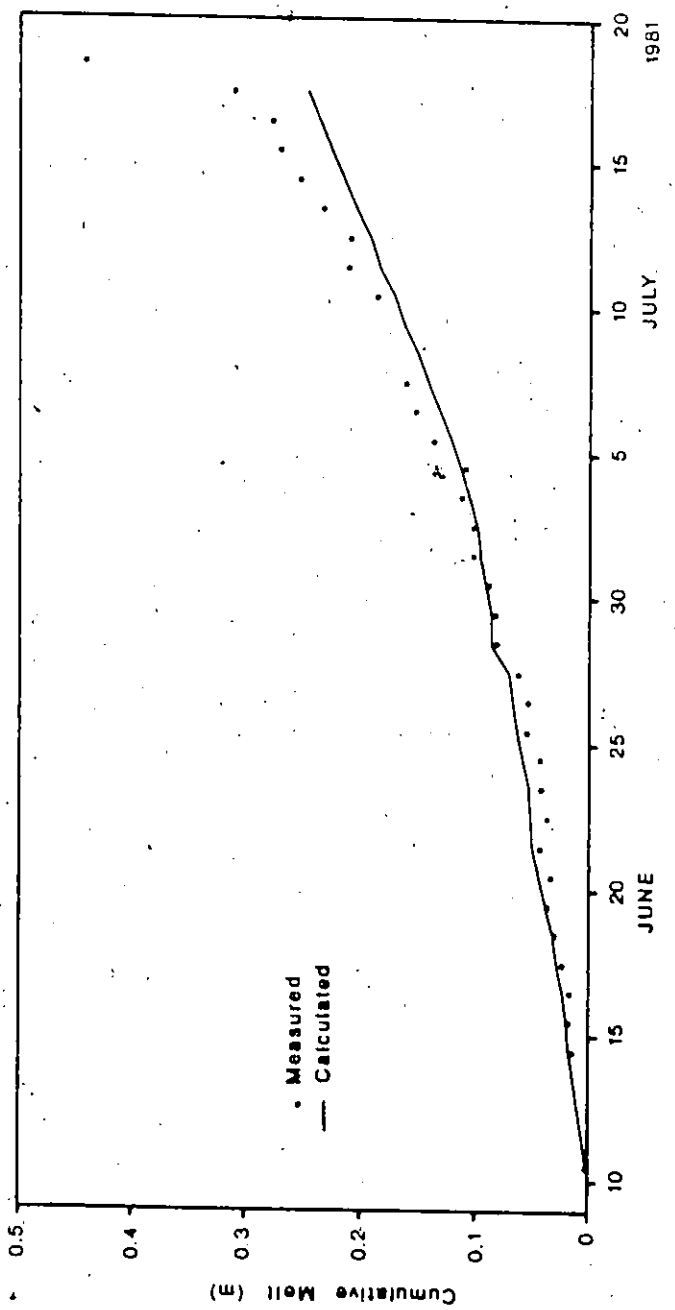

Figure 5.13. Measured and computed cumulative melt from the lower ice surface, 1981.

There were substantial deviations of the model results from the observed conditions. These are attributable to inadequacies in both the data and the model. An improved understanding of the radiation regime of melting ice is required to enhance the calculation of internal melt and hence ablation from the upper ice surface. Additional values of the surface roughness coefficient are needed to determine its variability with surface conditions.

The model can be improved by incorporating the calculation of the ice temperature profile. This would permit the calculations to commence in the premelt period and allow the effects of diurnal freezing or cold periods during decay to be examined. Water temperature calculated from the radiation absorbed by the water would eliminate the need to measure the water temperature but determining a correct value for the thermal conductivity of water in the later part of the decay period would remain a problem.

CHAPTER 6

TWO-DIMENSIONAL ICE MELT MODEL

6.1 Model Description

The one-dimensional ice melt model can adequately describe the melt occurring at a site, but gives no indication of the behaviour of the ice on the remainder of the lake. To accomplish this latter goal, the spatial aspects of the melt processes must also be taken into consideration. In the model described in this chapter, the three dimensional problem posed above is reduced to an array of simpler two-dimensional ones by determining the change in ice thickness along transects normal to the shore (Fig. 6.1). The structure of each transect (Fig. 6.2) consists of a number of points where the melt is calculated one-dimensionally. A generalized flow chart for this model is given in Fig. 6.3.

6.1.1 Data Requirements and Initialization

The information required by the model, in addition to that indicated in Table 5.1, is given in Table 6.1. The lake water level is the only item that requires daily update as the others are necessary for the model initialization.

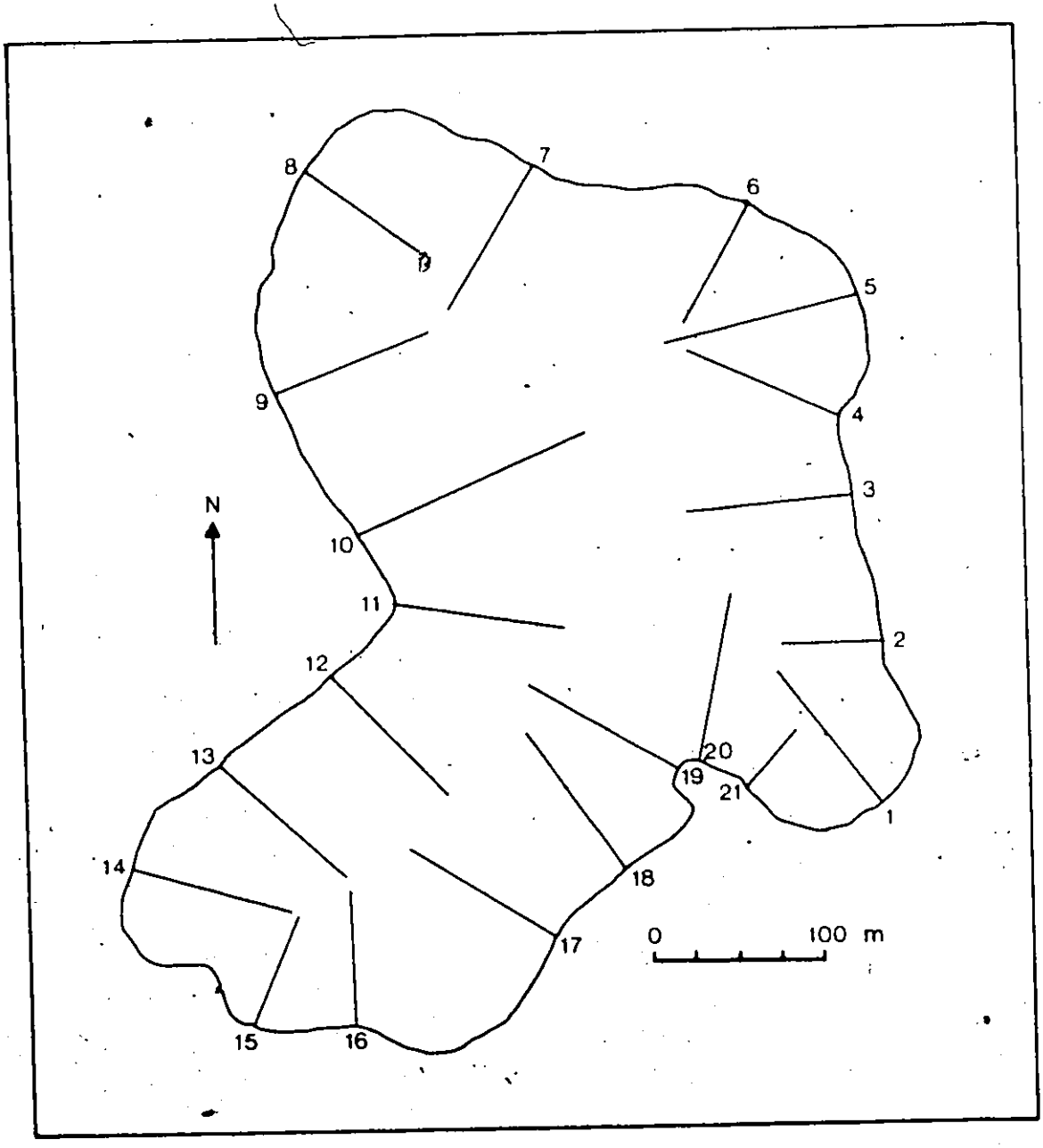

Figure 6.1. Location and name of transects used by the two-dimensional model.

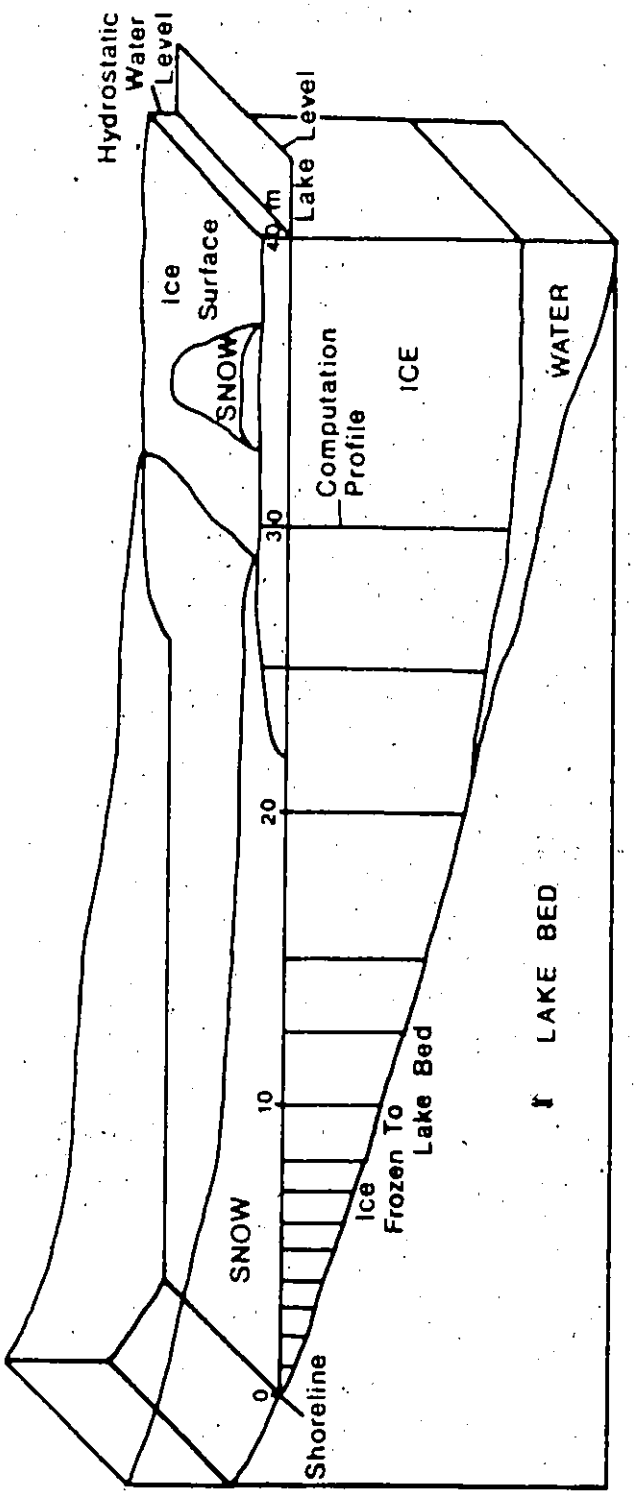

Figure 6.2. Idealized section across the edge of the lake ice cover showing the premelt conditions. The computational sites are superimposed on the front face and the diagram is consistent with the assumptions in the two-dimensional model.

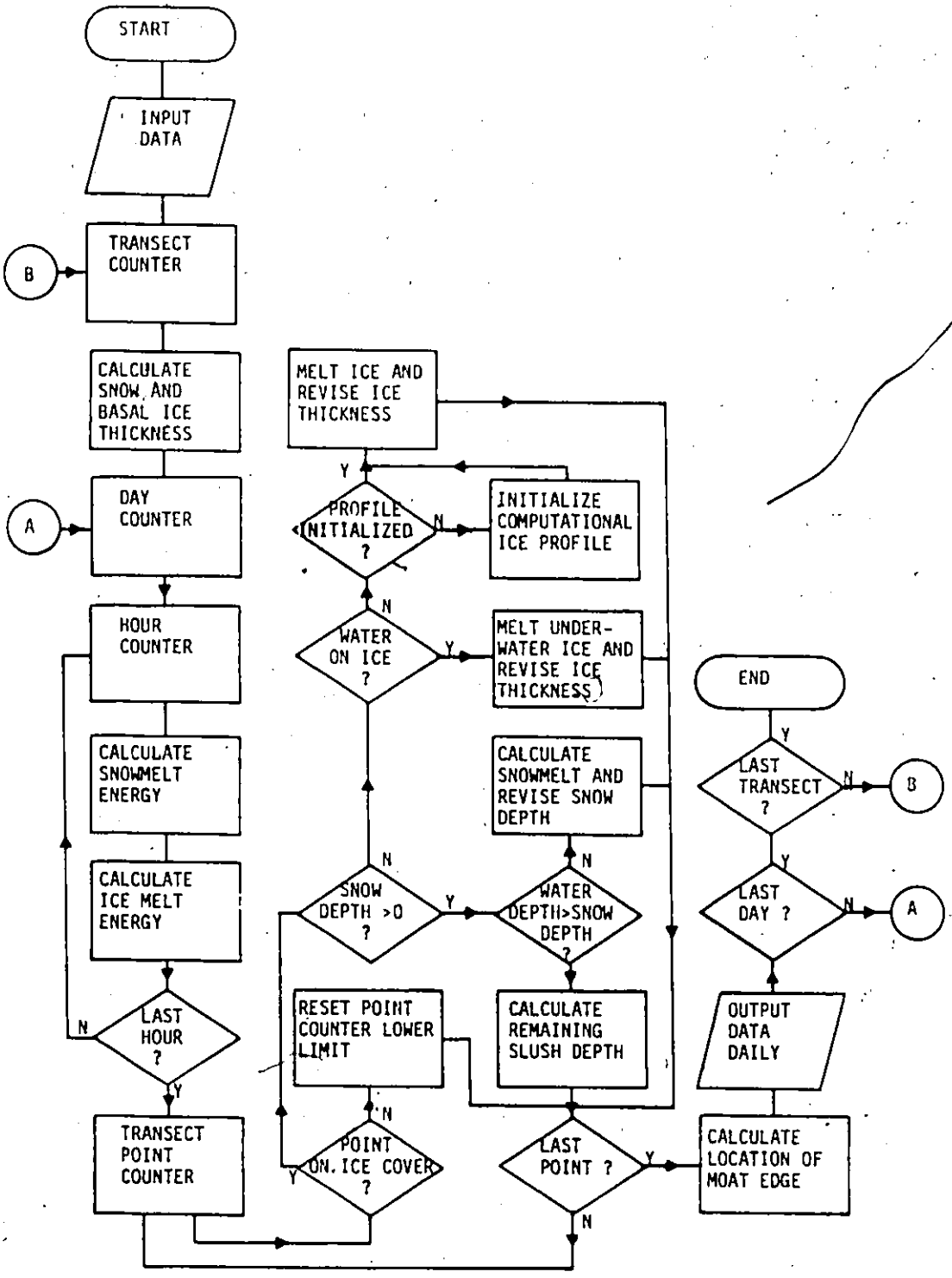

Figure 6.3. Simplified flow chart of the two-dimensional ice melt model.

Table 6.1

Input and Output Variables for the Two-Dimensional Model

Input

Variable	Frequency	Symbol
Lake depth	Once/point	
Ice thickness	Once/point	H
Snow depth	Once/point	h'_s
Distance from shore	Once/point	d
Number of points in transect	Once	
Snow surface roughness	Once	z_{os}
Lake level	Daily	h_w

Output

Variable	Frequency	Symbol
Snow depth	Daily/point	h'_s
Ice thickness	Daily/point	H
Basal ice thickness	Daily/point	h_b
Hydrostatic water level	Daily/point	h_{wl}
Distance of moat edge from shore	Daily/transect	d_e
Distance from shore to edge of ice frozen to lake bed	Daily/transect	d_{fz}
Ice thickness at moat edge	Daily/transect	h_{ie}
Index to indicate if ice has fractured at moat edge	Once/transect	

The locations of the transects were chosen to be as representative of the ice and lake conditions for as large an area as possible in order to minimize the number of transects required. This resulted in 21 selected transects spaced at approximately even intervals around Small Lake. The number of points selected varied with each transect and the upper limit was arbitrarily set at 20. Near the shore where the ice cover froze to the lake bottom, the points were located 1 m apart. As Figure 6.2 indicates, the point spacing increased to 5 m within 15 m of the shore with a 10, 20 and 50 m point separation being used beyond. The furthest point was never more than 150 m from the shore.

Values for snow depth, ice thickness and bathymetry for these points were obtained from the maps of each, contained in Chapters 3 and 4. Where possible, the transects were located where the original snow depth and bathymetry data had been obtained, thus permitting the direct use of the observed values. The selection of a value for the initial ice thickness was more complicated since the known thicknesses were widely spaced and drilling near the zone frozen to the lake bottom was minimized to avoid damage to the ice auger blades. Field observations have demonstrated an inverse relationship between snow depth and ice thickness (Fig. 4.9). When this relationship was combined with measured snow depths, an

estimate of the ice thickness was obtained for points where actual values were not available.

Bottom-fast ice was assumed to occur when the estimated ice thickness exceeded the water depth. The validity of this assumption depends upon the snow conditions during the period of ice growth. With no snow, the ice thickness would exceed the water depth due to the buoyant nature of ice. At the other extreme, a heavy snow cover would depress the ice below the hydrostatic water level and if there were no flooding of the snow to produce snow-ice (or white ice), the resulting ice would be less than the lake depth. Since the necessary snow information is not available, this criterion for selecting the location of the ice frozen to the lake bottom provides a reasonable compromise.

Snow-ice can form on Arctic lakes early in the winter (Schindler et al 1974), but since it was observed only sporadically during the study years, its presence was ignored. However, the refreezing of snowmelt water at the snow-ice interface to produce basal ice (also a form of white ice) occurs each spring and adds appreciably to the ice thickness (Woo and Heron 1981, Woo et al 1982). Marsh and Woo (1984) found that deeper snowpacks have thicker basal ice layers due to a greater cold content in the substrate to sustain a longer period of ice growth. The 1981 data of Marsh and Woo (1984) from Resolute, combined

with those obtained at Small Lake are combined in Fig. 6.4 to provide the following empirical relationship.

$$(6.1) \qquad h_b = ((0.0156\ h_s) - 0.0012)^{1/2}$$

where h_b is the basal ice thickness and h_s is the snow depth. Eq. 6.1 was used to estimate the basal ice thickness where the lake ice was frozen to the lake bottom since this environment is comparable to the land sites where the other basal ice measurements were made. Elsewhere on the lake ice, the snowcover is temporally variable and the substrate is much warmer, hence the cold content of the ice varies greatly and is not as large. During snowmelt, field observations showed that, on floating ice, basal ice is not well developed. Its thickness varied from 0 to 0.07 m of poorly refrozen snow grains and did not relate well to snow depth. For snow thicknesses less than about 0.08 m, basal ice was usually absent and with snow exceeding 0.08 m, a mean basal ice thickness of 0.02 m is applied to the model.

Snow depth observed during the premelt snow survey (h_s) were used in the model. These depths were corrected for the densification and melt (h_m) that occurred during the ripening period and the reduction of depth due to basal ice growth (h_b).

$$(6.2) \qquad h'_s = h_s\ \rho_{sd} / \rho_{sw} - h_b - h_m$$

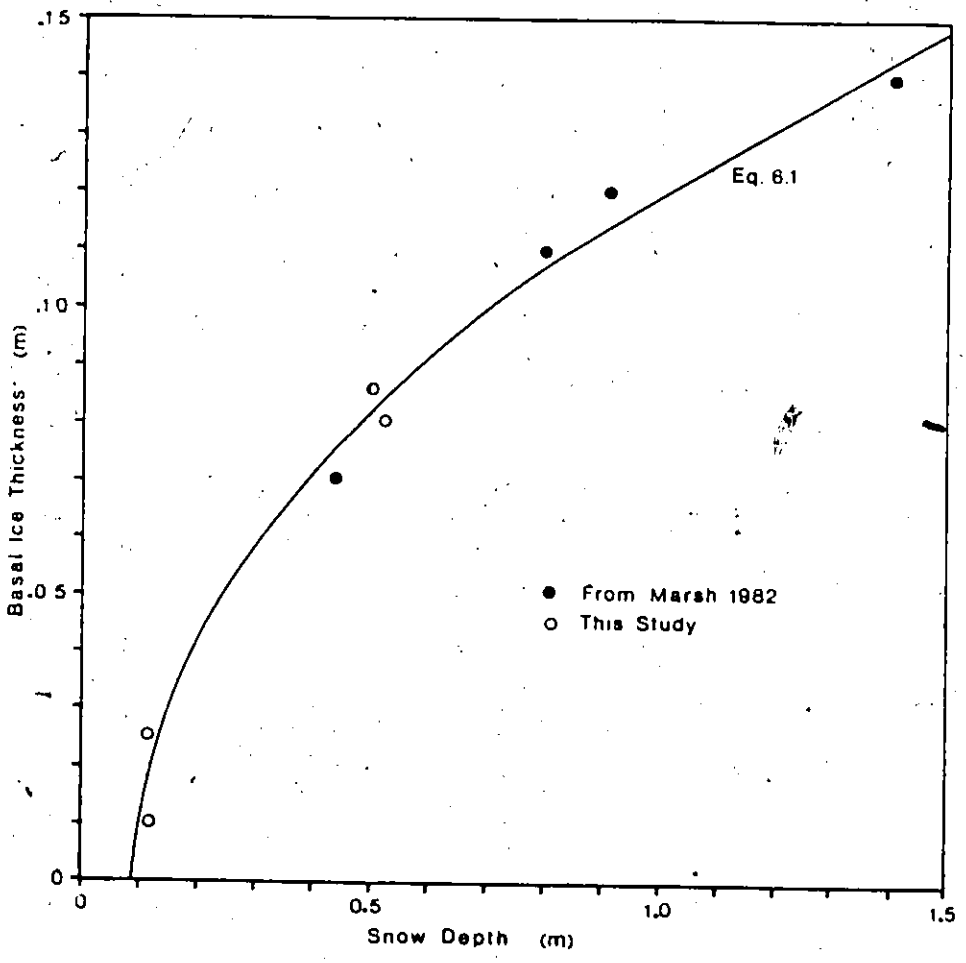

Figure 6.4. Effect of snow depth on the thickness of basal ice.

where h'_s is the revised snow depth, ρ_{sd} is the density of a typical dry snowpack (320 kg/m³), and ρ_{sw} is the density of a melting snowpack (500 kg/m³).

6.1.2 Snowmelt

The energy balance approach outlined in Heron and Woo (1978) and Woo and Heron (1979) was used to calculate snowmelt (see Eq. 5.6 to 5.13). Net radiation over snow was estimated as a residual of the radiation balance, Eq. 5.5.

$$(6.3) \quad Q^*_s = (1 - \alpha_s)\, K\downarrow + L^*_s$$

The longwave radiation balance (L^*_s) is the same for melting ice and snow since both are at 0°C and so would incoming shortwave radiation ($K\downarrow$). To estimate the snow surface albedo (α_s), for any particular time during the snowmelt season, the model makes use of an empirical equation by Woo and Dubreuil (1984) for the Resolute snow cover (Fig. 6.5).

$$(6.4) \quad \alpha_s = \alpha_{s1} - ((\alpha_{s1} - \alpha_{s2}) / \exp(2.22 - 0.166\, T) + 1)$$

where T is the time in days since the beginning of the snowmelt and α_{s1} and α_{s2} are the snow albedos at the beginning and end of the melt period. Values of 0.80 and 0.48 respectively were used. The decrease in snowcover thickness is

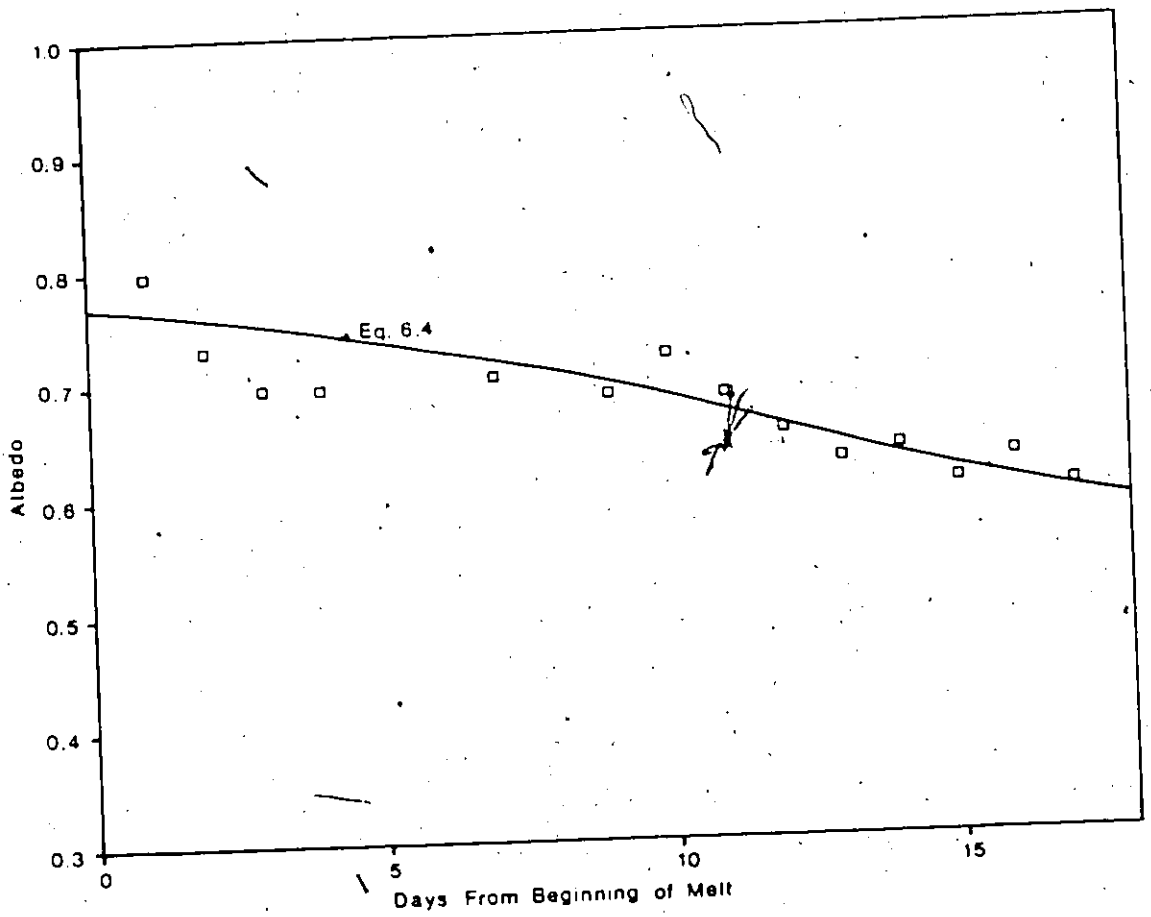

Figure 6.5. Decay of snow albedo during melt for a site outside Resolute, 1981.

$$(6.5) \qquad dh_s/dt = (Q^*_s + Q_H + Q_E + Q_p) / \rho_{sw} L_f$$

to estimate the fluxes of sensible and latent heat (Q_H, Q_E), a snow surface roughness of 0.003 m was used while the snow density during the melt period was approximated by 500 kg/m³ (Heron and Woo 1978, Woo and Heron 1979).

Throughout the melt period, the lake level rose to slush the thin snow cover along the shore. With a layer of water over the snow, the energy balance conditions are radically altered, rendering the above snowmelt computations inapplicable. This situation was complicated by the fact that once the internal cohesion was overcome, the slush became buoyant and often floated along the moat, rather than melting in situ. To simplify the problem the observed mean daily rate of slush loss of 0.07 m was used in the model.

6.1.3 Ice Melt

Ice melt did not occur at any point until the snow at that site was eliminated. For the main part of the ice cover which was not frozen to the lake bottom or under water, ice melt was calculated using the procedures outlined in Chapter 5. However, the spacing of the layers in the profile was increased from 0.02 m to 0.05 m to reduce the computational resources required. The calculation of ice melt along the shore was complicated by

the formation of the moat and the ponding of water on the ice. Wake and Rumer (1979) have examined the melting of submerged lake ice, but their model was untested since the value of the coefficients and their variability with environmental conditions was unknown. For the Small Lake ice cover, the observed mean daily melt rate of 0.031 m was used to estimate the upper surface melt of ice under water, regardless of whether it was white or black ice or whether the ice was frozen to the lake bottom. Internal ice melt was ignored because visual examination of newly risen ice indicated little internal melt except along the triple grain boundaries. However, where the ice was free from the lake floor but still under water, the ice bottom melt was calculated.

6.1.4 Moat Development

An initial moat is formed when rising water level floods the ice that is frozen to the lake bottom. Billfalk (1981) approached this process theoretically by considering the deflection of an ice beam with one end frozen to a river.

$$y = h_w (1 - \exp(-vx) (\sin vx + \cos vx)) \quad (6.6)$$

where y is the deflection of the ice surface, h_w is the total water level change, x is the distance from the fixed end and

$$(6.7) \qquad v = (M / 4Y.(H^3/12))^{1/4}$$

Here, M is the modulus of foundation for water (10^4 m/m^2), Y is the elastic modulus of ice. Equation 6.6 assumes uniform ice properties, rapid loading of the ice cover (less than several minutes) and the response of the ice cover is elastic. These assumptions do not hold strictly for the Small Lake ice cover, yet Eq. 6.6 is able to duplicate the observed ice deflections when suitable values of the elastic modulus of ice are selected (Fig. 6.6). However, the elastic modulus parameter loses its physical meaning because it now incorporates the effects of an ice creep component. Its value is therefore much lower than those reported in the literature for melting ice (Barnes 1960). The inclusion of the ice creep component prevents accurate day to day estimation of this parameter and hence Eq. 6.6 is not operationally useful. Figure 6.6 provides an illustration. On the day following the successful fit of Eq. 6.6, the edge of the bottom fast zone retreated 2 m inshore. Eq. 6.6 yielded a rapid response but the ice cover required several days to deform to the new shape.

In view of these deficiencies, a simple model of the moat development in the initial stages was based on the geometry shown in Table 6.2. Field observation shows that the shorefast ice remained frozen to the lake bottom

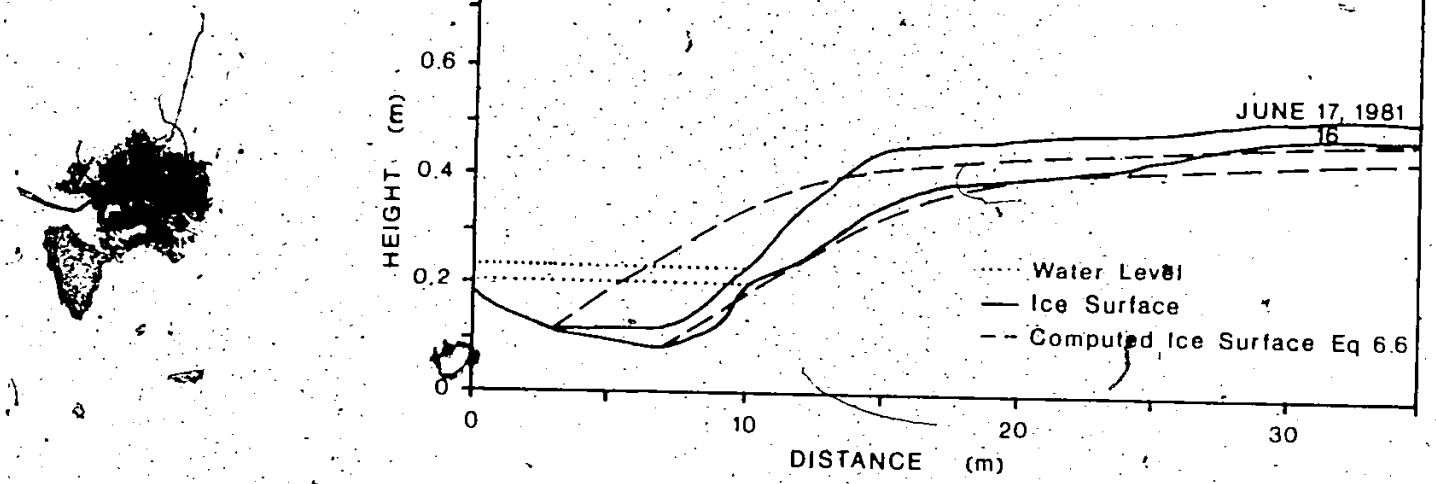

Figure 6.6. Observed ice surface elevation at edge transect U on two selected days. Predicted surface elevations for both dates are also plotted. In Eq. 6.6 h was set to 0.75 m and Y to 6.5 x 10^7 N/m^2.

until the basal or other type of white ice had melted. Only then could sufficient shortwave radiation passing through the ice cause melting at the mud-ice interface and permitting a subsequent detachment of the ice from the lake floor. Thus the extent of basal ice indicates the boundary of the shore zone where the ice was frozen to the lake bottom. The distance from this boundary to where the lake ice rises out of the water (distance B in Table 6.2) was determined by field measurement at the time of fracture to be 3.0 m. The other widths at earlier times were ignored since the chosen value will strongly influence when the ice edge will fracture and hence must be optimized for this period. This will result in an underestimation of the moat width in the early stages of moat development.

With rising water level, the ice fractured at the edge of the frozen zone under the moat and at the edge of the moat as Billfalk's (1981) work indicates. These results also indicate a relationship between ice thickness and the water level rise at the time of fracture. Field data obtained in 1981 just prior to or after the fracturing show such a relationship (Fig. 6.7). Billfalk's (1981) curve for non-melting ice is non-linear while a line provides a reasonable description of the Small Lake observations.

Table 6.2

Moat Geometry at the Time of Fracture

Distance from Water Surface to Ice Surface (A)	Distance from Edge of Frozen Zone to Edge of Moat (B)
0.34 m	2.20 m
0.33	2.98
0.34	4.50
0.30	3.60
0.24	2.25
0.24	3.20
	3.00
0.39	1.20
	1.60
0.57	3.50
0.29	2.50
0.25	4.90
0.59	3.50
0.50	4.00
0.45	4.30
0.52	4.00
0.47	2.40
0.45	1.86
0.48	1.90
	3.00
0.28	3.75
	1.60
	3.90
	3.02 mean

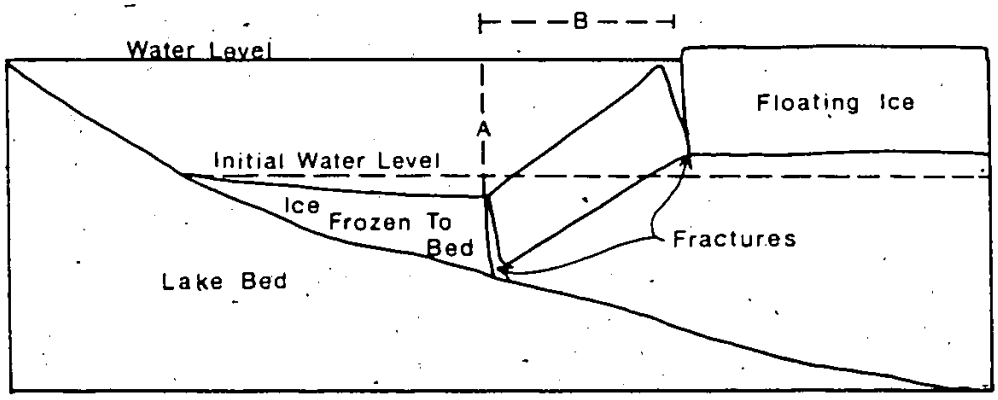

MOAT CROSS SECTION

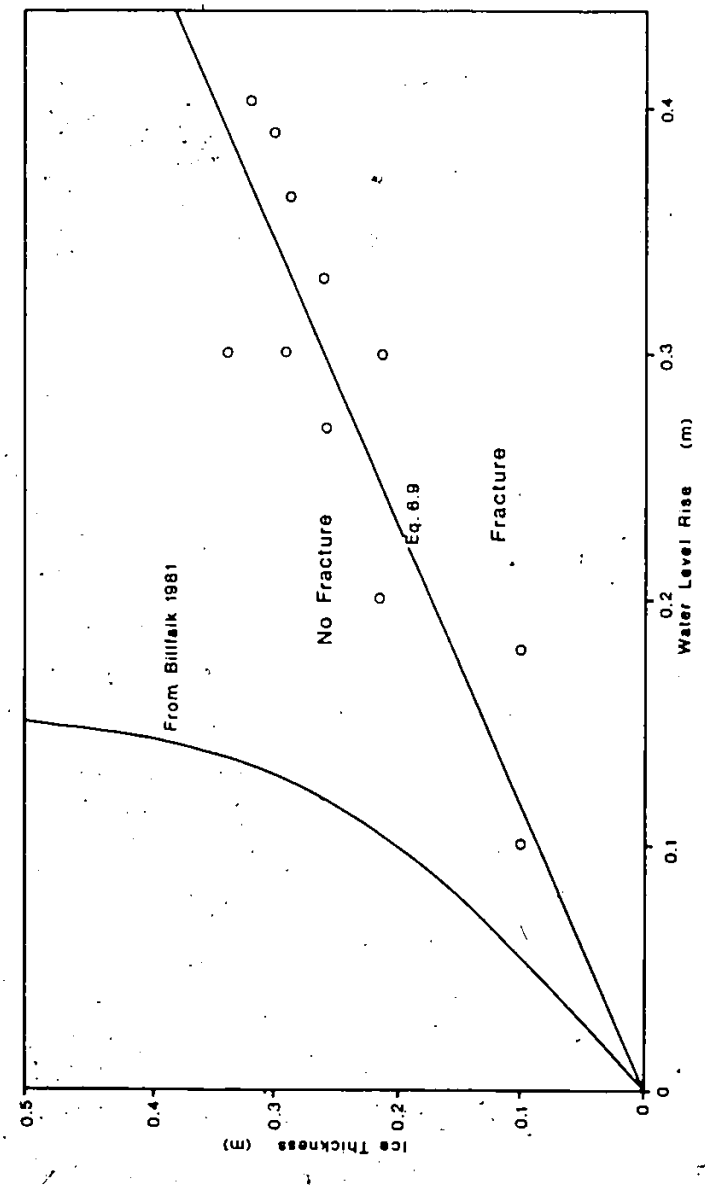

Figure 6.7. Critical water level rise necessary for the fracture of an ice cover with an edge frozen to the shore

$$h_f = 0.87\, h_w \qquad (6.8)$$

where h_f is the ice thickness at which fracturing occurs and h_w is the increase in the water level from the initial level. Since Eq. 6.8 is empirical it is probably not valid in situations when the water level rises faster or higher than observed in this case. The ice thickness and time of fracture is likely influenced by the amount of ice creep which in turn is dependent upon the applied stress and the duration of stress application. Fortunately, Eq. 6.8 is applicable in 1980 as well since the behaviour of the water levels are similar.

When fracturing occurs, major cracks are found along the moat edge and when the ice emerges, it usually breaks free of the main ice cover, moves along the moat and melts within a few days. These floes and any remaining submerged ice are ignored in this model because they constitute a limited area of ice cover, and thus cause only a small error. Besides fracturing, ice can break free of the shore in two ways, 1) the basal ice is melted and the ice floats to the surface or 2) the ice melts completely near the shore. In these cases, there is little cracking and the new moat edge is the edge of the floating ice.

Once the ice cover has broken free of the shoreline, the retreat of the ice edge and the growth of the moat will be due to a combination of mechanical and

thermal processes. These processes, described in Chapter 4, are poorly understood and for this model the mean daily rate of ice edge retreat for 1981, (1.8 m/d) was used. This rate will underestimate edge retreat for periods of high winds and waves when ice loss can reach 5.0 m/d. A vertical ice edge is also assumed, since the submerged ice tongue only becomes extensive (up to 2 m) during storms and is usually much smaller.

The thickness of the ice edge was determined by

$$h_{ie}(T) = (H_2 + H_1) / (d_2 - d_1) \qquad d_1 < d_e < d_2 \tag{6.9a}$$

$$h_{ie}(T) = (H_1 + h_{ie}(T-1)) / (d_e - d_1) \qquad d_e(T) < d_1 \tag{6.9b}$$

where h_{ie} is the ice edge thickness at time (T) or (T-1), H is the ice thickness at adjacent points 1 and 2 on the ice cover, d is the distance to these points from the original shore.

When the entire ice cover is detached from the shore, it moves about the lake, controlled by wind speed and direction, causing highly variable moat widths. These movements are not modelled, the position of the ice cover was manually plotted based on field observations.

6.1.5 Model Output

The thickness of lake ice, basal ice, snow, water depths as well as the ice edge location and thickness were

output daily for each point. Such information from all transects, together with field data for ice sheet movement, were then plotted manually on maps to show the spatial variation of lake ice thickness.

6.2 Results

The model was run for the period from the beginning of melt until the ice cover broke into two large pieces. This major fragmentation occurred on July 17, 1980 and on July 12, 1981 resulting in 31 and 32 computation days respectively. Computution involved 21 transects evenly distributed around the shoreline.

6.2.1 The Transects

The transects displayed two modes of behaviour. For about half of the transects, the ice cover melted free of the shore while in the remaining cases, fracturing freed the ice from the shore.

An example of a transect that melted free of the shore is shown by the diagram in Fig. 6.8. The initial snowcover was thin yielding only 0.03 m of basal ice at its thickest point. Snow melted rapidly and was gone by June 11th with the basal ice disappearing on the following day. Water ponded on the ice surface to produce an initial moat 3 m wide and 0.02 m deep at the ice edge. This ponding lasted only one day. As the basal ice melted on

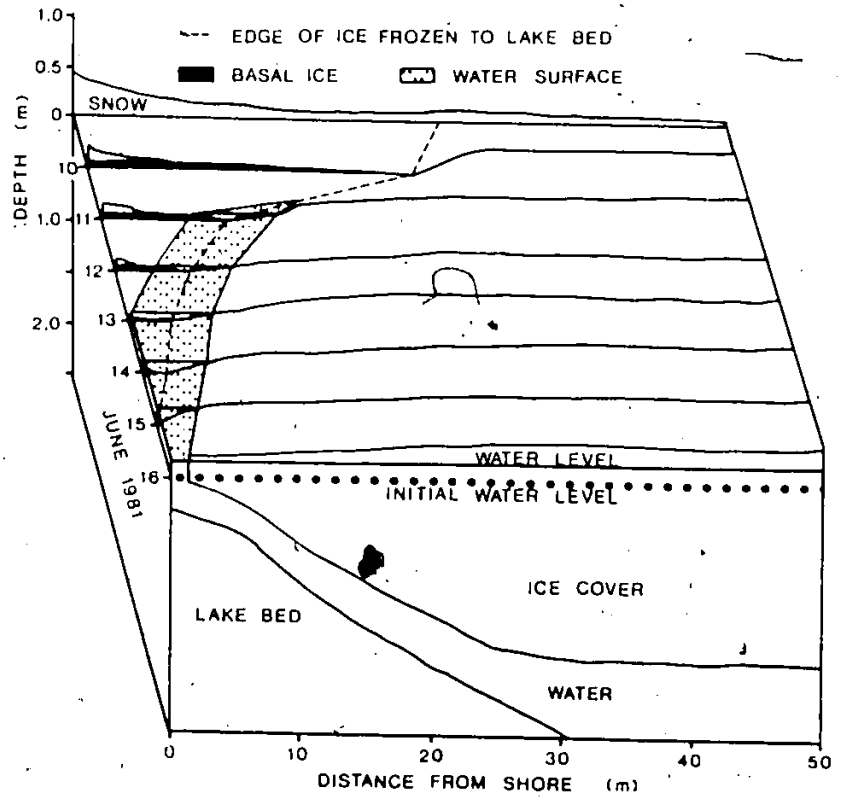

Figure 6.8. Predicted conditions at transect 20 during the initial phase of moat development, 1981.

June 12th, the ice edge floated free of the shoreline. The moat was then enlarged by ice edge retreat at a rate of 1.8 m/d.

The conditions at the transects where fracturing occurred are more complex (Fig. 6.9). With a snow depth of 1.2 m, basal ice thickness reached 0.14 m at the shoreline. Snow or ice melt continued until June 13, 1981 before water was first ponded 15 m from the shore and approximately 5 m beyond the edge of the snowdrift on the lake. The zone where lake ice was frozen to the bottom extended to 20 m from the shore. During the following week, to June 19th, the width of the moat varied between 5 and 9 m. Moat width was controlled by the extent of the snowdrift and the bottom-fast zone, both of which retreated shoreward independently due to differences in snow and ice melt rates. The depth of water increased throughout this period, reaching a maximum of 0.30 m at the boundary between the frozen and unfrozen bottom zones. Between the water and the snowcover lay a zone of slush typically 1 m in width. By June 20th, the snow had melted and the edge of the moat reached the shoreline. The width of the moat continued to decrease until June 22nd when the ice fractured 5 m from the shore and the second phase of moat development began. When the ice fractured, 2 m of the transect remained frozen to the lake shore.

The timing of the various phases of moat

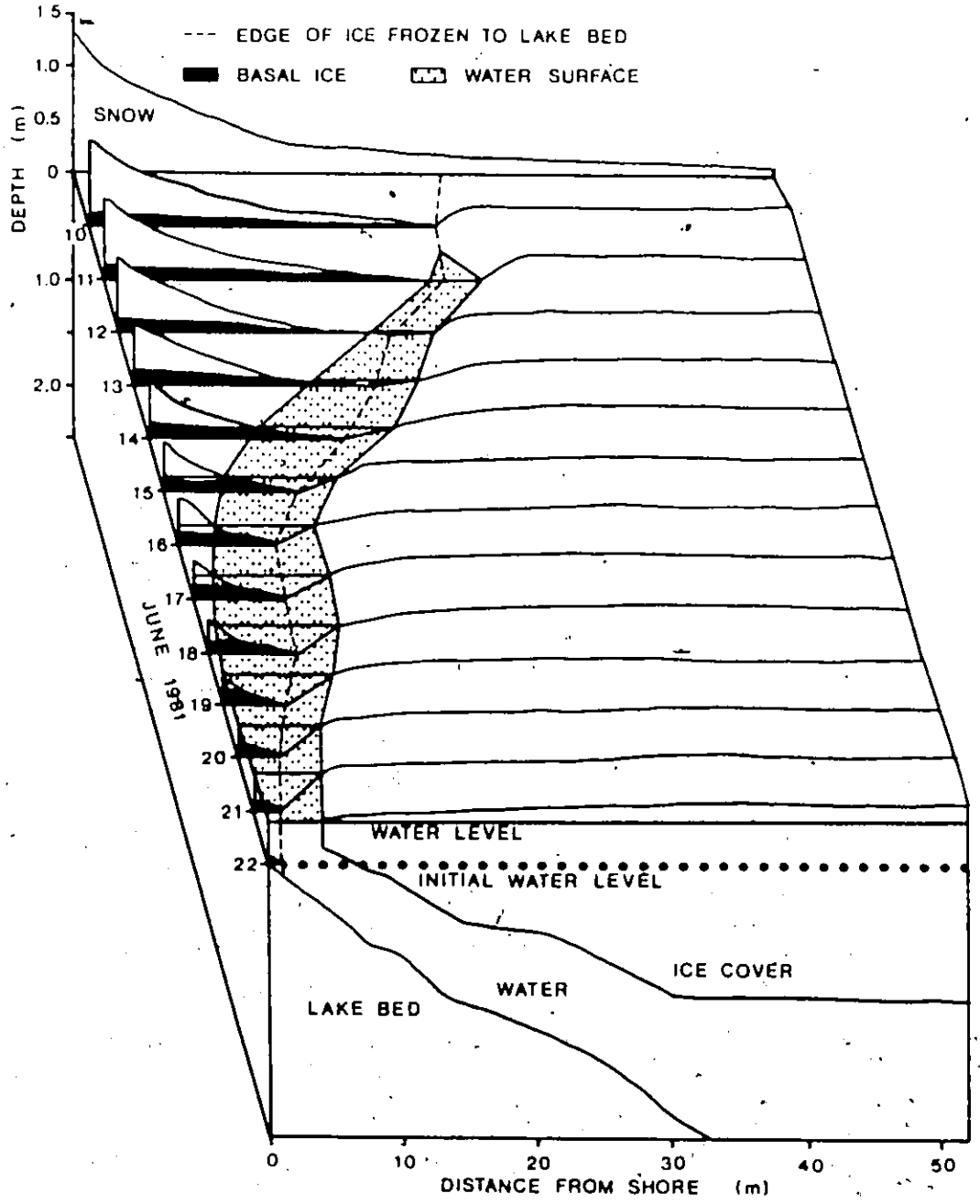

Figure 6.9. Predicted conditions at transect 10 during the initial phase of moat development, 1981.

development differed between the two years of study, but all transects displayed patterns similar to the two examples described above.

6.2.2 Lake Ice Cover

The computed sequence of moat locations for all transects in 1981 is summarized for 3 selected days in the map of Fig. 6.10. The results for both years are similar although the events in 1981 took place five to seven days earlier than the previous year. Ponding began in the thin snow areas along the southeastern and eastern shore on June 17, 1980 and June 11, 1981. By June 19, 1980 and June 12, 1981, a complete moat surrounded the floating ice cover. The delay is related to the rate at which the water level rose and the thickness of snow and basal ice. Lake ice was first detached from the shore on June 18, 1980 and on June 12, 1981, again at the eastern and southeastern parts of the lake. From the rest of the lake edge, ice was released sporadically during the 10 days that folowed. In 1980, the final fracturing occurred on June 28th at two sites along the southern and western shores. In 1981, these were the same last sites where the ice was released from the lake edge (on June 22nd). After that, the ice cover was free to move about the lake.

The observed and computed sequence of events were comparable for both 1980 and 1981. One notable discrepancy

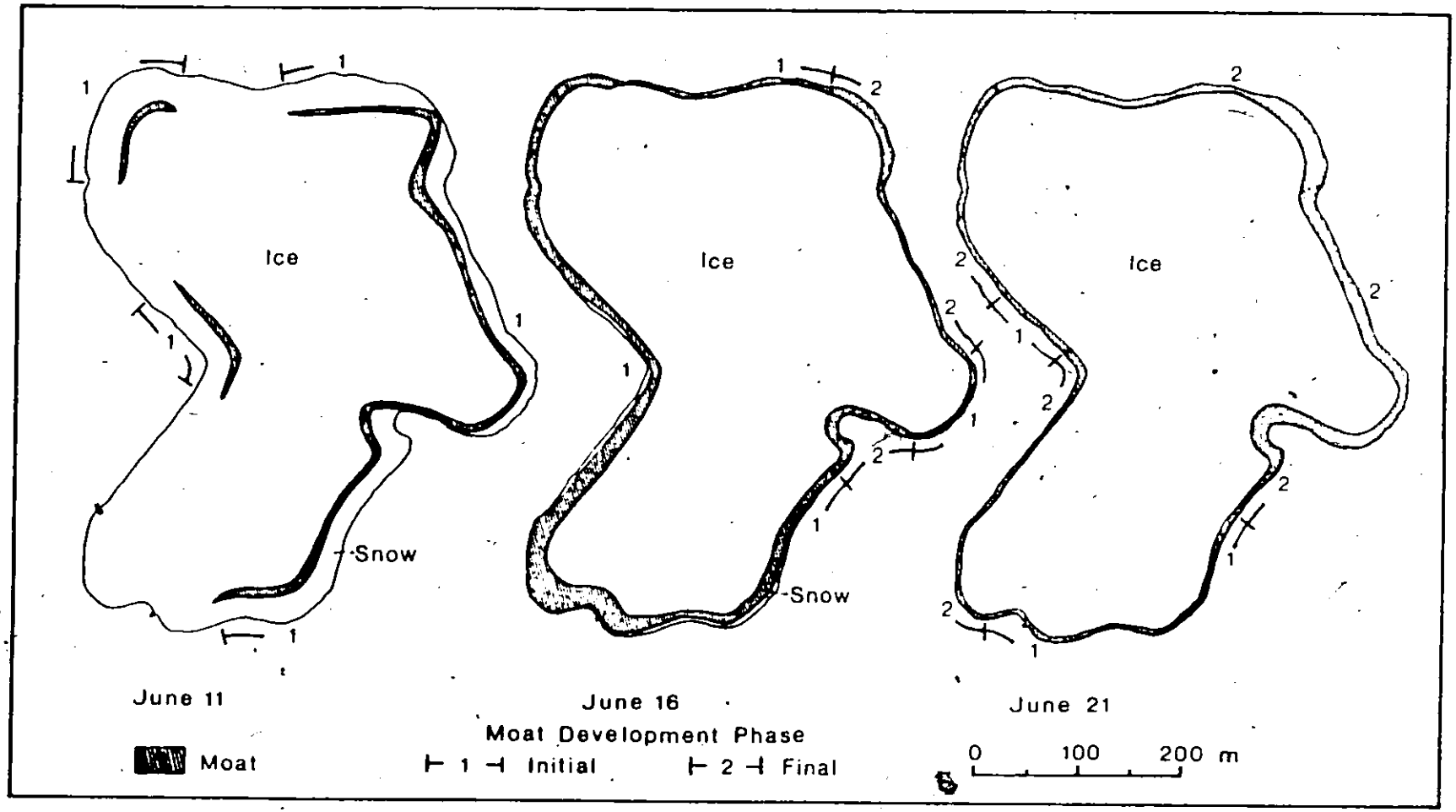

Figure 6.10. Calculated moat extent during the initial period of development for selected days, 1981. The development phase and size of the moat are indicated by the numerals along the shore.

is that the computed conditions occurred approximately two days earlier than conditions on the lake, a feature that will be examined later. After the ice is free to move in the lake, the extent of the ice cover is controlled by the rate of ice edge retreat, the length of time since retreat started and the lake shape. The observed and computed ice covers during the initial drift phase of their decay are shown for 1981 in Fig. 6.11. The 1980 field data were less reliable because they were derived almost exclusively from oblique photographs. This may account for the poorer fit between the observed and computed values. Where the shoreline is relatively straight, the fit is reasonable and the shapes of the observed and computed ice covers are similar, except where concentrated overland flow has caused additional melt. The greatest discrepancies occur in 'Gauge Bay', 'Tent Bay' and 'Low Point'. In the latter area, the computed area of ice loss is overestimated. This is due to the fact that the computed ice edge release occurred earlier than the observed date, and the computed edge retreat rate was higher than the actual value. After the main ice body was released from the two shallow bays, the thin ice near the edges decayed to such an extent that 10 m of the edge disintegrated rapidly into a mass of loose crystal fragments which quickly melted. Thus the observed shape of the ice cover near Gauge Bay never became as pointed as was indicated by the computations.

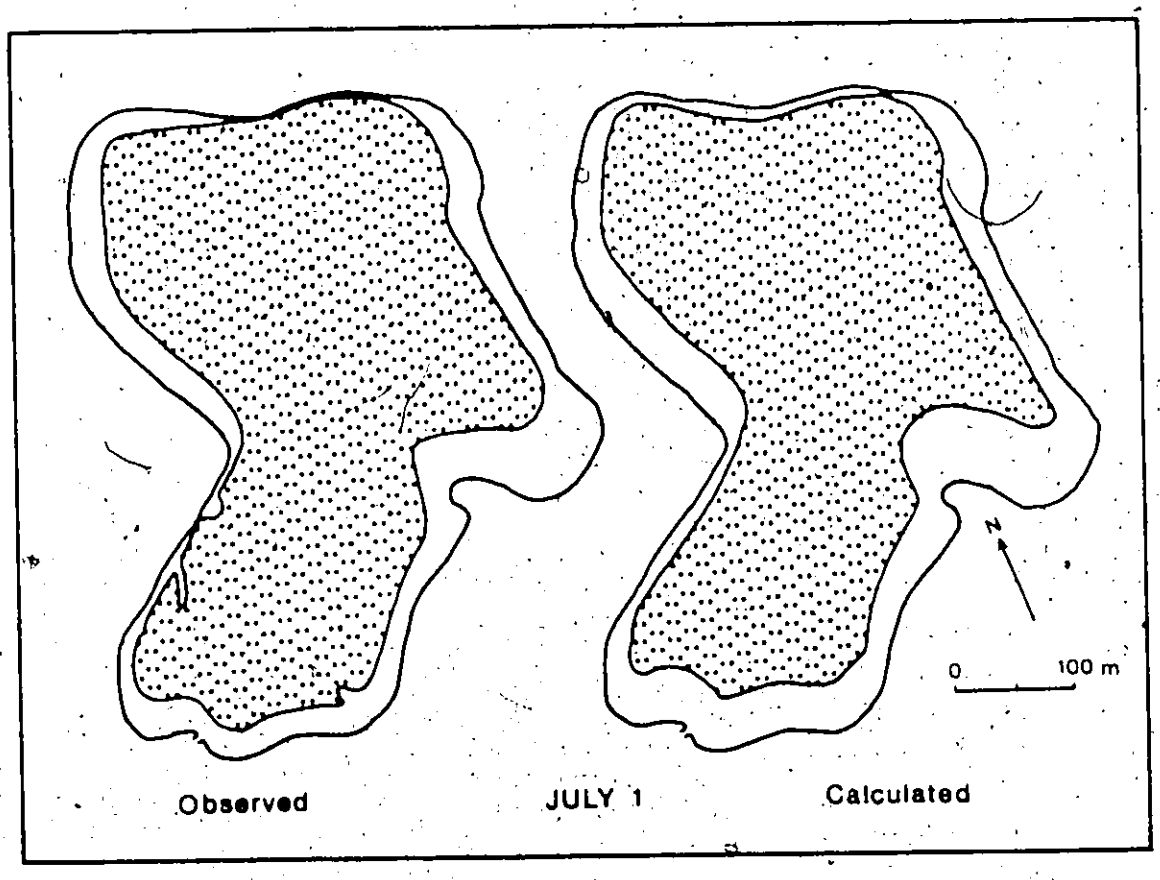

Figure 6.11. Observed and calculated ice coverage for Small Lake on three selected dates, 1981. This figure is continued on the following page.

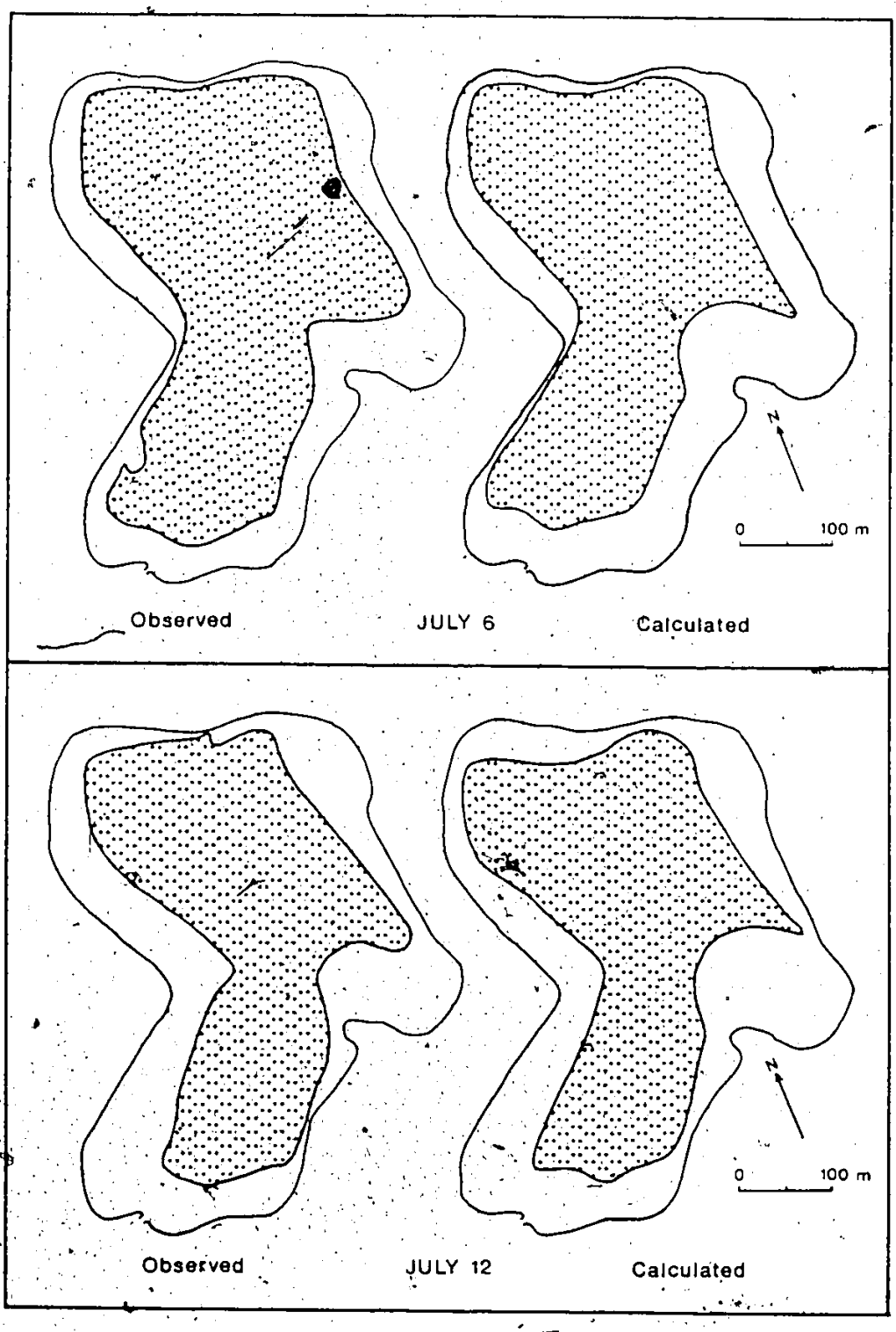
N
0
100 m
Observed
JULY 6
Calculated
N
0
100 m
Observed
JULY 12
Calculated

6.2.3 Moat Conditions

Most of the observed information from the moat was used to develop the model and therefore is not suitable for testing the calculated results. One feature used to evaluate model performance is the distance from the shore to the inner edge (towards the centre of the lake) of the initial moat. The location of the ponded water edge reflects the combined influence of the initial snow and basal ice thickness and the disposition of the bottom-fast ice. As the snow and basal ice melted, the inner edge of the pond shifted shorewards as is shown by the computed results from three transect in 1980 and 1981 closest to the observation locations (Fig. 6.12). The computed edge of the moat started further offshore than observed. It was often difficult to distinguish between temporarily ponded snowmelt water and the moat when it was forming. Part of the difference in Fig. 6.12 is also due to delays in establishing the measurement site. Most of the error is attributable to the initial assumption that the thickness of the ice frozen to the lake bed is equal to the lake depth. Thus this ice flooded as soon as the lake level rose. However, this error has little overall effect on the melting of the ice cover.

After the computed moat edge was about 10 m from the shore, the observations and computed results are roughly comparable although there are large discrepancies.

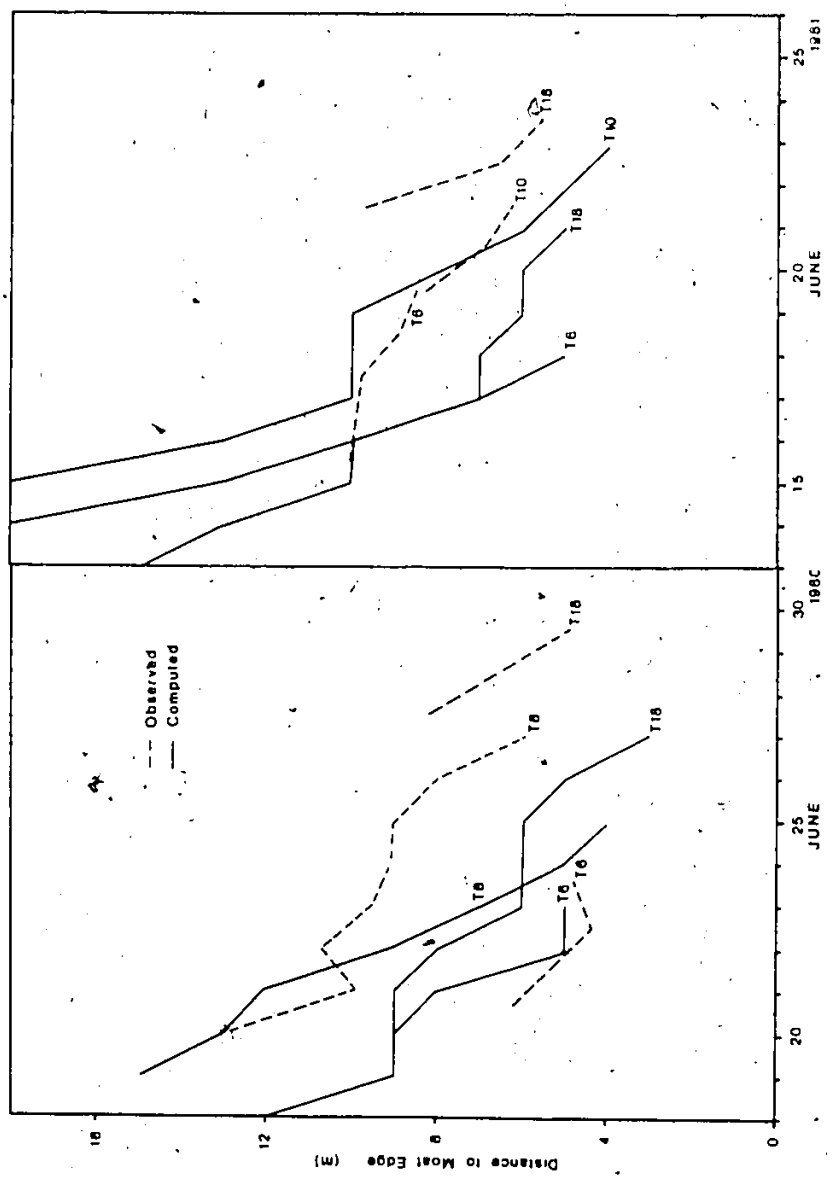

Figure 6.12. Observed and computed shoreward movement of the moat edge during development.

The most notable difference is that the calculated results precede the observations by approximately two days. The computed moat edge also comes closer to the shore before the initial moat phase ended. The possible causes of these model results are discussed later in this section. The calculated results displayed a number of periods in which no movement of the moat edge occurred. This is due to the fixed distance from the edge of bottom-fast zone to the moat edge and the interval between computation points on the transect used in the model. Observations indicated that the moat edge rarely remained static for long. It should be noted that the two cases of moat edge movement away from the shore in 1980 are probably the result of measurement error. In addition, observed moat conditions could vary over short distances along the shoreline.

Given the above limitations, there is a reasonable correspondence between the observed and computed rates of moat edge retreat during the later stages of the initial moat formation. This indicates that the bottom-fast ice was melting free from the lake shore and the boundary shifted shoreward in a realistic manner.

The mode and date of ice release from the shore line can also be used to test the model performance (Fig. 6.13). In 1981, the model indicated that the ice melted free of the shore from Beach Bay, along the eastern shore to Low Pt., while fracturing occurred along the southern

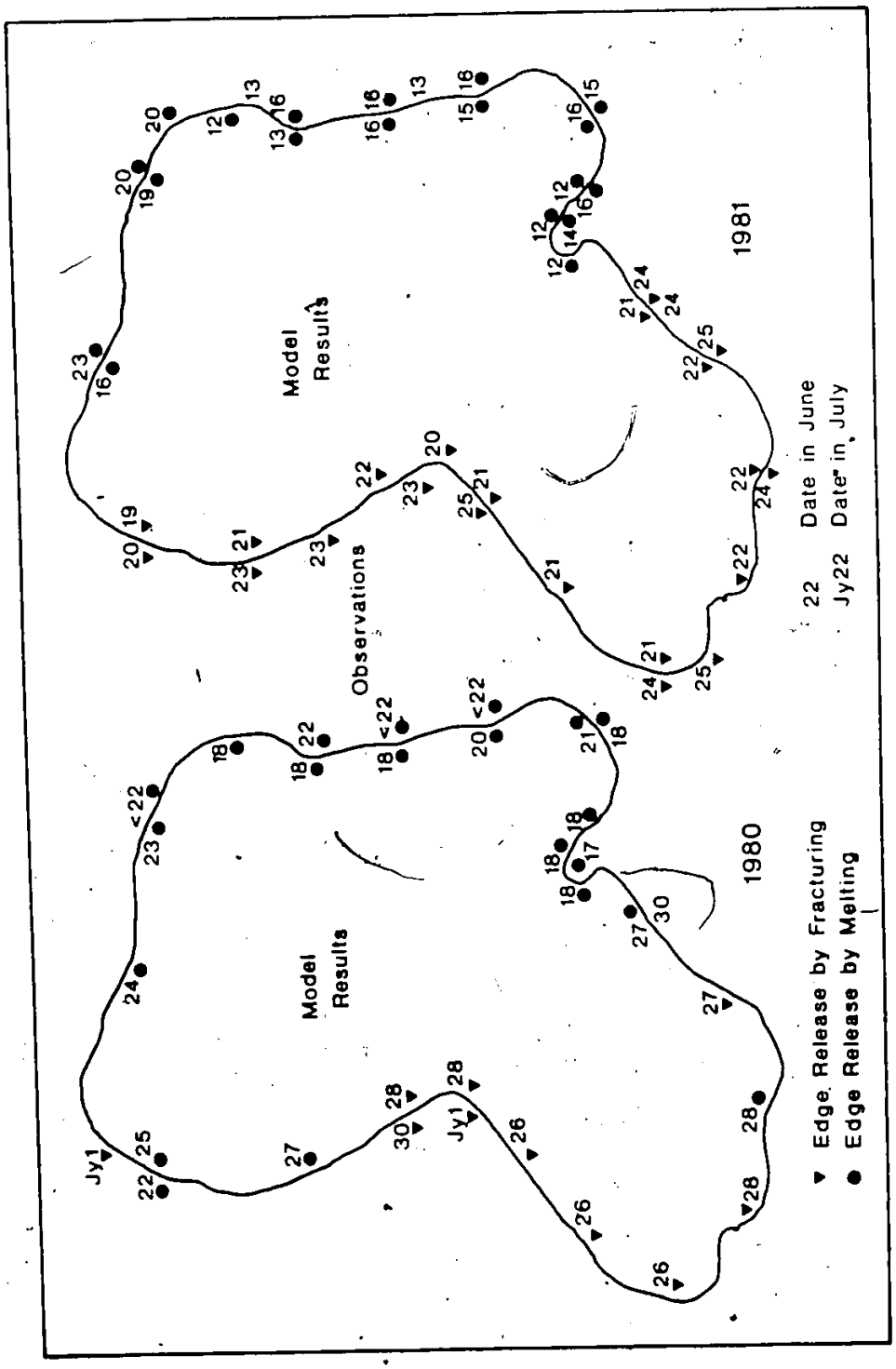

Figure 6.13. Observed and predicted date and nature of ice release from the shoreline. Model results are indicated within the lake area while the corresponding observations are displayed on the shore.

and western sectors. This pattern was verified by field observations. In 1980, the model yielded similar conditions except for several transects which melted free along the southern and western shores, and one fracture site located near Tent Bay. These were the only three cases (14% of all transects) where the model misclassified the mode of ice release.

The date of the ice release is important in determining when the ice cover is free to drift and when the edge retreat of the floating ice can begin. Detailed observations in 1981 (Fig. 6.14), indicate that the computed dates averaged 2.2 days earlier than the observed. In 1980, the model ice release dates are 1.5 days earlier than the observed dates. This time error is more evident for the sites released by fracturing, and these fractures tended to occur much later in the season.

Three main reasons may contribute to the above systematic error. 1) Since both modes of ice edge release were affected, it is possible that the snow cover used in the model is thinner than it should have been or the snow or ice melt rates were too large. These errors would have allowed the basal ice to melt too early, and allow the ice edges to break free in advance of the observed dates. 2) It is also possible that the there was white ice formed by the slushing of snow or by wave splash along the shore that went unnoticed in the field. During melt, this type

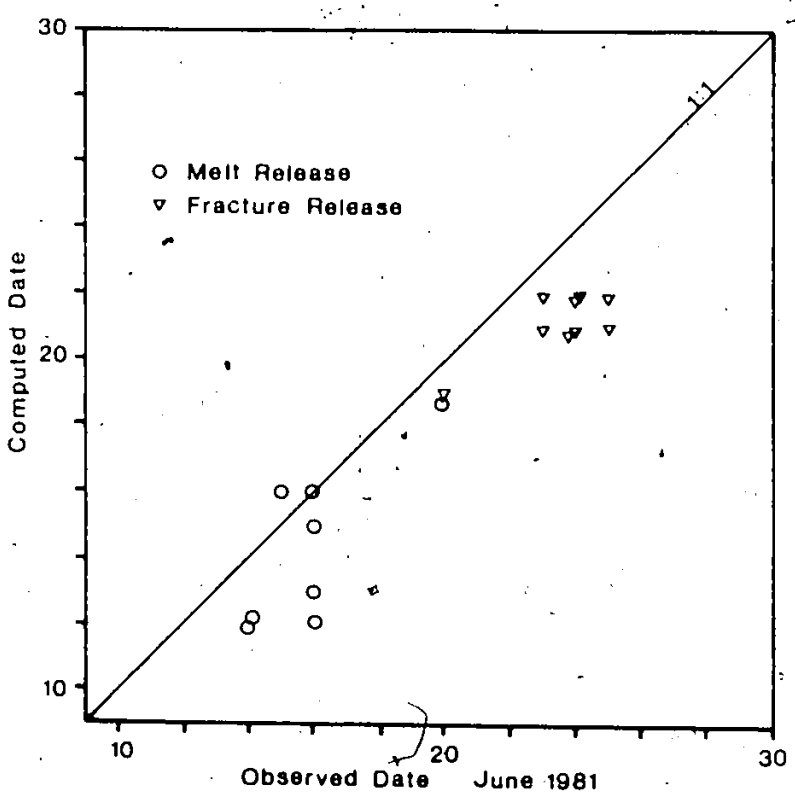

Figure 6.14. Comparison of the observed and calculated dates of ice edge release from the shore, 1981.

of ice is virtually indistinguishable from melting basal ice and would be of sufficient thickness to delay the release of the ice edge for several days. 3) Fracturing of the ice edge in the model is determined by the thickness of the ice at the moat edge (Eq. 6.8) and the water level rise, typically 0.3 to 0.4 m/d. An error of 0.03 m in estimating the moat edge ice thickness will produce a 1 day error in the timing of the ice fracturing. Such an error in determining ice thickness easly arises out of imprecision in estimating ice melt beneath the ponded water. It can also be due to inaccuracies in the lake bathymetry or the assumption that the bottom-fast ice was the same as the bathymetric depth. The last two factors will produce a systematic error. Interpolation between points or a finer grid would reduce the systematic error.

It is difficult to isolate the relative importance of the factors described above. Field evidence from 1981 suggests that the computed edge of the zone in which ice is frozen to the lake bed was 1 to 2 m closer to the shore at the time of fracturing than it should have been. Thus the fracturing was immediately due to the third factor described above but either of the first two factors could have contributed.

6.2.4 Edge Thickness of the Floating Ice Cover

The computed edge thickness of the floating ice

cover for a typical transect is given in Fig. 6.15. This transect melted free of its shore and thus the initial edge thickness was only 0.08 m. As the edge retreated into the main ice cover, edge thickness increased, attaining a maximum of 1.06 m on June 3rd when the thicker ice was reached. Following this, thickness decreased rapidly. The observed ice thickness exceeded the computed values, and this error is attributable to both the empirical edge retreat function used in the model and overestimation of the melt rate for the floating ice described in Chapter 5. An example of the observed and computed ice thickness along a transect is shown in Fig. 6.16. Again, the melt computation error mentioned above is involved and has resulted in the computed thicknesses being too small. When this error is removed (about 0.4 m), the correspondence between the observed and calculated transects would improve over most of the transect. However, the lack of points near the ice edge does not permit the rapid changes in ice thickness to be predicted well. Also, no allowance is made in the model for increased water heat flux close to the ice edge.

6.2.5 Ice Cover Area

The predicted position of the ice edge was plotted for all transects and the area of the predicted ice cover was planimetered. The results for 1980 and 1981 are shown

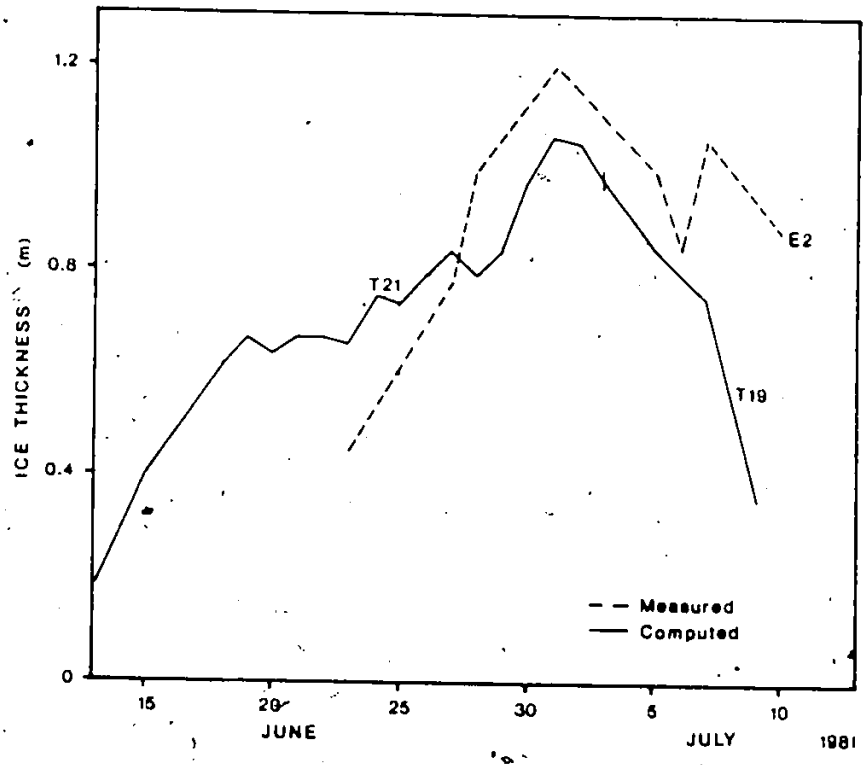

Figure 6.15. Measured and computed edge thickness of the Small Lake ice cover, 1981.

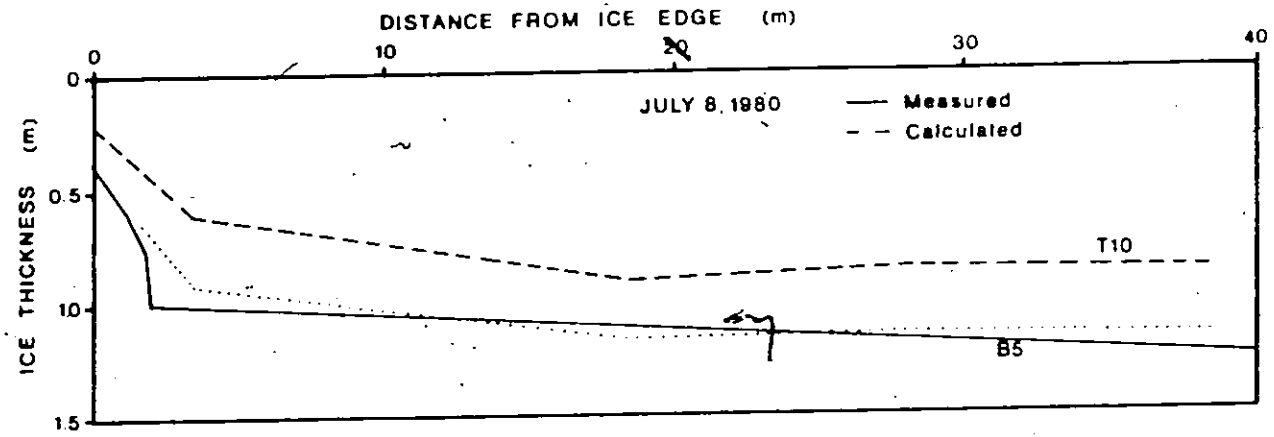

Figure 6.16. Measured and computed ice thickness along a transect from the ice edge, 1980. The dotted line indicates the bottom of the ice if the overestimation of melt by the one-dimensional model is corrected.

in Fig. 6.17. Initially, when the moat was formed and the ice broke free of the shore, there was only a small decrease in the lake ice cover. Once the moat completely surrounded the ice, the decrease in ice cover area was nearly linear, because of the constant edge retreat rate used in the model and the geometry of the lake. As a result, the shape of the ice area curves for 1980 and 1981 are similar, though the 1980 curve lags the 1981 curve by about 5 days.

The observed ice cover areas are also shown in Fig. 6.17. The computed results for 1981 follow the observations closely but preceded the actual date by two days due to the early moat formation predicted by the model. The use of a constant edge retreat rate in the model causes the observed and computed curves to diverge after June 21, 1981 since the early ice edge loss is less than the mean rate used in the model. After approximately July 8th, the model edge retreat is exceeded by the actual rates and the ice cover area curves converge. In 1980, the observed ice cover maps were not as accurate as 1981, and this leads to a large difference from the predicted results.

6.2.6 Summary

The two dimensional ice decay model described in this chapter performed well. In general the results from

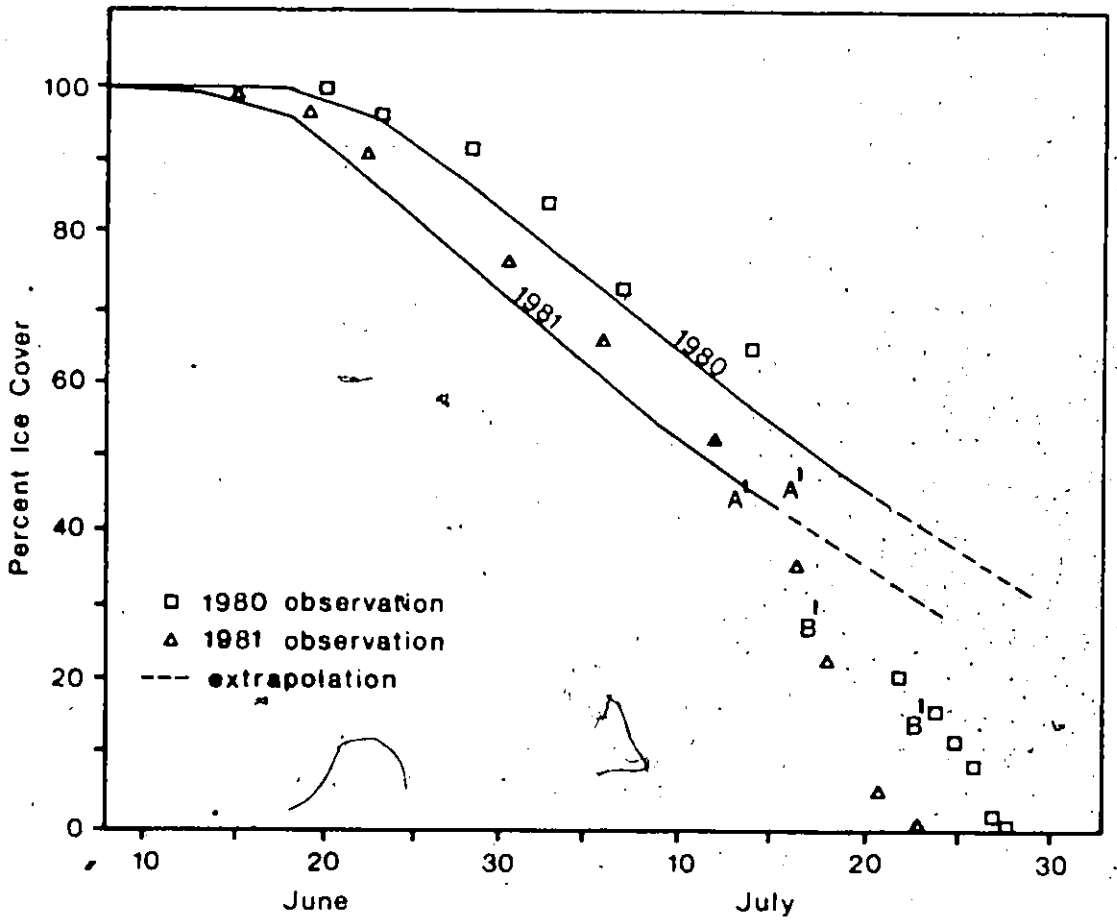

Figure 6.17. Observed and predicted ice cover area for Small Lake, 1980 and 1981. The date when the ice cover broke into two pieces is indicated by (A) while the major fragmentation is shown by (B).

the model compare favourably with field observation during the period of moat formation. However, the computed date when the ice cover broke free of the shore was about 2 days later than observed. This has little effect on the computed mode of edge release. In 1981, no transects were mis-classified with respect to the mode of ice release while in 1980, there were only 4 misclassifications.

Once the ice cover detached from the shore, a constant rate of ice loss was applied to the edge of the floating ice. The calculated and observed ice cover areas are comparable. The usage of a constant edge retreat rate in the model has noticeable effects, but the magnitude is small compared to the errors resulting from the computation of ice release from the shore. The shape of the predicted ice cover departed from the observations only at two locations in the lake where thin ice and shallow ice resulted in rapid ice loss early in the melt period.

The thickness of ice at the edge of the floating cover was determined by its initial thickness, the ice melt rate and the edge retreat. The temporal variation of edge thickness followed the observed trend, but the observed and computed ice thickness differed substantially both early and late in the melt period due to errors in the computed ice thickness and the rate of edge retreat.

Many of the discrepancies between the observed and

calculated ice conditions can be traced to the error that the edges of the ice cover became free of the shore approximately 2 days earlier than observed. This error may be caused by one or more of the following: the model snowcover or the basal ice along the shore were thinner than in reality, an underestimation of the initial ice thickness or an over-estimation of the snow or ice melt. Individual effects of each of these components cannot be isolated until more field data can be obtained.

CHAPTER 7

Conclusions

This study examined the decay of a small High Arctic lake ice cover to provide an improved understanding of its behaviour during melt. The spatial variability of the lake ice cover during decay was simulated with a two-dimensional, physically based model.

The energy balance computations are summarized in Table 7.1. The results indicate that absorbed radiation was the largest energy source followed by the flux of sensible heat from the atmosphere. The fluxes of heat from the lake water and latent heat as a result of condensation were small in comparison while the heat provided by precipiation was negligible. The only energy loss, other than that used for melt, was due to the net longwave flux. Internal melt energy was concentrated near the ice surface, lowering the surface ice densities by 400 kg/m^3 or more. Together with the surface melt energy, this resulted in about 75 percent of the decrease in ice thickness occurring from the upper ice surface. The accuracy of the one dimensional model used to predict ice thickness was reasonable but varied greatly with the quality of the data and parameters. Additional work on the absorption of radiation by ice and the variability of the aerodynamic roughness would improve the model accuracy.

Table 7.1

Summary of the Energy Balance and Ice Melt Components

Energy Flux Term	Percent of Total Input Energy	
	1980	1981
Sensible Heat	43	38
Latent Heat	6	12
Heat from Precipiation	negligible	negligible
Net Longwave Radiation	-13	-17
Absorbed Shortwave Radiation	42	41
Heat from Lake Water	9	10
Ice Melt	-87	-83

Ice Melt Component	Percent of Total Melt (WE)	
Upper Ice Surface Melt	40	39
Internal Ice Melt	49	49
Lower Ice Surface Melt	11	12

Most of the previous studies on lake ice melt have treated the problem one-dimensionally. However, a knowledge of the formation and growth of the moat of water along the lake perimeter is crucial in determining the ice cover extent for most of the decay period. The moat development could be divided into two phases. In the first, the moat is underlain by ice and is caused by flooding of the ice surface where the ice edge is frozen to the lake edge. Its position is determined by the nature of the snow cover, water level rise, and ice deflection and deformation. This phase ends when the the ice either melts free of the lake bottom or fractures at the edge of the moat. A critical water level rise is necessary to fracture a given thickness of ice. In the second phase, the moat grows as ice is lost from the edge of the floating ice cover. Transfer of heat from the warm moat water produces melting but in addition, the mechanical action of waves is responsible for removing fragments from the edge of the ice cover. Over the melt period, more than 40 percent of the ice cover area is lost in this manner. Other mechanisms of ice loss from the edge of the floating ice cover, such as shore-ice interaction during ice drift and the stranding of ice during water level drops produce negligible ice loss.

The two-dimensional model that was developed to simulate the spatial aspects of ice decay performed well

despite the many necessary simplifications. The predicted behaviour of the moat compared favourably with that observed in the field and the ice thickness was comparable to measured values. While there were some discrepancies in the shape of the predicted ice cover, the calculated and observed ice cover areas were similar.

Energy balance models require more data than the simple index methods, but are more versatile. The data requirements for the two-dimensional model are no more stringent than the one-dimensional energy balance case, and little additional data are required. The model can be improved easily when more knowledge of some of the processes becomes available. The model becomes spatially transferable when the modifications outlined below are made. The present model is applicable to medium to small Arctic lakes. It cannot be used for the very shallow ponds which freeze completely, since the ice cover tends to fragment early in the melt period as the ice breaks free of the bottom in a haphazard manner. For the deeper ponds, where the ice is thicker, stronger, and remains intact when it is released from the lake bottom, the model can be applied, but with reduced accuracy during the period of initial moat formation. With some modification, this model can be used for temperate and subarctic lake ice covers. For these environments, one major change involves a computation of the thermal profile of the ice because of

intense nocturnal cooling of the ice which refreezes much of the meltwater released by internal melt on the previous day, and thus altering the ice density profile and strength. Another modification involves the radiation absorption component due to the presence of a thick layer of highly reflective white ice on the lakes.

The ice decay model loses its accuracy when the lake ice is more strongly influenced by water currents. Under these conditions, the heat flux from the water increases and the bottom melt is large and spatially variable. A similar problem exists when a lateral input of warm water from a stream locally accelerates the melt along the shore. The model is also unable to deal with the final phase of ice decay. During this period, the ice cover breaks up into progressively smaller pieces. The rate of fragmentation is determined by the ice strength and the stresses imposed.

Research on several aspects of lake ice melt can further strengthen the model. Among these is the nature of the radiation regime of the ice cover which indirectly controls the ice strength. Ice strength is related to the ice porosity, which in turn is affected by the internal melting of the ice. As internal melt is dependent on the radiation absorption, a good estimate of the radiation absorption coefficients under a variety of ice conditions and environments will enhance the model (cf. Grenfell and

Maykut's (1977) approach for sea ice). It may also allow the ice albedo to be determined from the ice properties and thus reduce the data requirements. Another area for future investigation should involve the mechanical strength of melting ice. Ice strength plays an important role in the initial moat formation, loss along the ice edge and fracturing and final disintegration of the ice cover. A better understanding of ice strength during decay would permit the spatial ice decay model to be expanded to include the ice dynamics. This information would eliminate some of the empirical relationships currently employed in the model.

Continued northern development and the need for impact assessments has resulted in a need to be able to model environmental conditions in order to determine potential effects. This also applies to lakes which are an important feature in northern environment. As Fox et al (1979) have indicated, none of the current limnologic models are applicable to ice covered lakes. The two-dimensional model of ice decay used in this study can be incorporated into lake models to allow the behaviour of the lake during ice decay to be simulated. The approach used is flexible and the procedures can be easily modified to meet the requirements of each situation. Used in conjunction with existing ice growth models, this approach will permit the development of an annual lake ice model.

REFERENCES

Adams, W.A., 1975. Light intensity and primary productivity under sea ice containing oil. *Beaufort Sea Project Tech. Report*, 29. Dept. Fisheries and Environment, Victoria.

Adams, W.P., 1976. A classification of freshwater ice. *Musk-ox*, 18, 99-102.

Adams, W.P., 1981. Snow and ice on lakes. in Gray, D.M. and Male, D.H (eds, *Handbook of Snow*, Pergamon Press, Toronto, 437-474.

Alestalo, J., 1980. Systems of ice movement on Lake Lappajarvi, Finland. *Fennia*, 158, 27-39.

Allen, W.T.R., 1977. *Freeze-up, Break-up and Ice Thickness in Canada*. Pub. CLI-1-77, Atmospheric Environment Service, Fisheries and Environment Canada, Ottawa, 185p.

Andrews, J.T., McGee, R. and McKenzie-Pollack, L., 1971. Comparison of elevation of archaeological sites and calculated sea levels in Arctic Canada. *Arctic* 24, 216-228.

Ashton, G.D., 1983. Lake ice decay. *Cold Regions Sci. and Technol.*, 8, 83-86.

Ashton, G.D., 1984. Deterioration of floating ice covers. in Lunardi, V.J. (ed.), *Proc. Third International Offshore Mechanics and Arctic Engineering Symp.*, A.S.M.E., 26-33.

Baker, D.G., Baker-Blocker, A., DeWitt, B.H. and Dixon, D.W., 1976. Objective prediction of ice formation, freeze-up and break-up on the Great Lakes. *Jour. of App. Met.*, 15, 1033-1040.

Barnes, D.F., 1959. Preliminary report on Lake Peters, Alaska, ice studies. *Proc. of 2nd Annual Arctic Planning Session*, GRD Res. Note 29, Air Force Cambridge Research Center, 102-110.

Barnes, D.F., 1960. An investigation of a perennially frozen lake. *Air Force Surveys in Geophys.*, No. 129, 134p.

Barnes,D.F. and Hobbie,J.E.,1960. Rate of melting at the bottom of floating ice. *U.S.G.S.*, Prof. Paper 400-B, B392-B394.

Barnes,H.T., 1910. On the apparent sinking of surface ice in lakes. *Science*, 31, 856-857.

Bilello,M.A.,1980. Maximum thickness and subsequent decay of lake, river and fast sea ice in Canada and Alaska. *C.R.R.E.L. Report*, 80-6, 160p.

Bilello,M.A.,1967. Water temperatures in a shallow lake during ice formation, growth and decay. *C.R.R.E.L.*, Res. Report 213, 20p.

Billfalk,L.,1981. Formation of shore cracks in ice covers due to changes in the water level. *International Symp. on Ice*. I.A.H.R., Quebec, 650-662.

Bolsenga,S.J.,1978. Photosynthetically active radiation transmission through ice. *N.O.A.A. Tech. Memo.* ERL GLERL-18, 48p.

Bolsenga,S.J.,1981. Radiation transmittance through lake ice in the 400-700 rangs. *J. Glaciol.* 27, 57-66.

Bostock,H.L.,1972. Physiographic subdivisions of Canada. in Douglas,R.J.W. (ed.), Geology and Economic Minerals of Canada, Geol. Surv. Can. Econ. Report 1, Dept. of Energy, Mines and Resources, Ottawa, 10-30.

Browman,L.G.1974. Channels in ice. in *Advanced Concepts and Techniques in the Study of Snow and Ice Resources*. National Academy of Sciences, 224-234.

Carson,C.F. and Hussey,K.M.,1960. Hydrodynamics of three Arctic lakes. *J. Geol.* 68, 585-600.

Chieh,S.H., Wake,A. and Rumer,R.R., 1983. Ice forecasting model for Lake Erie.*J. Waterways. Port and Coastal Eng.* 109, 392-415.

Cook,F.A.,1958. Temperatures in permafrost at Resolute, N.W.T. *Geogr. Bull.*, 12, 5-18.

Cruikshank,J.G.,1971. Soils and terrain units around Resolute, Cornwallis Island. *Arctic*, 224, 195-209.

Dilley,J.F.,1978. *Heat Transfer Analysis of Nearshore Ice Formation. Growth and Decay Utilizing a Numerical Simulation Model.* Ph.D. Thesis, University of Pennsylvania, 245p.

Doronin,Y.P.,1970. *Thermal Interaction of the Atmosphere and the Hydrosphere in the Arctic.* Israel Program for Scientific Translations, Jerusalem, 244p.

Doronin,Y.P. and Kheisin, D.E., 1977. *Sea Ice.* Amerind Publishing Co., New Delhi. 323p.

Energy, Mines and Resources, 1974. *National Atlas of Canada.* MacMillan of Canada, Toronto, 254p.

Fox,P.M., LaPerriere,J.D. and Carlson,R.F.,1979. Northern lake modeling: aliterature review. *Water Resour. Res.*, 13, 1065-1072.

Gidding,J.G. and LaChapelle,E.,1963. Diffusion theory applied to radiant energy distribution and albedo of snow. *J. Geophys. Res.* 66, 181-189.

Goldman,C.R., Mason,D.T. and Hobbie,J.E., 1967. Two Antarctic lakes. *Limnol. Oceanogr.* 12, 295-310.

Goodrich,L.E.,1970. Review of radiation absorption coefficients for clear ice in the spectral region, 0.3 to 3.0 microns. *Div. of Building Res. Tech. Paper*, 331. Nat. Res. Council of Canada, Ottawa.

Gorelkin,N.Y., Kazakov,A.M. and Nurbayev,D.D.,1980. Penetration of solar radiation into the water masses of the Charbak Reservoir. *Soviet Hydrology: Selected Papers* 19, 144-147.

Greene,G.M.,1981. Simulation of ice-cover growth and decay in one dimension on the Upper St. Lawrence River. *N.O.A.A. Tech. Memo.* ERL GLERL-36, 82p.

Greene,G.M. and Outcalt,S.I., 1985. A simulation of river ice cover thermodynamics. *Cold Region Sci. Technol.* 10, 251-262.

Grenfell,T.C.,1979. The effects of ice thickness on the exchange of solar radiation over the polar oceans. *J. Glaciol.* 22, 305-320.

Grenfell,T.C. and Maykut,G.A.,1977. The optical properties of ice and snow in the Arctic Basin. *J. Glaciol.* 18. 445-463.

Grenfell,T.C. and Perovich,D.K.,1981. Radiation absorption coefficients of polycrystalline ice from 400-1400 nm. *J. Geophys. Res.* 86(C8), 7447-7450.

Grenfell,T.C. and Perovich,D.K.,1984. Spectral albedos of sea ice and incident solar irradiance in the southern Beaufort Sea. *J. Geophys. Res.* 89(C3), 3573-3580.

Heron,J.R. and Woo,M.K.,1978. Snowmelt computations for a High Arctic site. *Proc. Eastern Snow Conf.* 35, 162-172.

Hibler,W.D.,1979. A dynamic thermodynamic sea ice model. *J. Phys. Oceanogr.* 9, 815-846.

Hill,H.,1967. A note on temperatures and water conditions beneath lake ice in spring. *Limnol. Oceanogr.* 12, 550-552.

Hobbie,J.E.,1962. *Limnological Cycles and Productivity of Two Lakes in the Alaskan Arctic.* Ph.D. Thesis, Indiana University, 124p.

Hobbie,J.E.,1973. Arctic limnology: a review. in Britton,M.E. (ed), *Alaska Arctic Tundra*, Arctic Institute of North America, Tech. Paper 25, 127-168.

Hobbs.P.V.,1974. *Ice Physics.* Claredon Press, Oxford, 837p.

Huppert,H.E. and Josberger,E.G., 1980. The melting of ice in cold stratified water. *J. Physical Oceanogr.*, 10, 953-960.

Irvine,W.M. and Pollack,J.B.,1968. Infared properties of water and ice spheres. *Icarus* 8,324-360.

Josberger,E.G.,1980. The effect of bubbles released from a melting ice wall on the melt driven convection in salt water. *J. Phy. Oceanogr.* 10, 474-477.

Judge,A.S.,1977. Calculation of permafrost thickness. in Bliss,L.C. (ed), *Truelave Lowland. Devon Island. Canada: A High Arctic Ecosystem.* The University of Alberta Press, Edmonton, 26-30.

Ketcham,W.M. and Hobbs,P.V.,1969. An experimental determination of the surface energies of ice. *Phil. Mag.* 19, 1161-1173.

Kivisild,H.R.,1970. River and lake ice terminology. Paper 1.0 in *Ice and Its Action on Hydraulic Structures*, I.A.H.R. Symp., Reykjavik.

Koerner,R.M.,1963. Glaciology, winter 1961-1962. in The Devon Island expedition, 1960-1964, *Arctic* 16, 57-62.

Lachenbruch,A.H.,1957. Thermal effects of the ocean on permafrost. *Bull. Geol. Soc. Am.* 68, 1615-1630.

Langleben,M.P.,1966. On the factors affecting the rate of ablation of sea ice. *Can. J. Earth Sci.*, 3, 431-439.

Langleben,M.P.,1972. Decay of an annual sea ice cover. *J. Glaciol.* 11, 337-343.

LaPerriere,J.D., Tilsworth,T. and Casper,L.A., 1978. *Nutrient Chemistry of a Large. Deep Lake in Subarctic Alaska.*. Corvallis Environmental Research Laboratory, U.S. Environmental Protection Agency, Corvallis, 128p.

Latimer,J.R.,1972. Radiation measurement. *Technical Manual Series* 2, International Field Year for the Great Lakes, 53p.

Maguire,R.J.,1975. Effects of ice and snow cover on transmission of light in lakes. *Scientific Series* 54, Inland Waters Directorate, Environment Canada, Ottawa, 24p.

Maguire,R.J.,1975b. Light transmission through snow and ice. *Tech. Bull.* 91, Inland Waters Directorate, Environment Canada, Ottawa, 4p.

Marsh,P and Woo,M.K.,1984. Wetting frbnt advance and freezing of melt water within a snow cover. 1. Observations in the Canadian Arctic. *Water Resour. Res.* 20, 1853-1864.

Maykut,G.A. and Untersteiner,N., 1971. Some results from a time-dependent thermodynamic model of sea ice. *J. Geophysical Res.*, 76, 1550-1575.

Maxwell,J.B.,1980. The climate of the Canadian Arctic Islands and adjacent waters. *Climatological Studies* 30, Atmospheric Environment Service, Environment Canada, Ottawa. 1120p.

Meisner,A.D.,1955. Heat flow and depth of permafrost at Resolute Bay, Cornwallis Island, N.W.T., Canada. *Trans. Am. Geophys. Union* 36, 1055-1066.

Michel,B.,1978. *Ice Mechanics*. Laval University Press, Quebec, 499p.

Michel,B. and Ramseier,R.O.,1971. Classification of river and lake ice. *Can. Geotech. J.* 8, 36-45.

Muguruma,J. and Kikuchi,K.,1963. Lake ice investigation at Peters Lake, Alaska. *J. Glaciol.*, 2, 687-708.

Parkinson,C.L. and Washington,W.M.,1979. A large scale numerical model of sea ice. *J. Geophys. Res.* 84(C1), 311-337.

Perey,F.G.J. and Pounder,E.R.,1958. Crystal orientation in ice sheets. *Can. J. Phys.* 36, 494-502.

Pivovarov,A.A.,1972. *Thermal Conditions in Freezing Lakes and Rivers*. John Wiley and Sons, New York, 136p.

Polyakova, K.N.,1977. Long-range forecast of the strength of the melting ice cover in the Volgograd Reservoir in spring. *Soviet Hydrology: Selected Papers* 16, 217-221.

Ramseier,R.O. and Weaver,R.J.,1975. Floating ice thickness and structure determination - heated wire technique. *Technical Bulletin* 88, Inland Waters Directorate, Environment Canada, Ottawa, 8p.

Rigler,F.,1975. *Char Lake Project. Final Report 1974.* Canadian Committee for International Biological Project, 95p.

Roulet,N.T.,1981. *Variability of the Quality and Quantity of Light Penetrating a Winter Lake Cover*. M. Sc. Thesis, Trent University.

Rumer,R.R. and Yu,P.M., 1978. Modelling ice dissipation in eastern Lake Erie. *J. Great Lakes Res.*, 4, 194-200.

Russel-Head,D.S.,1980. The melting of free-drifting icebergs. *Annals of Glaciol.* 1, 119-122.

Schindler,D.W., Welch,H.E., Kalff,J., Brunskill,G.J., and Kritsch,N., 1974. Physical and chemical limnology of Char Lake, cornwallis Island (75° N Lat). *J. Fisheries Res. Board of Canada*, 31, 585-607.

Scott,J.T. and Ragotzkie,R.A., 1961. *Heat Budget of an Ice Covered Inland Lake.* Tech. Report 6, Department of Meteorology , University of Wisconsin, 52.

Semtner,A.J.,1976. A model for the thermodynamic growth of sea ice in numerical investigations of climate. *J. Physical Oceanogr.* 6, 379-389.

Shaw,J.B., 1965. Growth and decay of lake ice in the vicinity of Schefferville (Knob Lake), Quebec. *Arctic*, 18, 123-132.

Shulyakovskii,L.G. (ed),1966. *Manual of Forecasting Ice-Formation for Rivers and Inland Lakes.* Israel Program for Scientific Translations, Jerusalem, 245p.

Shumskii,P.A.,1964. *Principles of Structural Glaciology.* Dover Publications Inc., New York, 497p.

Starosolszky,O.(ed),1980. *Multilingual Ice Terminology, Addendum 1.* International Association for Hydraulic Research, Section on Ice Problems. Research Centre for Water Resources, Budapest, 24p.

Swinzow,G.K.,1961. Ice cover of an Arctic proglacial lake. *C.R.R.E.L. Res. Report* 155, 43p.

Taylor,A., Judge,A., and Desrocher,D.,1983. Shoreline regression: its effect on permafrost and the geothermal regime, Canadian Arctic Archipelago. in *Proc. Fourth International Conf. on Permafrost.*, National Academy Press, Washington, 1239-1244.

Thorsteinsson,R.,1958. Cornwallis and Little Cornwallis Islands, District of Franklin, Northwest Territories. *Geol. Surv. of Canada Memoir* 294, 134p.

U.S. Navy,1952. *A Functional Glossary of Ice Terminology*. U.S. Navy Hydrographic Office Publicaion No. 609, Washington, 88p

Wake,A. and Rumer,R.R., 1979. Effect of surface meltwater accumulation on the dissipation of lake ice. *Water Resources Res.*, 15, 430-434.

Wake,A. and Rumer,R.R.,1979b. Modeling ice regime of Lake Erie. *J. of Hydraul. Div. A.S.C.E.* HY7, 827-844.

Washburn,A.L. and Stuiver,M.,1985. Radiocarbon dates from Cornwallis Island area, Arctic Canada - an interim report. *Can. J. Earth Sci.* 22, 630-637.

Weller,G.E.,1969. Radiation diffusion in Antarctic ice media. *Naure* 221, 355-356.

Wetzel,R.G.,1975. *Limnology*. W. B. Saunders Company, Toronto, 743p.

Williams,G.P., 1965. Correlating freeze-up and break-up with weather conditions. *Can. Geotech. J.*, 11, 313-326.

Williams,G.P., 1968. Freeze-up and break-up of fresh water lakes. *Ice Pressures against Structures*, Proc. of a Conference at Laval University, 1966. National Research Council of Canada Technical Memorandum 92, 203-212.

Williams,G.P., 1969. Water temperatures during the melting of lake ice. *Water Resources Res.*, 5, 1134-1138.

Willaims,G.P., 1971. Predicting the date of lake ice breakup. *Water Resources Res.*, 7, 325-333.

Woo,M.K.,1980. Hydrology of a small lake in the Canadian High Arctic. *Arctic and Alpine Res.* 12, 227-235.

Woo,M.K. and Heron,R.,1979. Modelling basin snow storage in a High Arctic environment. *Proc. Can. Hydology Symp. 79*, Assoc. Committee on Hydrology, Nat. Res. Council of Canada, 207-216.

Woo,M.K., Heron,R. and Steer,P.,1981. Catchment hydrology of a High Arctic lake. *Cold Region Sci. Technol* 5, 29-41.

Woo,M.K. and Heron,R.,1981. Occurrence of ice layeers at the base of High Arctic snowpacks. *Arctic and Alpine Res.* 13, 225-230.

Woo,M.K., Heron,R., and Marsh,P.,1982. Basal ice in High Arctic snowpacks. *Arctic and Alpine* 14, 251-260.

Woo,M.K., Heron,R., Marsh,P. and Steer,P.,1983. Comparison of weather station snowfall with winter snow accumulation in High Arctic basins. *Atmosphere-Ocean* 21, 312-325.

Woo,M.K. and Dubreuil,M.A.,1984. Empirical relationship between dust content and Arctic snow albedo. *Cold Regions Sci. Technol.* 10, 125-132.